Crystal Structure of the Catalytic Domains of Membranous Adenylyl Cyclase with MANT-ITP and Electrophysiological Analysis of MANT Nucleotides in Cardiomyocytes

DISSERTATION

zur Erlangung des Doktorgrades der Naturwissenschaften (Dr. rer. nat.) der Naturwissenschaftlichen Fakultät IV - Chemie und Pharmazie - der Universität Regensburg
Lehrstuhl für Pharmakologie und Toxikologie

vorgelegt von

Melanie Hübner

aus Dresden

im Jahr 2010

Die vorliegende Arbeit entstand in der Zeit von November 2007 bis Juli 2010 unter der Leitung von Herrn Prof. Dr. R. Seifert am Institut für Pharmakologie und Toxikologie der Naturwissenschaftlichen Fakultät IV – Chemie und Pharmazie – der Universität Regensburg.

Promotionsgesuch eingereicht am: 28.07.2010

Tag der mündlichen Prüfung am: 27.08.2010

Prüfungsausschuß:

Vorsitzender:	Prof. Dr. Jörg Heilmann
1. Gutachter (1. Prüfer):	Prof. Dr. Roland Seifert
2. Gutachter (2. Prüfer):	Prof. Dr. Stefan Dove
3. Prüfer:	Prof. Dr. Sigurd Elz

Meinen Eltern

Danksagung

Mit Beendigung meiner Arbeit ist es an der Zeit, mich bei all den Menschen zu bedanken, die am Gelingen dieser Arbeit maßgeblich beteiligt sind.

Mein Dank für die Ermöglichung dieser Arbeit gilt zuallererst meinem Doktorvater Herrn Prof. Dr. Seifert, der mir nicht nur ein sehr spannendes Doktorthema zur Verfügung stellte, sondern mir zusätzlich wissenschaftliche (Auslands)-Aufenthalte an der University of Montana und am Universitätsklinikum Köln ermöglichte. Er hat mit großer Initiative meinen Stipendienantrag unterstützt, hilfreiche Ratschläge bei der Problembewältigung gegeben und mir immer ein offenes Ohr und eine große Geduld bei allen Diskussionen entgegengebracht. Dem Elitenetzwerk Bayern danke ich für die finanzielle und ideelle Promotionsförderung.

Weiterhin danke ich meinem Zweitgutachter Herrn Prof. Dr. Dove für Einblicke in die 3D-Struktur von Adenylylzyklasen, für zusätzliche Ideen beim Niederschreiben der Doktorarbeit und für die zügige Erstellung des Zweitgutachtens. Herrn Prof. Dr. Elz möchte ich dafür danken, daß er sich als Drittprüfer zur Verfügung stellt und Herrn Prof. Heilmann danke ich als Vorsitzenden für die Vervollständigung meiner Prüfungskommission.

Ohne meine netten Arbeitskollegen von der University of Montana hätte ich sicherlich nie solch tiefe Einblicke in die Röntgenkristallstrukturanalyse und Proteinaufreinigung erhalten. Ich danke daher Herrn Prof. Dr. Steve Sprang, Tung-Chung Mou, Dianne DeCamp, Celestine Thomas und Roslyn Pinson, daß sie mich so liebevoll in das „Center for Biomolecular Structure and Dynamics“ aufgenommen haben und mich während dieser Zeit auch persönlich unterstützt und begleitet haben.
Weiterhin kann ich der Arbeitsgruppe von Herrn Prof. Dr. Herzig an der Universität Köln, Institut für Pharmakologie, nicht genügend dafür danken, daß sie mich für eine gewisse Zeit in ihren Arbeitskreis aufgenommen hat und mir mit Rat und Tat bei der Bearbeitung elektrophysiologischer Aufgabenstellungen zur Seite stand. Ein großer Dank an Prof. Herzig, Dr. Jan Matthes, Sara Dizayee, Sigrid Kirchmann-Hecht und den Rest der Truppe. Es war sehr schön, ab und zu einen Freitagnachmittagssekt mit ihnen zu trinken!

Für immer unvergessen bleibt mir das „Doktoranden-Team“ der Pharmakologie und Toxikologie von der Universität Regensburg. Ich denke, daß wir nicht nur wissenschaftlich, sondern auch persönlich eine unheimlich intensive Doktorandenzeit zusammen verbracht haben, auch wenn ich Euch oft „verlassen“ habe. David, Heidrun, Higgl, Irena, Katharina, Lisa, Martin, Matthias, Miriam, sowie Postdoc Erich, Andrea und Petra – es war schön mit Euch! Außerdem möchte ich mich gerne bei unseren fleißigen technischen Assistentinnen Gertraud Wilberg, Astrid Seefeld und Susanne Brüggemann für die Durchführung von AC-Assays und sonstige Hilfestellungen bedanken. Vielen Dank an Herrn Prof. Kees für die zusätzliche Betreuung der Doktorarbeit und das abschließende Gegenlesen.

Meinen Freunden, die stets für mich da waren und nie müde wurden, mich anzuspornen, gilt mein weiterer Dank. Meinen Schulfreundinnen Anne-Katrin und Claudia, danke ich fürs Zuhören, für aufbauende Worte und für viele gemeinsame Stunden, die maßgeblich zum Gelingen der Arbeit beigetragen haben. Dr. Martin Meyer möchte ich dafür danken, daß er mir das Selbstbewusstsein für einen „2. Anfang“ zurückgegeben hat. Dr. Matthias Desch, Chris Hanson und Denis Lehmann möchte ich sehr fürs Korrekturlesen danken. Vor allem Denis hat in den letzten Wochen großartige „Aufbauarbeit“ geleistet.

Zu guter Letzt, möchte ich mich bei meiner tollen Familie, meinen Eltern Herrn Prof. Dr. Manfred und Ute Hübner, meiner Schwester Anke und Wolfgang, sowie meinen Großeltern, bedanken. Ihr habt mich nicht nur moralisch und finanziell unterstützt, sondern ward immer ein wunderbarer Rückhalt in schwierigeren Zeiten und die besten Ratgeber, die man sich wünschen kann.

Das Studium jeglicher neuen Wissenschaft…
gleicht einer Reise in ferne Länder.
Alexander von Humboldt (1769-1859)

Abbreviations

AA	amino acid
AC $5^{-/-}$	AC 5 knockout
AD	Analog-Digital
Amp	ampicillin
ATP	adenosine 5'-triphosphate
β-AR	β-adrenergic receptor/β-adrenoceptor
bp	base pair
CaM	calmodulin
cAMP	cyclic adenosine 3',5'-monophosphate
CLS	collagenases
Da	Dalton
FRET	fluorescence resonance energy transfer
FS	forskolin
GPCR	G protein-coupled receptor
GppNHp	guanosine 5'-[β,γ-imido]triphosphate
GTPγS	guanosine 5'-[γ-thio]triphosphate
HRP	horseradish peroxidase
$I_{Ca,L}$	L-type calcium current
I-V	current - voltage relationship
Kan	kanamycin
KO	knockout
LTP	long-term potentiation
mAC	mammalian membranous adenylyl cyclase
MANT	N-methylanthraniloyl
MD	molecular dynamics
min	minute(s)
MP-FS	7-acetyl-7-[O-(N-methyl-piperazino)-γ-butyryl)]-forskolin
MWCO	molecular weight cut off
NDP	nucleoside 5'-diphosphate
NTP	nucleoside 5'-triphosphate
NTPγS	nucleoside 5'-[γ-thio]triphosphate
OD_{600}	optical density at 600 nm
PDB	RCSB Protein Data Bank
PI	protease inhibitors
PKA	cAMP-dependent protein kinase A
PKC	protein kinase C
rpm	rotations per minute
RMSD	root mean square deviation
sAC	soluble adenylyl cyclase
sGC	soluble guanylyl cyclase
SDS - PAGE	sodium dodecyl sulphate - polyacrylamide gel electrophoresis
S.E.M.	standard error of mean
SOB	super optimal broth
SR	sarcoplasmatic reticulum
SSRL	Stanford Synchrotron Radiation Lightsource
UMT	the University of Montana
UR	the University of Regensburg
VDCC	voltage-dependent calcium channels
WC	whole cell
WT	wild type

1. Introduction

1.1. Adenylyl cyclases

1.1.1. AC isoforms

Adenylyl cyclases (ACs) convert adenosine 5'-triphosphate (ATP) to pyrophosphate and cyclic adenosine 3',5'-monophosphate (cAMP), a second messenger that plays an important role in many different biological systems. The physiological activity of ACs is mainly regulated by G protein-coupled receptors (GPCRs) that are located in the plasma membrane and induce a GPCR-mediated signaling cascade in the cell. The term already indicates that GPCRs couple to G proteins, either to stimulatory G proteins, such as $G_{s\alpha}$, or to inhibitory G proteins, such as $G_{i\alpha}$. These proteins interact directly with AC and *via* activation cAMP is produced. Generation of cAMP influences a variety of cellular responses, such as embryogenesis (Bellen *et al.*, 1987), hormone secretion (Dyachok *et al.*, 2008), regulation of vascular smooth muscle (Hardman, 1984), cardiac contraction (Okumura *et al.*, 2003a), olfaction as well as learning and memory (Wang and Storm, 2003).

In humans, one soluble and nine membrane-bound AC isoforms are responsible for cAMP production (Buck *et al.*, 1999; Hanoune and Defer, 2001; Kamenetsky *et al.*, 2006). The unique soluble AC isoform (sAC) is not further discussed here, but it should be mentioned that this enzyme does not have membrane domains and is not regulated by G proteins, but stimulated by calcium and bicarbonate. It resembles cyanobacterial AC and plays a role in sperm motility and fertilization. Based on differences in the regulatory properties of membranous AC (mAC), they can be classified into four different categories:

- ACs 1, 3 and 8 are stimulated by Ca^{2+}/calmodulin (CaM) (class I);
- ACs 2, 4 and 7 are stimulated by $G_{\beta\gamma}$ (class II);
- ACs 5 and 6 constitute class III and are $G_{i\alpha}$/Ca^{2+} inhibited and
- AC 9 is the only member of class IV, because it is the only AC isoform that is not activated by forskolin (FS).

FS is a natural diterpene, derived from the roots of *Coleus forskohlii*, an Indian plant and it is the most effective direct activator of ACs 1-8. Unfortunately, ACs are expressed only at low levels, and there is a lack of isoform-specific antibodies. Therefore, tissue distribution is detected mainly *via* PCR and Northern blotting, but also using functional assays, such as the AC activity assay (Sunahara *et al.*, 1996; Hanoune and Defer, 2001; Göttle *et al.*, 2009). Another possibility to comprehend the role and function of individual AC isoforms was achieved by changing the gene level of AC isoforms in knockout (KO) and overexpression studies (Schaefer *et al.*, 2000; Yan *et al.*, 2007; Sadana and Dessauer, 2009). Most cells express not only one single AC isoform. But some AC isoforms have a specific expression

pattern, and a physiological role can be assigned due to their localization. ACs 1 and 8 are associated to learning and memory, AC 3 plays a role in olfaction and ACs 5 and 6 regulate cardiac contractility (Table 1).

Isoform	Expression in tissue	Physiological roles	Genetic approach
AC 1	brain, adrenal medulla	learning, memory, synaptic plasticity, opiate withdrawal	AC $1^{-/-}$ mice: ↓ LTP, ↓ pain response, ↓ neuronal excitotoxicity, ↓ withdrawal behavior, ↑ ethanol sedation Overexpression: enhanced memory
AC 2	brain, lung, skeletal muscle, heart	arrest of cell proliferation, synaptic plasticity	
AC 3	olfactory epithelium, pancreas, brain, heart, lung, testis	olfaction, sperm function	AC $3^{-/-}$ mice: ↓ odorant-induced signaling, ↓ pheromone detection
AC 4	no specific expression	mood disorders, depression, photo reception	
AC 5	heart, striatum, kidney, liver, lung, testis, adrenal	cardiac contraction, motor coordination, opiate dependency, pain responses	AC $5^{-/-}$ mice: ↑ life span, ↓ age-induced myopathy, ↓ pain response, abnormal coordination, ↓ morphine response Overexpression: ↑ basal AC activity
AC 6	heart, kidney, liver, lung, brain, testis, skeletal muscle, adrenal	cardiac contraction	AC $6^{-/-}$ mice: ↓ stimulated AC activity Overexpression: ↑ response to catechol-amine, but no histological abnormalities
AC 7	brain, platelets	ethanol dependency, depression	Overexpression: ↑ morphine tolerance, ↑ ethanol effect
AC 8	brain, lung, pancreas, testis, adrenal	learning, memory, synaptic plasticity , LTP, opiate withdrawal	AC $8^{-/-}$ mice: ↓ LTP, ↓ withdrawal behavior, ↓ ethanol consumption
AC 9	no specific expression (eg. brain-hippocampus)	polymorphism relevant in asthma treatment, learning, memory	AC 9 gene deletion is embryonically lethal
sAC	testis, but detected in all tissues	sperm capazitation, fertilization	

Table 1. Expression pattern and physiological role of mACs and sAC. Specific physiological roles and expression levels were identified, using the above mentioned techniques (Sadana and Dessauer, 2009).

It is important to understand that some AC isoforms have very similar physiological roles. As already mentioned AC 1 which is primarily expressed in brain, particularly in hippocampus, neocortex, entorhinal cortex and cerebellar cortex, is most likely connected to learning and memory, together with AC 8. Mice having a gene deletion of AC 1 showed normal growth and unchanged motor behavior and lifespan, but decreased Ca^{2+} stimulated activity in brain, decreased long-term potentiation (LTP) and deficiency in spatial memory (Wu *et al.*, 1995). However, abnormalities in LTP could be reversed by FS, indicating that another AC isoform - most likely AC 8 - also contributes to these effects. Furthermore, ACs 1 and 8 mediate morphine response. These two enzymes are quite similar in their regulatory profile, because they are, together with AC 3, regulated by Ca^{2+}-bound CaM. However, ACs 1 and 8 are mainly stimulated by direct binding of CaM to a CaM binding site, whereas AC 3 is inhibited *via* CaM-dependent protein kinase II (Kamenetsky *et al.*, 2006).

Regulation of ACs can vary between the different isoforms, but all of the transmembrane isoforms are stimulated by $G_{s\alpha}$. $G_{\alpha olf}$ is also a stimulatory G protein predominantly expressed in olfactory tissue and it also activates AC. $G_{i\alpha}$ inhibits only some of the AC isoforms, such as ACs 5 and 6, but also CaM stimulated AC 1. The $G_{\beta\gamma}$-subunit can be either stimulatory (group II and III) or inhibitory (group I). ACs are further regulated by divalent cations. The presence of Mn^{2+} and Mg^{2+} stimulates the enzyme, but submicromolar concentrations of free Ca^{2+} inhibit ACs 5 and 6. In contrast, high, non-physiological concentrations of Ca^{2+} inhibit all AC isoforms, mainly by competition with Mg^{2+} for binding to the catalytic site. In a feedback mechanism ACs are influenced by protein kinases (PKs). PKA inhibits ACs 5 and 6 by direct phosphorylation of the cytosolic domain. PKC can be stimulatory (AC 1; PKCδ and AC 7; PKCα/ζ and AC 5) or inhibitory (PKCα and AC 4; PKCδ /PKCε and AC 6). Additional kinases, such as tyrosine kinases, regulate indirectly AC activity which is not discussed here in more detail. Further regulation of ACs was shown by studying the interaction with different other proteins, such as Snapin or A-kinase anchoring protein (AKAP79), indicating high diversity of regulation (Beazely and Watts, 2006).

Even though we already know quite a lot about the differential expression pattern and regulation of ACs 1-9, there are still many important questions: why do we have 10 different AC isoforms, and is it possible to activate or inhibit specific isoforms selectively? The search for isoform-specific AC inhibitors/activators may further help in characterization of the physiological role of single AC isoforms and could be used to identify new pharmacotherapeutic targets. In several studies it was shown that substrate affinity and selectivity of AC inhibitors and activators are different for some AC isoforms (Gille *et al.*, 2004; Pinto *et al.*, 2009).

One possibility to characterize the different AC isoforms was the expression of full-length isoforms in mammalian and insect cells, but this was hampered by the non-availability of functional and pure protein and non-specificity of AC antibodies. The other possibility was the expression of the two functionally active catalytic domains C1 and C2 in *Escherichia coli* (Dessauer *et al.*, 1997). With these soluble proteins in hand biochemical, kinetic and structural studies became possible.

1.1.2. AC structure

The following chapter will focus on the complex structure of mammalian transmembrane ACs (Krupinski *et al.*, 1989). They consist of:

- a short variable cytosolic N-terminus, that is highly divergent and plays an important role in regulation (e.g. phosphorylation by PKCδ to inhibit AC 6; stimulation of ACs 5/6 by $G_{\beta\gamma}$),
- two hydrophobic transmembrane domains (M1 and M2) and
- two cytosolic domains, namely C1 and C2, that form the catalytic center (~ 40 kDa).

The membrane spans are not important for catalysis, but they do play a role for a close location of C1 and C2. The N-terminal and C-terminal part of C1 and C2, referred to as C1b and C2b, show the highest diversity among the different isoforms and also by comparing different species. Within both cytosolic domains are ~ 230 amino acids (AA) present that are responsible for catalysis. They are named C1a and C2a domains and their sequence is roughly 40% identical. The sequence homology of C1a and C2a of ACs 1, 2 and 5 is quite high. Therefore, even heterologous combinations of the two intracellular domains from different species and different isoforms can form a stable and active complex with each other. This was used ~ 13 years ago to characterize the catalytic domains by purification of C1a domain of AC 5 and C2a domain of AC 2 and subsequent analysis of the crystal structure of these two soluble domains (Tesmer *et al.*, 1997). Since then, this structure is used as the general functional model for mACs (Figure 1 B, Protein Data Bank 1AZS).

Looking at the structure we can see that the interface between the two domains is pseudosymmetrical. The crystal structure was obtained by cocrystallization with a water-soluble FS analog, 7-acetyl-7-[O-(N-methyl-piperazino)-γ-butyryl)]-forskolin (MP-FS). Figure 1 B shows a well-defined FS binding site in the cleft between C1 and C2. This pocket is structurally related to the active site that is on the opposite site of the catalytic cleft. Due to the fact that AC 9 has a different amino acid (AA) residue in this part of the binding site in comparison to ACs 1-8 (Y1082), it is not stimulated by FS, but FS-sensitivity can be restored by mutagenesis (Yan *et al.*, 1998). The basic principle for the existence of the FS binding site is discussed in literature (Tesmer *et al.*, 1997), but the search for a physiological FS analog

that might regulate ACs through this binding site was so far unsuccessful. One study detected a FS-like molecule in renal cysts of 15 patients suffering of polycystic kidney disease, but they could not clarify whether this molecule is physiologically relevant or might be derived from widely used dietary supplements that contain FS (Putnam *et al.*, 2007).

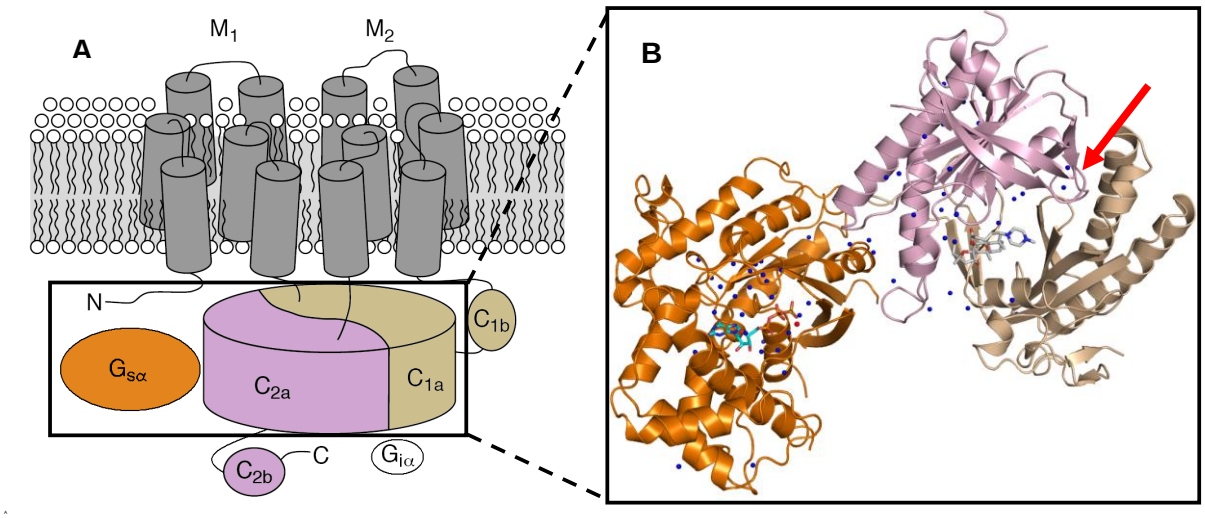

Figure 1. Scheme of mAC and crystal structure of catalytic domains in complex with $G_{s\alpha}$ and FS. On the left side (A) the protein is depicted with the transmembrane domains M1 and M2 and the cytosolic domains C1 and C2. The important interaction sites with physiological regulating G protein $G_{s\alpha}$ (*orange*) and $G_{i\alpha}$ (*white*) are also indicated. The right side (B) shows the first published crystal structure of the catalytic center of the protein (PDB 1AZS) (Tesmer *et al.*, 1997). C1a and C2a are colored *wheat* and *lightpink*, respectively. They carry a water-soluble FS analog (MP-FS) in their catalytic cleft (C-atoms *grey*, N-atoms *blue*, O-atoms *red*). $G_{s\alpha}$ is colored *orange* and carries GTPγS (C-atoms *cyan*, N-atoms *blue*, P-atoms *orange*, O-atoms *red*, S-atom *yellow)*. *Darkblue* spheres are water molecules and one *red* sphere shows one Mg^{2+} ion, interacting with GTPγS. The red arrow indicates the ATP binding site, responsible for catalysis.

Binding of the P-site inhibitor 2'-deoxy-3'-adenosine monophosphate and pyrophosphate into $G_{s\alpha}$/MP-FS – stimulated VC1/IIC2 complex was used to identify the active site of mACs and the structural principles for catalysis as well as P-site inhibition (Tesmer *et al.*, 1997; Dessauer *et al.*, 1999). The substrate-binding site showed that divalent cations such as Mn^{2+}, Ca^{2+} and Mg^{2+} bind into the catalytic site by a two metal ion mechanism. Mg^{2+} and Mn^{2+} stimulate ACs because they catalyze phosphoryl transfer in the active site, mainly by binding to the 'B' metal site. It is speculated that Ca^{2+} tends to favor the 'A' metal site thus leading to AC inhibition. Besides the substrate-binding site there are numerous other interaction sites. At the opposite site of the catalytic site at the C2 domain is a cleft between α2' and α3' helices that interacts with $G_{s\alpha}$. It is still discussed how $G_{i\alpha}$ interacts with the catalytic domains. Unfortunately no crystal structure of catalytic domains with $G_{i\alpha}$ could be achieved until now, but mutagenesis studies indicated that a cleft in the C1 domain that is on the opposite site of

the $G_{s\alpha}$ binding site could be the interaction site (Dessauer *et al.*, 1998) (Figure 1 A). Possibly, $G_{i\alpha}$ stabilizes the open inactive conformation of the catalytic domains.

It is quite interesting that C1 and C2 have relatively weak affinity for each other under basal conditions, but as soon as either FS or $G_{s\alpha}$ are present, basal activity can be stimulated by more than 100-fold and affinity for these two domains is increased even more, when both proteins are present together (Whisnant *et al.*, 1996). Unfortunately, it was not yet possible to crystallize mACs with only one of the two activators. But it may be possible that synergism of FS and $G_{s\alpha}$ is initiated by a slight rotation of the two domains that binds ATP more tightly, therefore, increasing catalytic activity.

The characterization of a more physiological homologous C1 and C2 crystal structure of mAC has not been achieved yet, mainly because of poor protein expression or due to instability of the expressed protein. There is also a crystal structure of the IIC2 homodimer available and this structure is very similar to the heterodimer except that it can bind two FS molecules (Zhang *et al.*, 1997). Primary sequence and regulation of mammalian soluble AC is significantly different to transmembrane ACs, but sAC have the same overall structure and employ the same two-metal ion mechanism for catalysis, as identified with the sAC homolog CyaC (Steegborn *et al.*, 2005).

1.2. Heart function

Many cellular mechanisms that are yet not totally elucidated are important for heart function. However, the focus will be on one main intracellular signal transduction in the myocardium, induced by the sympathetic nervous system (Figure 2). As soon as the body increases the oxygen demand due to psychological or physiological stress, the sympathetic nervous system is activated, the level of norepinephrine is increased and the contraction and cardiac output is elevated. On the cellular basis, norepinephrine is released from presynaptic vesicles after stimulation of sympathetic nerves and binds to membranous GPCRs, namely β_1- and β_2-adrenoceptors (β-AR) (Bristow *et al.*, 1990). Although β_1-ARs predominate over the other subtype in myocardium, β_2-ARs appear to couple more efficiently to ACs. The importance of the third β-AR (β_3-AR) in heart still remains to be elucidated (Lohse *et al.*, 2003). Agonists of β-AR turn on the GPCR pathway by activation of the stimulatory G protein that dissociates in $G_{s\alpha}$ bound to GTP and $G_{\beta\gamma}$. It has to be mentioned that β_2-AR signaling can also inhibit AC *via* inhibitory $G_{i\alpha}$ (El-Armouche *et al.*, 2003; Förster *et al.*, 2003). The $G_{s\alpha}$-subunit couples to AC and increases the production of second messenger cAMP. This intracellular messenger then activates cAMP-dependent protein kinase (PKA) that increases intracellular Ca^{2+} levels *via* phosphorylation of L-type Ca^{2+} channels and thus contraction of myocytes takes place. Phosphorylation of Ca^{2+} channels increases open probability of the

channels detected by an increase in Ca^{2+} influx ($I_{Ca,L}$) from the extracellular space into the cytosol (Reuter, 1983). The increase in intracellular Ca^{2+} further activates Ca^{2+} release from the sarcoplasmatic reticulum (SR), thereby mediating the positive inotropic effect. Relaxation of cardiomyocytes is also achieved *via* cAMP-dependent phosphorylation of phospholamban (PLB), a Ca^{2+} transporter in the SR. Activation of phospholamban initiates the Ca^{2+} reuptake into the SR. Another cAMP-dependent mechanism that further aids in cardiomyocyte relaxation is the phosphorylation of troponin I, modulating myofilament Ca^{2+}-sensitivity.

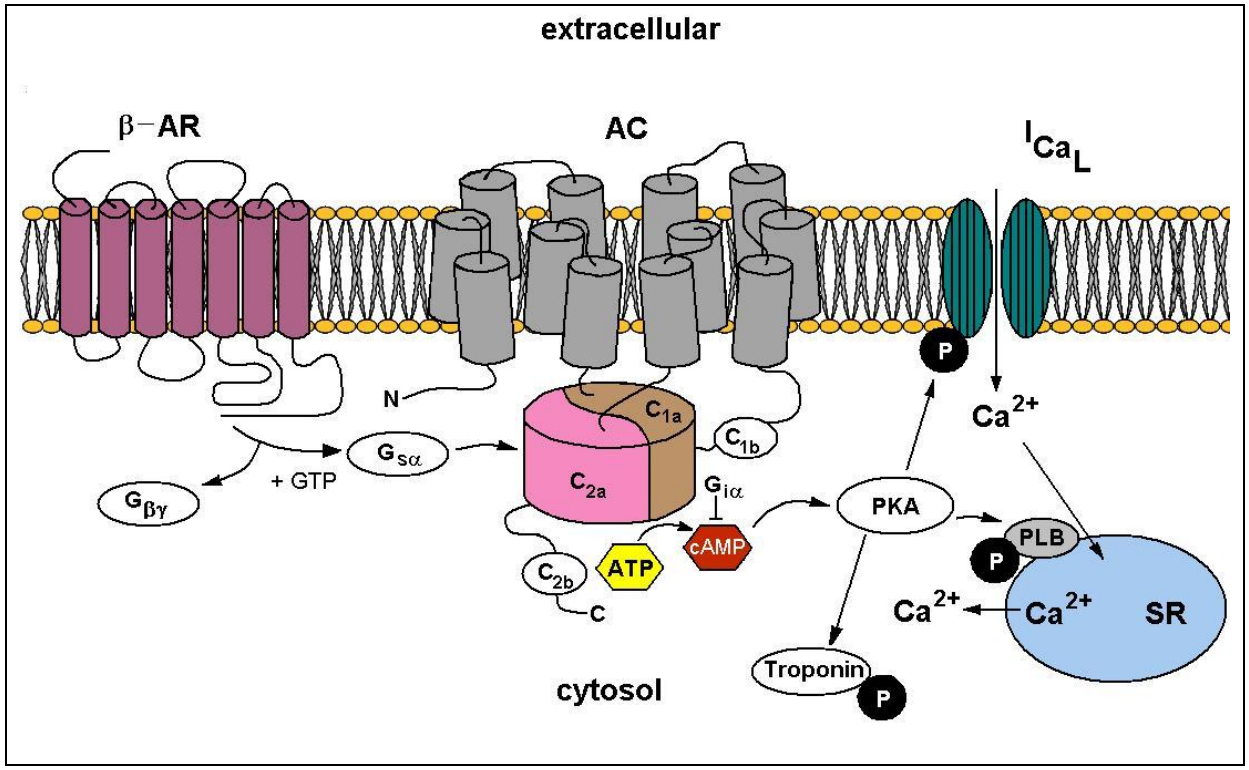

Figure 2. "Classical" cardiac β-AR signaling. The common pathway activates AC *via* $G_{s\alpha}$, increasing cAMP levels. *Via* activation of protein kinase A (PKA), several proteins are phosphorylated that regulate the calcium homeostasis of the cell and thereby influencing cardiac contractile behavior. PKA phosphorylates not only L-type calcium channels ($I_{Ca,L}$), phospholamban (PLB) and troponin, but also ryanodine receptors, myosin binding protein and protein phosphatase inhibitors (not shown here) (Lohse *et al.*, 2003).

1.2.1. Voltage-dependent calcium channels

Voltage-dependent Ca^{2+} channels (VDCC) are necessary for the function of nerve and muscle cells. Ca^{2+} channels are membranous heteromultimeric protein complexes that are selective for Ca^{2+} and regulate Ca^{2+} permeability by differences in membrane potential and Ca^{2+} gradient between the extracellular space and the cytosol. There are a variety of Ca^{2+} channels. The most important group consists of VDCC that are activated by depolarization of the cell membrane (Jones, 1998). According to their current properties, VDCC are subdivided into high voltage-activated and low voltage-activated channels (Ertel *et al.*, 2000). A very important high voltage-activated Ca^{2+} channel is the L-type (long-lasting) Ca^{2+} channel that exhibits high conductance for Ca^{2+} and Ba^{2+} ions (Mikami *et al.*, 1989). In heart, it

consists of four different subunits, a pore forming α_1-domain, a modulating intracellular β-domain, and a $\alpha_2\delta$-domain, that couples the extracellular α_2-subunit *via* transmembrane crossing δ-subunit to the pore forming domain. The membrane-traversing γ-subunit is not expressed in heart (Randall and Benham, 1999; Treinys and Jurevicius, 2008). The α_1-subunit is also functionally active when the other domains which stabilize and regulate the Ca^{2+} channel are not present. Regulation of the Ca^{2+} channel pore is mainly dependent on phosphorylation by PKA, but which phosphorylation site brings about activation could not be unequivocally established yet. C-terminal serine residues of the α_1- and β_2-subunit are thought to influence the activity of the whole channel (Dai *et al.*, 2009). However, many other factors such as divalent cations and cytoplasmic factors affect channel activity (Yamaoka and Kameyama, 2003). Alterations in L-type Ca^{2+} channel function and expression play a role in the development of hypertrophy and heart failure (Beetz *et al.*, 2009).

1.3. Pharmacotherapy of chronic heart failure

Cardiac insufficiency develops when the heart is unable to supply the organs with enough blood to maintain the oxygen demand of the organism. Patients suffer from a decreased exercise tolerance, dyspnea and fatigue, caused by changes in preload, afterload, heart contractility or heart rate. Mostly, the patients also complain about abdominal or leg swelling due to fluid retention. In Germany chronic heart failure is responsible for high health expenses, because it is one of the main reasons for hospitalization (Neumann *et al.*, 2009). Cardiac insufficiency is a very serious and complex disease. Many pathophysiological mechanisms are responsible for the development of heart failure, such as myocardial hypertrophy, altered Ca^{2+} homeostasis and the activation of the sympathetic nervous system. The heart tries to compensate the decrease in oxygen supply by activation of the sympathetic nervous system, but this can be very harmful for the cardiovascular system. Patients suffering of cardiac insufficiency show very high plasma norepinephrine concentrations that correlate with the severity of the disease (Thomas and Marks, 1978; Cohn *et al.*, 1984). Due to excessive catecholamine stimulation, the signal transduction is desensitized. If the receptor is constantly activated by β-AR agonists, phosphorylation of the receptor by β-adrenoceptor and cAMP-dependent protein kinases leads to internalization of the receptor, because β-arrestin binds to the phosphorylated receptor. This cytosolic protein initiates that the receptor is embedded in vesicles and removed from the cell membrane. Prolonged stimulation with catecholamines can lead to proteolysis of the receptor, so called down-regulation, together with a minimization of β-AR m-RNA (Engelhardt *et al.*, 1996; Lohse *et al.*, 1996). The positive inotropic effect of β-AR agonists is diminished due to down-regulation at the receptor level, assessed by decreased isoprenalin effects. In conclusion,

decreased β-AR density, especially of β_1-AR is experimentally demonstrated and is correlated with the severity of heart failure.

A standard therapy for chronic heart failure is, therefore, the treatment with β-AR blockers that antagonize the effects of constant stimulation of the sympathetic nervous system, either by blocking detrimental β_1-AR effects or by resensitizing the β-AR system (Lohse *et al.*, 2003). Especially cardioselective β_1-blockers, such as metoprolol or bisoprolol, as well as the β- and α_1-AR blocker carvedilol are useful drugs for the therapy of chronic heart failure. Many studies already demonstrated that β-blockers are the most important advance in heart failure therapy by decreasing severity of symptoms, increasing quality of life and reduction of mortality (Lechat *et al.*, 1998; Lohse *et al.*, 2003).

Medication of heart insufficiency depends on the clinical stage of the disease. The "ACCF/AHA guidelines for the diagnosis and management of heart failure in adults" (American College of Cardiology Foundation/American Heart Association) assist cardiologists in clinical decision making (Jessup *et al.*, 2009). In principle, chronic heart failure is subdivided into 4 clinical stages that determine the complex therapeutic approach. In addition to β-AR antagonists, angiotensin-converting enzyme inhibitors, angiotensin II receptor blockers, diuretics and digitalis are used as standard medication. Furthermore, the guidelines discuss additional medical approaches, such as vasodilators or aldosterone antagonists (Jessup *et al.*, 2009).

1.4. Adenylyl cyclase 5 in heart

ACs play a major role in the development of heart failure because chronic activation of cAMP signaling, induced by overexpression of β-AR, $G_{s\alpha}$ or PKA, results in cardiomyopathy (Iwase *et al.*, 1997; Engelhardt *et al.*, 1999; Antos *et al.*, 2001). The heart expresses all AC isoforms, except AC 8 (Defer *et al.*, 2000). AC 1 is only present in sino-atrial node. ACs 5 and 6 are predominant and very closely related in terms of regulation (only PKC regulation quite different). At birth both isoforms are expressed equally and are most abundant in neonatal heart, but in adult heart AC 5 is dominant (Tobise *et al.*, 1994). Due to preparation of a specific AC 5 mouse monoclonal antibody it could be detected that AC 5 is increased in heart with left ventricular hypertrophy in response to pathophysiological stress (Hu *et al.*, 2009). To understand the physiological role of both isoforms in heart and to identify if the isoforms couple to various signaling pathways, KO and overexpression studies were carried out (Okumura *et al.*, 2003a; Tang *et al.*, 2006; Tang *et al.*, 2008).

1.4.1. AC 5 knockout mice

No compensatory increase in expression of other AC isoforms is detected in AC $5^{-/-}$ mice. Especially the remaining AC 6 does not adopt the missing AC 5 activity. Basal AC activity is

decreased by ~ 35%. Stimulated AC activity with isoproterenol, FS and GTPγS was also diminished by 27-40%, indicating that AC 5 contributes to overall AC activity in a quite high amount, i.e. ~ 30-40% (Okumura *et al.*, 2003a). Interestingly, there was a total loss of carbachol-induced AC inhibition in comparison to WT mice. Carbachol is a muscarinic agonist that inhibits AC activity *via* $G_{i\alpha}$. Parasympathetic regulation seems to be mediated *via* AC 5 and could be the reason for an increased basal heart rate in AC $5^{-/-}$ mice. No change in basal cardiac function was detected, but isoproterenol-stimulated left ventricular ejection fraction (LVEF) was significantly reduced. Electrophysiological measurements showed no differences in L-type Ca^{2+} current, but isoproterenol stimulation was significantly reduced and Ca^{2+} mediated inhibition was annihilated. Expression of G proteins and β-AR was not altered. Another KO model showed increased basal contraction of perfused hearts and decreased sensitivity to β_1 agonists, but also a significant reduction of $G_{s\alpha}$ expression (Tang *et al.*, 2006).

The influence of AC 5 gene deletion in the development of heart failure was of considerable interest. Pressure overload by aortic banding was used as heart failure model. The aorta thoracalis was constricted to generate an increased pressure in the left ventricle. In contrast to WT mice, left ventricular function was not altered in KO mice. AC $5^{-/-}$ mice are protected against heart failure under stress conditions. Furthermore myocardial apoptosis is reduced in cardiomyocytes (Okumura *et al.*, 2003b). Gene deletion of AC 5 protects against oxidative stress. The KO mice have an increased life span (~ 30%) and age-induced cardiac myopathy is significantly reduced (Yan *et al.*, 2007). However, it should be mentioned that beside of cardiac effects, AC 5 is also highly expressed in striatum and there it plays a role in the dopaminergic system. AC $5^{-/-}$ mice develop Parkinson-like symptoms, such as abnormal coordination and bradykinesia that can be partially compensated by selective D_1 and D_2 agonists that stimulate remaining AC isoforms (Iwamoto *et al.*, 2003).

Studies on transgenic mice with deletion of AC 6 detected no change in basal AC activity. However, under stimulated conditions AC 5 is decreased *via* proteosomal degradation, leading to a reduced PKA activity and stimulated left ventricular contractile function (Tang *et al.*, 2008).

1.4.2. AC 5 overexpression

An increased AC 5 expression in mice led to increased basal cAMP levels, elevated PKA activity and phospholamban phosphorylation. This increase in basal AC activity influences basal cardiac function, because heart rate is increased in transgenic mice. However, cardiac β-AR signaling is not altered, because β-AR agonists did neither influence L-type Ca^{2+} channel activity in isolated cardiomyocytes, nor was there any change in heart rate and contractility after agonist infusion (Tepe *et al.*, 1999). Interestingly, AC 5 overexpression significantly improved β-AR dysfunction in a hypertrophic mouse model (Tepe and Liggett,

1999). Overexpression of $G_{\alpha q}$ in cardiomyocytes resulted in hypertrophy and decreased cardiac contractility in vivo, due to a lack of basal as well as stimulated AC activity and an almost 50% decrease in AC 5 expression. As soon as AC 5 expression is restored in mice that overexpress $G_{\alpha q}$ and AC 5, dysfunction of β-AR signaling and cardiac contractility are compensated. The same happened when AC 6 was overexpressed with $G_{\alpha q}$ (Roth *et al.*, 1999). AC 6 overexpression in mice did not influence basal heart rate and contraction, but increased cardiac response to β-adrenergic stimulation (Gao *et al.*, 1999).

In order to summarize all the studies that were performed to characterize ACs 5 and 6 in heart, it has to be stated that production and utility of cAMP is clearly not one simple mechanism: under stress conditions cAMP might be harmful (as illustrated in the AC $5^{-/-}$ model), but it can be quite beneficial when other factors are altered (overexpression of ACs 5 or 6 in $G_{\alpha q}$ transgenic mice). Overexpression or gene deletion of AC 6 did not provoke any pathophysiological changes. In contrast, AC 6 is often stated to be beneficial in heart failure therapy (Phan *et al.*, 2007).

1.5. AC inhibition

AC regulation *via* stimulation with AC activators or inhibition with antagonists could have many pharmacotherapeutic applications. Especially, the tissue-specific distribution of some isoforms, to mention ACs 1, 5, 7 and sAC, may be used to develop drugs against Alzheimer's disease, heart failure, alcoholism, drug abuse and male fertility (Pierre *et al.*, 2009).

Inhibitors of AC 5 may be useful drugs for the therapy of heart failure and could increase longevity (Chester and Watts, 2007; Okumura *et al.*, 2009). Inhibition of AC 1 *via* specific AC 1 inhibitors could be used for neuroprotection. Deletion of AC 1 in mice significantly attenuated neuronal death induced by glutamate in primary cultures of cortical neurons (Wang *et al.*, 2007). Prevention of excitotoxicity *via* inhibition of AC 1 could be used for the treatment of stroke and neurodegenerative diseases (Watts, 2007).

1.5.1. MANT nucleotides

This group of potent AC inhibitors are nucleotides that possess a small fluorophore, N-methylanthraniloyl (MANT), bound to the 2' or 3' O-ribosyl group of the nucleotides (Jameson and Eccleston, 1997). Therefore, they can be used in fluorescence studies to detect enzyme kinetics. Various MANT nucleotides are available as fluorescent probes. Figure 3 shows the structure of the MANT nucleotides and gives an overview about structural changes that were applied to improve stability. The fluorophore possesses an additional advantage; it increases the lipophilicity, and thus could facilitate the passage through the cell membrane.

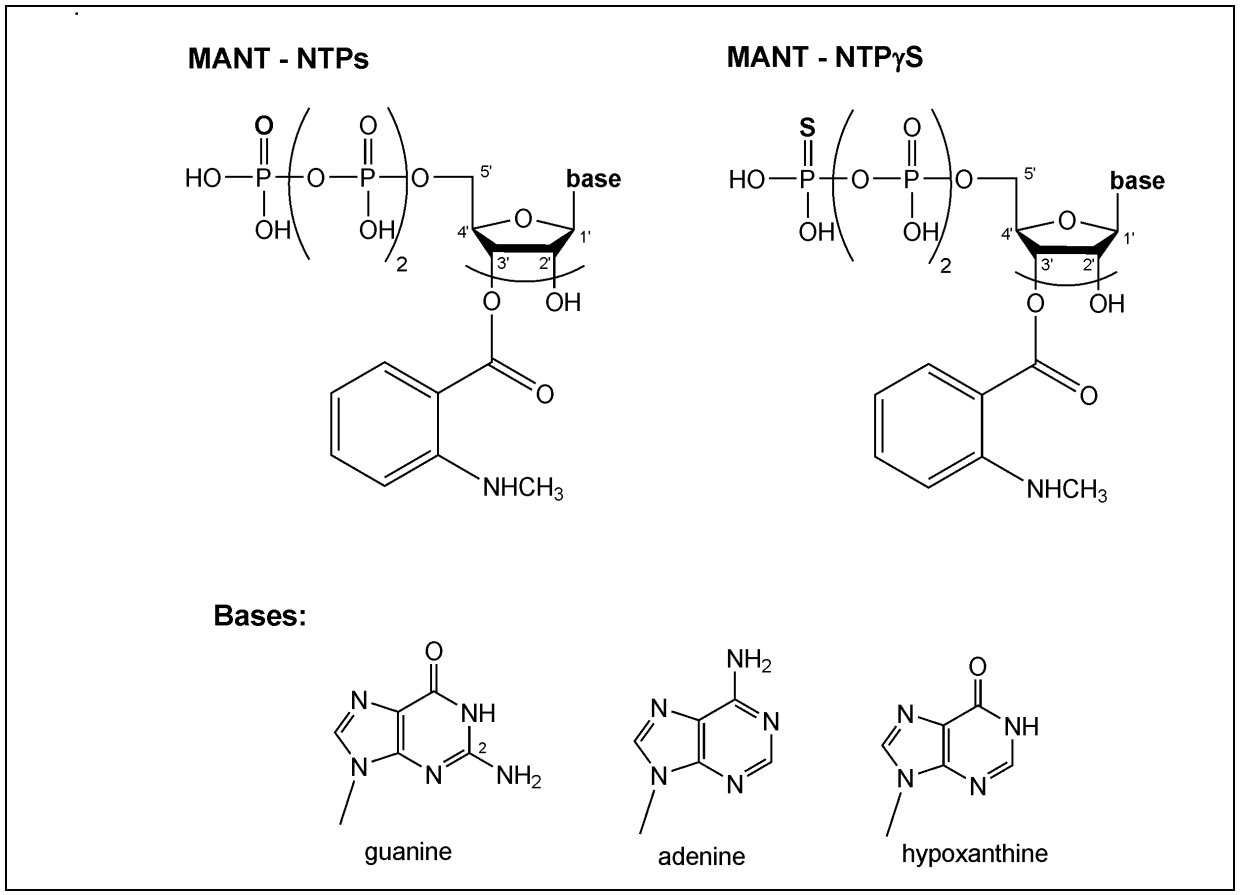

Figure 3. Structure of MANT nucleoside 5'-triphosphates (NTPs) and MANT nucleoside 5'-[γ-thio]-triphosphate (NTPγS). Represented are the MANT nucleotides used for crystallography and patch-clamp experiments, MANT-ITP, MANT-GTP, MANT-ITPγS, MANT-GTPγS and MANT-ATP. The MANT-group isomerizes between the 2' and 3'-O-ribosyl function.

The following data suggest that MANT nucleotides are very potent AC inhibitors and that they express their inhibitory effect by competition for the ATP-binding site using Lineweaver-Burk analysis (Gille and Seifert, 2003b; Gille *et al.*, 2004).

In the search for a test system to study kinetic interaction of receptor/G protein coupling, these fluorescent nucleotides were examined to establish a fluorescent high-throughput screening method. Until now, most studies are performed with radiolabeled nucleotides, such as [^{35}S]GTPγS, [α-^{32}P]GTP azidoanilide or [γ-^{32}P]GTP (Gierschik *et al.*, 1994; Laugwitz *et al.*, 1994). MANT-GTPγS and MANT-GppNHp were already tested on purified G proteins and showed relatively high affinity and changes in fluorescence upon G protein binding (Remmers and Neubig, 1996; Remmers, 1998). Gille and Seifert tested MANT-GTPγS and MANT-GppNHP for their affinity to recombinant $G_{s\alpha}/G_{i\alpha}$ fusion proteins, expressed in a 1:1 ratio with the formyl peptide receptor or the β_2-adrenergic receptor (Gille and Seifert, 2003a). MANT-GTPγS had a 30- to 300-fold lower affinity to $G_{s\alpha}/G_{i\alpha}$ fusion proteins compared to GTPγS. The K_i values of both MANT nucleotides for the different G_α fusion proteins were

250 – 1,120 nM for MANT-GTPγS and 1,200 – 5,700 nM for MANT-GppNHp, indicating that MANT nucleotides can bind and also inhibit G proteins, but very surprisingly with much lower affinity than mACs (Gille and Seifert, 2003b; Gille and Seifert, 2003a).

To ensure that MANT-GTPγS inhibits GTPγS-stimulated AC in the $G_{s\alpha}$-membrane preparation, AC activity assays on $G_{s\alpha}$-deficient S49*cyc*$^-$ lymphoma cell membranes were conducted (Gille and Seifert, 2003b). This $G_{i\alpha}$-model system showed AC inhibition under Mg^{2+} conditions when GTPγS or GppNHp were applied. But under Mn^{2+} conditions $G_{i\alpha}$ is blocked and GTPγS or GppNHp cannot activate the G protein. Nevertheless, MANT-GTPγS and MANT-GppNHp still showed an inhibitory effect on AC activity under Mn^{2+} conditions, with K_i values of 53 nM and 160 nM, respectively. The production of cAMP was reduced by direct inhibition of AC and not *via* $G_{i\alpha}$.

1.5.1.1. AC inhibition by MANT nucleotides

During the last years, many other MANT nucleotides were tested for their inhibitory potency on mACs.

MANT nucleotide	AC 1	AC 2	AC 5	AC 6	Cardiac AC	VC1/IIC2 + FS + $G_{s\alpha}$-GTPγS
MANT-ITP	3* 24*	14* 65*	1* 13*	3* n.d.	4* 24*	0.7 ± 0.1 n.d.
MANT-GTP	90$^+$ 1,500*	620$^+$ 3,700*	55$^+$ 760*	91$^+$ n.d.	21* 780*	18 ± 6 n.d.
MANT-ITPγS	41$^+$ 300*	120$^+$ 450*	31$^+$ 150*	43$^+$ n.d.	8* 26*	19 ± 3.3 n.d.
MANT-GTPγS	62$^+$ 990*	360$^+$ 1,800*	35$^+$ 550*	48$^+$ n.d.	23* 340*	24 ± 4.1 n.d.
MANT-ATP	210$^+$ 3,200*	850$^+$ 5,700*	200$^+$ 2,000*	280$^+$ n.d.	64* 2,000*	16 ± 6.4 n.d.
MANT-ATPγS	160* 1,400*	380* 2,300*	77* 1,100*	72* n.d.	67* 770*	n.d. n.d.
MANT-XTP	1,100 ± 100 n.d.	3,000 ± 200 n.d.	1,300 ± 400 n.d.	n.d. n.d.	1,300 ± 400 n.d.	1,200 ± 370 n.d.

Table 2. Inhibition of mAC activity/catalytic activity by MANT nucleotides. AC activity assays were conducted with 5 mM $MnCl_2$ or $MgCl_2$ and 100 µM FS. The catalytic activity of VC1/IIC2 was measured with 10 mM divalent cation and 100 µM FS. K_i values were calculated using obtained IC_{50} and K_m values (Cheng-Prusoff equation). Standard deviations (SD) were generally smaller than 20% of the means. Mean values ± SD are integrated using 4-5 independent duplicate experiments of at least 2 different membrane preparations or protein batches. Values taken from (Göttle *et al.*, 2009) are labeled with (*) and from (Gille *et al.*, 2004) are labeled with ($^+$). The other values are taken from (Geduhn, 2009). Abbreviation: n.d. = not done

Table 2 gives an overview about the K_i values (in nM) of different MANT nucleotides under Mn^{2+} and Mg^{2+} conditions on recombinant ACs 1, 2, 5 and 6 in Sf9 insect cell membrane preparations, on catalytic domains C1/C2 and on cardiac AC membrane preparations. MANT-ITP turned out to be the most potent AC 1/5 inhibitor known so far (K_i ~ 1-3 nM) and it also had the highest inhibitory effect on purified catalytic AC subunits C1/C2 (K_i ~ 0.7 nM). Furthermore, MANT nucleotides inhibit ACs 1 and 5 with a much higher potency than AC 2, and this is explained by differences in the binding pocket that change affinity, because two amino acid residues are different. Therefore, it is possible that changes in the MANT nucleotide structure, for instance in the MANT-group, may influence the selectivity profile of these substances for a specific AC isoform.

1.5.1.2. MANT nucleotides as fluorescent probes

Due to the fact that MANT nucleotides are fluorescent, we have a good tool in hand to study the kinetics of AC/nucleotide interaction. With the help of the purified catalytic subunits VC1 and IIC2 we could study the molecular interactions of MANT nucleotides with the protein *via* fluorescence analysis. MANT nucleotides interact directly with the two protein domains thereby changing fluorescence properties (Figure 4). MANT nucleotides show a direct emission peak at ~ 450 nm, when excited at 350 nm (blue line). This fluorescence is increased when the MANT-group of the nucleotide gets into a more hydrophobic environment and the emission peak shows a "blue-shift" to ~ 420 nm. Furthermore the nucleotide can trigger a fluorescence resonance energy transfer (FRET) from W1020 of IIC2 to the MANT-group, as soon as the nucleotide comes into closer distance to the binding site (Mou *et al.*, 2006). The dashed black lines in Figure 4 show endogenous fluorescence of C1/C2 tryptophan and tyrosine residues excited at 280 nm, when no MANT nucleotide is present. As soon as C1 and C2 are mixed with MANT nucleotide a FRET at ~ 420 nm in the emission spectra (λ_{em} = 300 - 500 nm) is detected, that increases by addition of FS, because FS promotes C1/C2 assembly. Several MANT nucleotides were tested using fluorescence spectroscopy, but only MANT-ITP showed a very strong increase of basal FRET and direct fluorescence after addition of C1 and C2 and without FS (Figure 4 C and D). The application of FS afterwards had only minor effects on FRET and direct fluorescence. It seems that MANT-ITP already promoted the catalytic subunit assembly without the presence of FS. Compared to MANT-ITP, MANT-GTP showed a smaller effect on basal FRET and direct fluorescence (Figure 4 A and D). In contrast, MANT-XTP had almost no influence on FRET and direct fluorescence (Figure 4 E and F).

Finally, it is important to mention, that MANT nucleotides are racemates, so the tested nucleotides are a mixture of two isomers. For comparison of the potency of pure isomers, we

need the pure 2'- or 3'-deoxy compounds, but until now only some are commercially available, and the synthesis is very difficult.

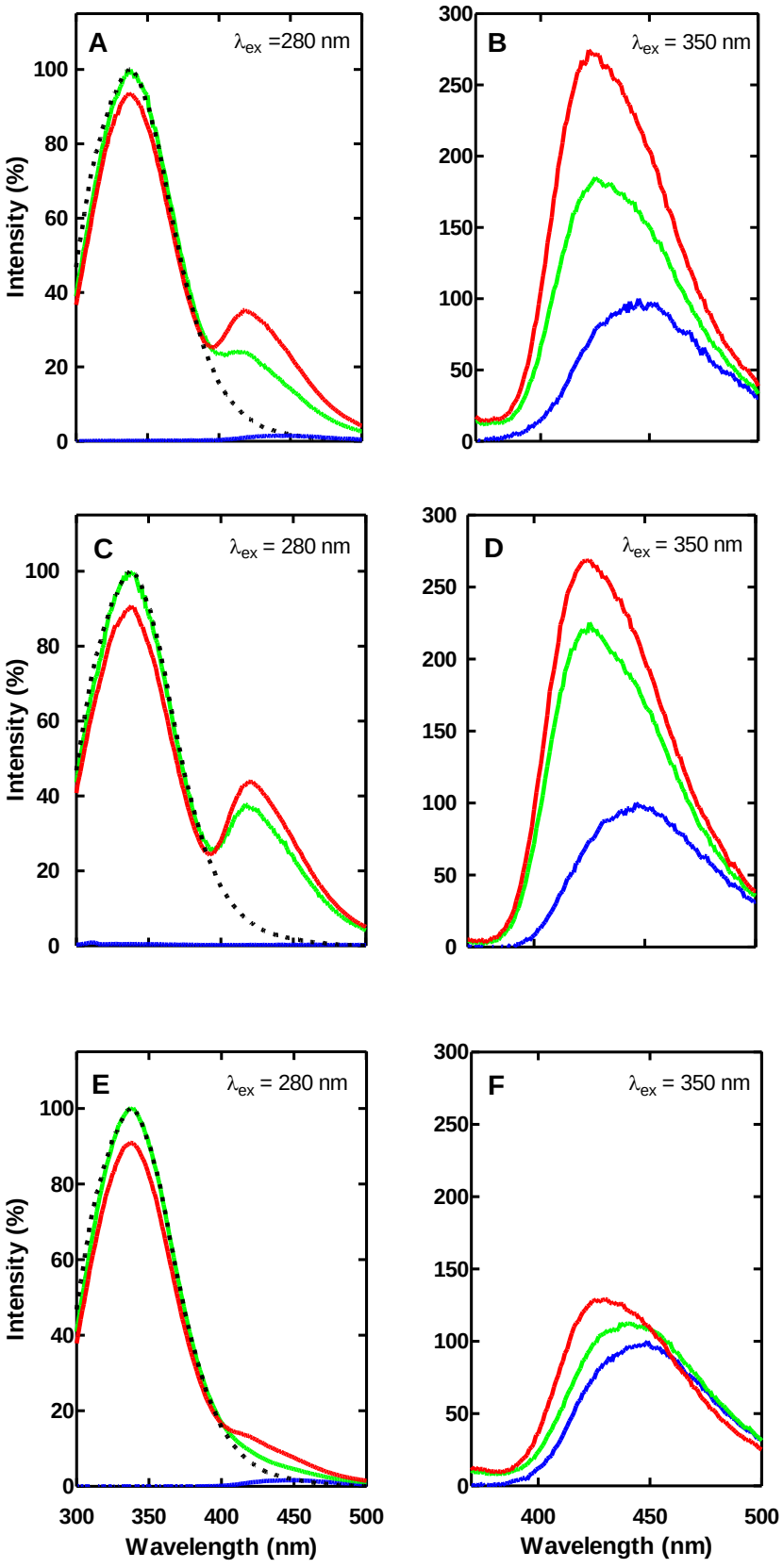

Figure 4. Fluorescence emission spectra of MANT-GTP (A/B), MANT-ITP (C/D) and MANT-XTP (E/F).

Emission at λ_{ex} = 280 nm (λ_{em} = 300 - 500 nm) and at λ_{ex} = 350 nm (λ_{em} = 370 - 500 nm) are represented. Experiments were conducted at 25°C in the presence of MANT nucleotides (1 µM), VC1 (5 µM) and IIC2 (25 µM) without and with FS (100 µM). Reactions mixtures contained a buffer of 100 mM KCl, 10 mM $MnCl_2$ and 25 mM HEPES/NaOH, pH 7.4. Three independent experiments with at least two different batches of VC1/IIC2 were performed. Measurements were accomplished by Cibele Pinto and Roland Seifert while working at the University of Kansas, Lawrence, KS. Fluorescence intensities are shown in %.

1.5.2. Other AC inhibitors

The classical AC inhibitors are P-site inhibitors, adenosine analogs that bind to the ATP binding site and block pyrophosphate release (Johnson *et al.*, 1989; Desaubry *et al.*, 1996). Therefore they inhibit AC only in the presence of pyrophosphate. The most potent P-site inhibitors consist of 3'-mono- or polyphosphates and 2',5'-dideoxyribose moieties. P-site inhibitors tested on purified AC from bovine and rat brain showed quite high potency in the nM range ($IC_{50} \sim 10$ nM) and no effect on other effector proteins of the cAMP signal cascade, such as PKA and phosphodiesterase (Desaubry and Johnson, 1998). However, there is one drawback; these substances are not very isoform-specific (Johnson *et al.*, 1997). Another class of compounds that also belongs to the group of P-site inhibitors, including 1*R*,4*R*-3-(6-aminopurin-9-yl)-cyclopentane-carboxylic acid hydroxyamide, selectively inhibited AC 5 in comparison to AC 2 and 3, but the IC_{50} values were in the µM range. The above-mentioned compound showed a reduction of myocardial apoptosis under excessive β-AR stimulation with isoprenalin (Iwatsubo *et al.*, 2004).

One group of competitive inhibitors are dideoxy nucleotides, such as β-L-2',3'-dideoxy adenosine 5'-triphosphate, but nothing is published about their isoform-selectivity (Shoshani *et al.*, 1999). Therefore, MANT nucleotides are a good starting point for the development of pharmacotherapeutics, because they show a competitive enzyme inhibition, a high potency and partial isoform-selectivity (Gille *et al.*, 2004; Mou *et al.*, 2005).

1.6. Aims of the project

1.6.1. Purification of C1/C2 and crystallization

MANT nucleotides are potent inhibitors of mACs that bind to the catalytic center of the enzyme and exhibit K_i values in the nanomolar range. We were particularly interested to understand the molecular mode of AC inhibition by different MANT nucleotides. Previous studies showed that the catalytic site of AC is quite flexible and binds a diverse range of nucleotides (Mou *et al.*, 2006; Suryanarayana *et al.*, 2009). The catalytic site of C1/C2 can accommodate large chemical alterations of nucleotide inhibitors. Furthermore, the MANT nucleotides differ from each other in their fluorescence properties. Large differences in direct fluorescence and FRET were detected when the MANT nucleotides were mixed with C1/C2 and stimulated by FS. These data indicate that MANT nucleotides can have different localization in the catalytic site of the protein and that there are alternate binding modes possible. MANT-ITP is the most potent mAC inhibitor known so far (Göttle *et al.*, 2009).

However, the reason for this high affinity binding on molecular basis is still unknown. The first aim of this study was to elucidate the structural basis for the interaction of MANT-ITP with mAC. In order to achieve this aim, X-ray crystallography was used. The catalytic domains C1a and C2a of mAC were purified and activated by $G_{s\alpha}$-GTPγS and FS. The crystal structure of this complex, bound to MANT-ITP:Mn^{2+}, was determined and compared to the published crystal structure of mAC with MANT-GTP. Both nucleotides consist of a purine base and have very similar structures. MANT-ITP just misses an NH_2 group at C2 of the guanine ring. Until now it was expected that the base substitution has relative little impact on nucleotide-affinity, because purine as well as pyrimidine bases are well tolerated and show high affinity (Mou *et al.*, 2006). However, the deletion of the NH_2 group increased potency of MANT-ITP for mACs by up to 50-fold compared to MANT-GTP and furthermore C1/C2 assembly assessed by fluorescence spectroscopy was quite different for both ligands. Therefore, we wished to understand the binding mode of MANT-ITP in more detail and to identify the role of the different nucleotide substituents (base, phosphate chain, MANT-group) for nucleotide affinity. Possibly, the base plays a much more important role on overall binding affinity as what was expected before.

1.6.2. Effect of MANT nucleotides in intact cells

ACs play a major role in the GPCR signal transduction and due to their specific tissue distribution they could be used as pharmacological targets in the development of therapeutics for various diseases. Due to the fact that chronic heart failure is a common and serious disease and inhibition of AC 5 seems to be cardioprotective, as assessed by AC $5^{-/-}$ mice and inhibition of myocardial apoptosis with P-site inhibitors, development of selective AC 5 inhibitors is a good starting point for future heart failure therapy (Okumura *et al.*, 2003b; Iwatsubo *et al.*, 2004). Inhibitors of AC 5 could reduce apoptotic processes in patients suffering of cardiac insufficiency. With the discovery of MANT nucleotides that are potent and competitive AC inhibitors, we have a good basis for further development of isoform-specific drugs. However, all these compounds have so far only been tested in membrane preparations that recombinantly express a specific AC isoform or they were tested in tissue membrane preparations (Gille *et al.*, 2004; Göttle *et al.*, 2009). As read-out, AC activity was assessed, but not yet the functional consequences of AC inhibition.

Therefore, we studied the effects of MANT nucleotides in intact murine cardiomyocytes. Due to the fact that the signal cascade in cardiomyocytes is predominantly influenced by mAC activity, measurement of L-type Ca^{2+} channel activity can be used to study the effects of mAC inhibitors. One MANT nucleotide, MANT-GTPγS, already showed inhibition of basal and isoprenaline-stimulated voltage-dependent Ca^{2+} channels in ventricular cardiomyocytes of WT mice, indicating that ACs play a major role in cardiac signaling. The inhibitory effect was attenuated when cardiomyocytes of AC $5^{-/-}$ mice were treated with MANT-GTPγS, indicating that this AC inhibitor mainly influences L-type Ca^{2+} currents *via* AC 5 inhibition (Rottländer *et al.*, 2007).

The aim of our current study was to assess if other MANT nucleotides, specifically MANT-ITP, exhibit a larger pharmacological effect in intact cells. Additionally, we used as “negative control” a MANT nucleotide that inhibits AC only with modest potency, MANT-ATP. MANT-GTPγS can also inhibit G proteins with low affinity (Gille and Seifert, 2003a). Therefore, the second aim of our study was to examine the effects of NTPs with higher selectivity for AC relative to G proteins, MANT-ITP and MANT-ATP.

Furthermore, we wanted to assess the stability of the MANT nucleotides in intact cells. Until now, the inhibitory potencies of MANT nucleotides were tested in membrane preparations, using a regenerating system to stabilize the tested nucleotides against enzymatic degradation. We examined the effect of the hydrolysis-sensitive phosphate group relative to the hydrolysis-resistant phosphorothioate group in MANT-NTP *versus* MANT-NTPγS on Ca^{2+} channel regulation by the application of MANT-GTPγS and MANT-ITPγS.

The structure of MANT nucleotides does not allow good absorption of the substances through the cell membrane. Therefore, we used the whole cell patch clamp technique to apply the MANT nucleotides directly into the cell through the pipette solution.

Within this work we wanted to clarify the following questions:

1. Do we see differences in L-type Ca^{2+} current inhibition in correlation to their AC 5 inhibitory effect?
2. How stable are MANT-NTPs that are not protected from degradation by phosphatases in comparison to MANT-NTPγS?
3. What is the incubation time for the MANT nucleotides until they express an inhibitory effect on L-type Ca^{2+} current after administration of the substances through the pipette?

2. Materials and Methods

2.1. Materials

2.1.1. Equipment

Analytical balance	BP211D, Sartorius, Göttingen
	SBC21, Scaltec Instruments, Göttingen
Autoclave (steam sterilizer)	Varioklav 135 S, Thermo Scientific, Erlangen
Cell lysis	Multiquick handblender, 300 Watt, Braun
Centrifuge	Multifuge 3 L-R, Heraeus, Hanau
	Super T-21, Sorvall, Thermo Scientific
Heating plate and stirrer	IKAMAG RCT basic, IKA Werke, Staufen
	MR3001, Heidolph Instruments,Schwabach
Incubator shaker	Innova 43, New Brunswick Scientific
Myocyte isolation:	
Heated circulating bath	F423, Haake, Berlin
Langendorff-setup	University of Cologne, custom-made
Patch-clamp setup:	
Analog-Digital converter	Digidata 1440A, Axon Instruments, Moleculare Devices, Sunnyvale, CA, USA
Battery	Solarpower; energy supply for microscope
Faraday cage	University of Cologne, custom-made
Main amplifier	Axopatch 200A and B, Axon Instruments
Microelectrode amplifier (preamplifier)	CV 201 AU and 203 BU headstage, Axon
Inverse microscope	Nikon Diaphot, Nikon Instruments Europe
Micromanipulator	MO-102/ MHW-103, Narishige, London, UK
pH-meter	Orion EA940, Thermo Fisher Scientific
	pH526, WTW, Weilheim
Pipette puller	P97 pipette puller, Sutter Instruments, USA
Power supply for SDS-PAGE/Western Blot	Power Pac Basic Power Supply, Bio-Rad
Protein purification	Äkta FPLC, GE Healthcare, Freiburg
	BioLogic DuoFlow Systems, Bio-Rad
Ion-exchange columns	Mono S 5/50 GL, GE Healthcare
	HiTrap Q FF 1 ml, GE Healthcare
	Q Sepharose FF, GE Healthcare
Hydroxyapatite column (HAP-column)	CHT Ceramic Hydroxyapatite Type I resin, Bio-Rad

Affinity columns	HisTrap FF 5 ml, GE Healthcare
	Profinity IMAC Ni-charged resin, Bio-Rad
	Talon Superflow resin, BD Biosciences
Size exclusion columns	Superdex 75 10/300, GE Healthcare
	Superdex 200 10/300, GE Healthcare
Sample loading	Superloop 50/150 ml, GE Healthcare
Empty columns	XK columns (e.g. 26/20), GE Healthcare
	University of Regensburg, custom-made
	Glass Econo-column, Bio-Rad
Shaking water bath	Julabo SW-20C, Julabo, Seelbach
Sterilizing oven	Heraeus, Hanau
Ultra centrifuge (rotor and equipment)	TGA 45 (TFT4594), Kontron Instruments
Vertical electrophoresis system	Mini-PROTEAN Tetra Cell, Bio-Rad, München
Western Blot	Mini Trans-Blot Cell, Bio-Rad
X-ray film processor	Cawomat 2000 IR, CAWO, Schrobenhausen

2.1.2. Chemicals/enzymes

Acrylamide 30% (m/v)	acrylamide/bis-acrylamide	Sigma-Aldrich, Taufkirchen
Antibiotics	Ampicillin sodium salt	USB, Cleveland, Ohio, USA
	Kanamycin monosulfate	Sigma-Aldrich
Antibodies	primary: 6xHIS (mouse)	Clontech, Mountain View,
	0.5 mg/ml IgG2a (1:5000 dilution)	CA, USA
	secondary: HRP anti-mouse (goat)	Santa-Cruz Biotechnology,
	0.4 mg/ml IgG (1:1000 dilution)	Heidelberg
β-ME	β-mercaptoethanol	Sigma-Aldrich
BSA	bovine serum albumin	Sigma-Aldrich
Coomassie blue	brilliant blue R 250	Sigma-Aldrich
$CaCl_2 \cdot 2H_2O$	calcium chloride dihydrate	Merck, Darmstadt
Collagenase	type 1 and 2, Worthington	CellSystems, St. Katharinen
CsCl	caesium chloride	Roth, Karlsruhe
CsOH	caesium hydroxide	Sigma-Aldrich
Detection Reagent 1/2	Peroxide and Enhancer solution	Thermo Scientific, Erlangen
DMSO	dimethyl sulfoxide	Sigma-Aldrich
DNase I	desoxyribonuclease, bovine	Sigma-Aldrich
DNA-Marker	Gene Ruler 1kb DNA-Ladder	Fermentas, St. Leon-Rot
DTT	dithiothreitol	Sigma-Aldrich/GERBU

EDTA/ EGTA	ethylenediaminetetraacetic acid/ ethylene glycol-bis (2-aminoethylether)-N,N,N',N'-tetraacetic acid	Sigma-Aldrich
Glucose	D(+)-glucose	Merck
Glycerol	87% (v/v) solution	Applichem, Darmstadt
Glycine		Merck
HCl	hydrochloric acid	Merck
HEPES	4-(2-hydroxyethyl)-1-piperazine-ethanesulfonic acid	Sigma-Aldrich USB, USA
Heparin	Liquemin® 5000 I.E./ml	Roche, Grenzach-Whylen
Imidazole	1,3-diazacyclopenta-2,4-diene	Sigma-Aldrich/Fluka
IPTG	Isopropyl β-D-thiogalactopyranoside	Fisher Scientific, Schwerte
KCl	potassium chloride	Roth
KH_2PO_4	potassium phosphate monobasic	Merck
K_2HPO_4	potassium phosphate dibasic	Sigma-Aldrich
Leupeptin	N-acetyl-L-leucyl-L-leucyl-L-argininal	GERBU, Gaiberg
MANT-ATP	MANT-adenosine 5'-triphosphate	Jena Bioscience, Jena
MANT-GTPγS	MANT-guanosine 5'-[γ-thio]triphosphate	
MANT-ITP	MANT-inosine-triphosphate	gift of Dr. J.Geduhn, UR
MANT-ITPγS	MANT-inosine 5'-[γ-thio]triphosphate	Jena Bioscience
$MgCl_2 \cdot 6H_2O$	magnesium chloride hexahydrate	Merck, Sigma-Aldrich
$MgSO_4 \cdot 7H_2O$	magnesium sulfate heptahydrate	Merck
Mg-ATP	adenosine-5'-triphosphate, Mg salt	Sigma-Aldrich
NaCl	sodium chloride	Merck, Sigma-Aldrich, Roth
$NaH_2PO_4 \cdot 1H_2O$	sodium dihydrogen phosphate	Merck
NaOH	sodium hydroxide	Merck
NH_4SO_4	ammonium sulphate	Merck
PEG 400/8000	polyethylene glycol	Merck
PMSF	phenylmethanesulfonyl fluoride	Roche/Sigma-Aldrich
Ponceau S	Acid Red 112, diazo dye	Sigma-Aldrich
Protein Standard	Precision Plus Dual Color Page Ruler #SM0669	Bio-Rad, München Fermentas
SDS	sodium dodecyl sulfate	Merck
TLCK	N-tosyl-L-lysine chloromethyl ketone	AppliChem/Sigma-Aldrich
TPCK	tosyl phenylalanine chloromethyl ketone	
Tris	tris(hydroxymethyl)aminomethane	Roth, Invitrogen
Trypsin inhibitor	Type II-L, Lima Bean	Sigma-Aldrich
Tween 20	Polysorbat 20	Merck

2.1.3. Consumables

Borosilicate capillaries	pipette manufacturing	Hilgenberg
Centrifugal filter devices	Centriprep YM-10, MWCO 10 kDa	Millipore
	Microcon YM-10, MWCO 10 kDa	Millipore
	Jumbosep 10K, MWCO 10 kDa	Pall Life Sciences USA
	Vivaspin MWCO 3, 10, 30 kDa	Sartorius Biotech
Cheesecloth	250 µm, nylon	Reichelt, Heidelberg
Cryo loop	Crystal Cap Copper Magnetic	Hampton Research
	Adjustable Mounted CryoLoop	Hampton Research
Crystallization trays	Cryschem 24 well plates	Hampton Research
	VDX 24 well plates	Hampton Research
Glass cover slides	circle and square forms (22 mm)	Hampton Research
Insulin syringe	1 ml, sterile	Becton Dickinson
Infusion set	Intrafix® air	B. Braun
Injection needles	21G, 22G, 27G BD Microlance	Becton Dickinson
Nitrocellulose membrane	0.45 µm Trans-Blot® Transfer medium	Bio-Rad
Mess dishes	35 x 10 mm Petri dish	Falcon
Photo film	Amersham Hyperfilm ECL	GE Healthcare
Pipette tips	10 µl, 200 µl, 1000 µl	Sarstedt
Test tubes	1.5 and 2 ml micro tubes	Sarstedt
	15 and 50 ml Falcon tubes	Sarstedt
Serological pipettes	1 ml, 5 ml, 10 ml, 25 ml, steril	Sarstedt
Single-use syringe	2 ml, 5 ml, 10 ml, 20 ml steril	B. Braun
Sterile filters	Filtropur S 0.2 µm	Sarstedt
	Sterifix 0.22 µm	B. Braun
Transfer pipette	disposable, 2 ml	Sarstedt
Vacuum grease	Dow Corning® vacuum grease	Hampton Research

2.1.4. Computer software

CCP4 program suite	Collaborative Computational Project No. 4, UK
Coot	Crystallographic Object-Oriented Toolkit, UK
Excel, PowerPoint, Word	Microsoft Office 2003, 2007
Endnote	Version X and X3, Thomson Reuters
Gene Runner	Version 3.01, Hastings Software
GraphPad Prism	Prism 5.0, GraphPad, USA
pClamp	pClamp6 and Clampex 10.2, Axon Instruments
PyMOL	DeLano Scientific, USA – now Schrödinger

2.2. Methods

2.2.1. Purification of mAC subunits C1/C2 and $G_{s\alpha}$

This chapter describes the procedure for protein purification of the following proteins (Hatley *et al.*, 2002):

VC1	catalytic subunit C1a of canine AC 5
IIC2	catalytic subunit C2a of rat AC 2
$G_{s\alpha}$	α-subunit of bovine stimulatory G protein

2.2.1.1. Plasmids

Plasmids used for the expression of the aforementioned proteins were a kind gift from Steve Sprang (PhD) and Tung-Chung Mou (PhD), University of Montana (UMT).

Plasmid	Characteristics	Application	Antibiotic resistance
pQE60-H6-VC1 (364-580)	4071 bp Restriction site Nco I - Hind III	protein expression of N-terminal HIS-tagged C1a of canine AC 5 (216 AA)	Ampicillin
pQE60-ArgC-IIC2	4030 bp Restriction site EcoR I - Hind III	protein expression of tag-less C2a of rat AC 2 (207 AA)	Ampicillin
pREP4 [M15]	low-copy plasmid 3740 bp Qiagen Cat. # 342010	expresses *lac* repressor protein, regulator of protein expression in *Escherichia coli* BL21	Kanamycin
pQE60-$G_{s\alpha}$-H6		protein expression of C-terminal HIS-tagged bovine $G_{s\alpha}$	Ampicillin

2.2.1.2. Bacteria

The following table shows the bacteria used for protein expression and plasmid amplification:

Bacteria	Application	Reference
Escherichia coli BL21-DE3, containing pREP4 plasmid	protein expression of VC1 and IIC2	gift of Drs. Steve Sprang and Tung-Chung Mou, UMT
Escherichia coli JM109	protein expression of $G_{s\alpha}$	gift of Drs. Steve Sprang and Tung-Chung Mou, UMT
Escherichia coli TOP10	plasmid amplification	One Shot® TOP10, Invitrogen

2.2.1.3. Preparation of heat shock competent cells

E.coli cells were plated on culture plates without antibiotics and incubated overnight. The next day, 10 ml LB media was inoculated and incubated overnight. Part of this stock was used to inoculate SOB media in a dilution 1:100. As soon as the optical density at 600 nm (OD_{600}) of 0.5 to 0.7 was reached, the suspension was placed in ice cold water for 15 min to stop bacterial growth. The media was replaced by centrifugation at 2,500 rpm at 4°C and the pellet was treated with RF1 buffer for 1 h on ice. The buffer was replaced by RF2 buffer and the cell suspension was divided into 100 µl aliquots, frozen in liquid N_2 and stored at -80°C.

RF1 buffer	pH 5.8
K^+-acetate	35 mM
$CaCl_2$	10 mM
$MnCl_2$	50 mM
RbCl	100 mM
Glycerol	15% (v/v)

RF2 buffer	pH 6.8
MOPS	10 mM
$CaCl_2$	75 mM
RbCl	10 mM
Glycerol	15% (v/v)

Buffers were sterile-filtered and pH-adjustment was done with 0.2 M acetic acid.

2.2.1.4. Transformation of *E.coli*

All the time we used freshly transformed *E. coli*, even though bacteria can be used for 4 weeks when stored at 4°C.

Competent *E.coli* cells were gently thawed in a warm hand and placed on ice for 10 min. After addition of 2-10 ng plasmid, cells were incubated for 30 min on ice. The cells were heated for 1 min at 42°C and immediately placed on ice for 3 min. After adding 900 µl LB or SOC medium the cells were incubated for 1 h without antibiotics at 37°C and 150 rpm. A small aliquot (ca. 100 µl) of the cell suspension is then plated on a selective culture plate (2.2.1.6) and incubated overnight at 37°C. A separate part of the overnight culture (700 µl) was frozen and stored at -80°C after addition of 300 µl 50% (v/v) glycerol.

2.2.1.5. Restriction digestion and sequencing

Restriction digestion was used to identify the quality of amplified DNA. Restriction endonucleases are enzymes, expressed by bacteria that can recognize and cleave specific base sequences in double stranded DNA. Enzymes and buffers used for analysis of our amplified DNA were purchased from NEB (New England Biolabs). For analytic detection of DNA fragments 0.1-0.5 µg DNA was digested with 1 µl restriction enzyme (~ 3-5 U) at a specific temperature in a 15 µl batch. After 2 h in a heating block, the digestion was terminated and the reaction was further evaluated by gel electrophoresis.

Another evaluation was performed by sequencing a specific DNA sequence of our amplified DNA to determine and assess the correctness of the nucleotide sequence. Sequence analysis of the Department of Pharmacology was carried out by Entelechon (Regensburg).

2.2.1.6. Culture media

Plasmid amplification was performed using the standard LB medium. Protein expression was achieved using special T7 medium. Media were autoclaved for 20 min at 121°C, 1 bar. Temperature-sensitive substances, e.g. antibiotics, were added to the media shortly before inoculation with bacteria or for the preparation of culture plates at around 50°C.

LB media, pH 7.4[1]:

Trypton	10.0 g
Yeast exract	5.0 g
NaCl	10.0 g
H_2O_{dest}	ad 1.0 L

[1]culture plates: addition of 15 g Agar

T7 media, pH 7.2

Trypton	20.0 g
Yeast extract	10.0 g
NaCl	5.0 g
Glycerol	2 ml
$KHPO_4$ (pH 7.2)	200 mM
H_2O	ad 1.0 L

Antibiotics were added with the following concentrations, depending on the bacteria used:

Antibiotic	Stock	TOP 10	BL21-pREP4	JM109
Ampicillin (Amp)	100 mg/ml in EtOH (50% v/v)	100 µg/ml	50 µg/ml	100 µg/ml
Kanamycin (Kan)	50 mg/ml in H_2O_{bidest}	-	50 µg/ml	-

For protein expression the plasmids were transformed into BL21-pREP4/JM109 cells and plated on LB Amp/Kan or Amp culture plates. The next day 100 ml LB media were inoculated by picking single colonies from the culture plate. The suspension was incubated overnight at 37°C and at 200 - 250 rpm in an incubator shaker. The next day, the overnight culture stock was centrifuged at 3,000 rpm and the pellet was used for inoculation of T7 expression media.

2.2.1.7. Expression and cell lysis of C1/C2 and $G_{s\alpha}$

Due to the fact that the expression level varied between the 3 different proteins, we used different expression protocols.

<u>VC1 protein expression</u>

VC1 is only expressed in very small amounts (~ 3 mg/12 L) and due to the fact that the protein is very unstable, expression was initiated at low temperature and for a short period.

Therefore, we inoculated 12 L T7 media with the overnight culture stock, incubated at 37°C until OD_{600} was ~ 0.8 and decreased the temperature to 25°C. As soon as OD_{600} was ~ 1.1 we induced protein expression with 30 µM IPTG. After expression for 4 h at 25°C the cells were harvested by centrifugation at 4,000 rpm for 20 min and the cell pellet was frozen in liquid N_2 and stored at -80°C.

IIC2 protein expression

In contrast to VC1, this protein is stable and can be expressed in large amounts (~ 30 mg/L). Therefore, protein expression can be performed overnight and in a smaller volume of one liter T7 media. The expression was started as soon as OD_{600} was ~ 0.8 and induced with 30 µM IPTG at 30°C. The next morning cells were collected by centrifugation at 5,000 rpm for 20 min. The cell pellet was drenched in liquid N_2 and also stored at -80°C.

$G_{s\alpha}$ protein expression

Due to the fact that the expression level for $G_{s\alpha}$ was not exuberant (~ 3 mg/L) we inoculated 10-12 L T7 media at 37°C with the overnight culture stock. Expression of $G_{s\alpha}$ was started at OD_{600} of 0.45 with 50 µM IPTG and continued at 30°C overnight. After 18 h the cells were harvested at 4,000 rpm for 20 min, frozen in liquid N_2 and stored at -80°C.

Cell lysis

The lysis buffers used for cell lysis are listed in the following table:

Lysis buffer	**VC1**	**IIC2**	**$G_{s\alpha}$**
NaCl	120 mM	50 mM	100 mM
Tris-HCl pH 8.0	50 mM	50 mM	50 mM
β-ME	1 mM	-	20 mM
DTT	-	2 mM	-
protease inhibitors	1x	1x	1x (only PTT, not LL)
H_2O_{dest}	ad 1500 ml	ad 200 ml	ad 1000 ml

Protease inhibitors (PI) are:

PTT	1,000x
TPCK	320 mg
TLCK	320 mg
DMSO	ad 5 ml
PMSF	350 mg
Isopropyl alcohol	ad 10 ml

LL	1,000x
Leupeptin	16 mg
Trypsin inhibitor II-L	16 mg
H_2O_{dest}	ad 10 ml

At the beginning we tried different cell lysis methods, e.g. homogenization with UltraTurrax (TP 18-10, IKA Werk) or ultrasound (Bandelin Sonoplus, Bandelin Electronics). However, the best lysis was achieved by homogenizing the frozen cell pellet together with lysis buffer with a Braun hand blender for 2 min until a viscous suspension without any chunks was achieved. Half of the lysis buffer was used to blend the cells the first time. Then lysozyme (freshly prepared in lysis buffer) was added in a final concentration of 0.2 mg/ml and the suspension was slowly stirred for 40 min at 4°C. All the following steps were performed at 4°C, using a cold room or refrigerator. A good lysis was achieved as soon as the suspension showed a mucous layer on top.

Then DNase I (also freshly prepared in lysis buffer) was added to the solution in a concentration of 8-10 µg/ml together with 1 mM $MgCl_2$ to break down the DNA. After stirring 20 min the mucous layer was dissolved and the suspension was centrifuged using ultracentrifugation at 35,000 rpm for 35 min. The obtained supernatant was applied to a protein purification column and the pellet was frozen in liquid N_2. The frozen pellet was again blended for 1 min with one quarter of lysis buffer and stirred for 20 min after adding 8-10 µg/ml DNase I and 1 mM $MgCl_2$. After ultracentrifugation we used the supernatant for protein purification and the remaining pellet was discarded. The second lysis was necessary to obtain a higher protein yield.

2.2.1.8. Protein purification

After cell lysis the supernatant contains all proteins that are expressed in the cell. To obtain a pure and functional protein, different purification steps had to be carried out depending on the protein. This chapter deals with the buffer solutions and columns used for purification of VC1, IIC2 and $G_{s\alpha}$.

Purification of VC1

The protein carries a hexahistidine tag at the N-terminus. Therefore, it can be purified using an affinity column for hexahistidine. We first tried to use a HisTrap FF 5 ml column, but the purification could be improved using Talon chromatography, because less contaminants were retained with this resin, increasing protein yield. An empty column was packed with 10 ml Talon resin, washed with H_2O_{dest} and equilibrated with 100 ml VC1 lysis buffer.

The supernatant (~ 1200 ml) was applied to the column using gravity flow and the flow rate was adjusted to ~ 2 ml/min. After loading (in general around 10 h) the column was washed with 50 ml Wash I buffer, followed by 25 ml Wash II buffer to clean the resin from non-specifically bound protein. Elution was started using Elution buffer and 2 ml fractions were collected. Fractions were analyzed using SDS-PAGE (2.2.1.9) and the fractions containing VC1 were pooled together. Pooled fractions (~ 12 ml) were diluted with buffer A to

decrease the final imidazole concentration to < 30 mM. The diluted protein solution was then further purified using two ion exchange columns.

Wash I buffer	pH 8.0
NaCl	500 mM
Tris-HCl	50 mM
β-ME	1 mM
PI	1x
H_2O_{dest}	ad 50 ml

Wash II buffer	pH 8.0
NaCl	50 mM
Tris-HCl	50 mM
β-ME	1 mM
PI	1x
H_2O_{dest}	ad 25 ml

Elution buffer	pH 8.0
NaCl	120 mM
Tris-HCl	50 mM
β-ME	1 mM
PI	1x
Imidazole	100 mM
H_2O_{dest}	ad 50 ml

A HiTrap Q FF 1 ml column was used as a precolumn to bind contaminating proteins and the Mono S 5/50 GL column was used for VC1 binding. Both columns were equilibrated with 10 ml buffer A. Protein solution was loaded onto the columns using a Superloop and a flow rate of 0.2 ml/min (Äkta FPLC). The columns were washed with 10 ml buffer A. The gradient elution runs only through the Mono S column and bypasses the HiTrap Q column. A fast gradient is run for 5x column volumes (CV) to 20% buffer B, followed by a slow gradient for 40x CV to 100% buffer B and fractions of 1 ml were collected.

Buffer A*	pH 7.0
HEPES	20 mM
$MgCl_2$	2 mM
EDTA pH 8.0	1 mM
DTT	2 mM
PI	1x
H_2O_{dest}	ad 350 ml

Buffer B*	pH 7.0
Buffer A + 1 M NaCl	250 ml

*buffers are filtered (0.22 µm filter)

In order to determine the fractions of interest, collected samples were applied to SDS-PAGE (2.2.1.9). The fractions containing VC1 were pooled together and concentrated using a centrifugal filter device. For crystallization work only fresh and not frozen concentrated VC1 was used.

Purification of IIC2

Since IIC2 was expressed as a tag-less protein, we could not use affinity chromatography. Therefore we started with an anionic exchange column and used a self-filled 50 ml Q Sepharose FF column. The supernatant after cell lysis was first filtered through a 0.45 µm filter to prevent clogging of the column. Flow rate was 5 ml/min. The column was equilibrated with 100 ml buffer D, loaded with the cell extracts (~ 200 ml) and washed with 100 ml

buffer D. A linear gradient from 50 to 350 mM NaCl (200 ml) was started, followed by a second linear gradient step (100 ml) to 1 M NaCl and 7 ml fractions were collected.

Buffer D	pH 8.0
Tris-HCl	50 mM
NaCl	50 mM
DTT	2 mM
PI	1x
H_2O_{dest}	ad 1.0 L

Buffer E	pH 8.0
Tris-HCl	50 mM
NaCl	1 M
DTT	2 mM
PI	1x
H_2O_{dest}	ad 1.0 L

Peak fractions were determined by SDS-PAGE (2.2.1.9) and the pooled fractions were loaded on a 50 ml HAP column (2.1.1) with a flow rate of 3 ml/min (equilibrated with buffer D). The column was washed with 100 ml buffer D and a gradient of 0 – 300 mM Na_2HPO_4 (in buffer D, pH 8.0) for 150 ml was run. IIC2 was eluted at ~ 100 mM Na_2HPO_4 concentration and collected in 9 ml fractions. The pooled fractions were dissolved in 3.6 M $(NH_4)_2SO_4$ to a final concentration of 1.2 M $(NH_4)_2SO_4$. A hydrophobic chromatography was applied using a HiTrap Phenyl 5 ml FF column. The protein solution was loaded onto the equilibrated column, washed with 75 ml buffer A, and linear gradient elution (50 ml) was started by the replacement of buffer A (1.2 M $(NH_4)_2SO_4$) against buffer B (no $(NH_4)_2SO_4$), 3 ml fractions were collected.

Buffer A	pH 8.0
Tris-HCl	50 mM
$MgCl_2$	1 mM
EDTA, pH 8.0	1 mM
PTT	1x
$(NH_4)_2SO_4$	1.2 M
H_2O_{dest}	ad 300 ml

Buffer B	pH 8.0
Tris-HCl	50 mM
$MgCl_2$	1 mM
EDTA, pH 8.0	1 mM
PTT	1x
H_2O_{dest}	ad 400 ml

The pooled fractions (~ 30 ml) containing IIC2 were filled into a dialysis membrane (MWCO 10 kDa) to remove $(NH_4)_2SO_4$ by dialysis with 3x 1.0 L dialysis buffer.

Dialysis buffer	pH 8.0
HEPES	20 mM
$MgCl_2$	2 mM
DTT	1 mM
EDTA, pH 8.0	1 mM
PI	1x

The protein sample was concentrated to ~ 2 ml and diluted in buffer D to a final volume of 50 ml. The first procedure with 50 ml Q Sepharose FF has to be repeated and afterwards the peak fractions were evaluated by SDS-PAGE (2.2.1.9). Fractions of interest were pooled together and concentrated using a centrifugal concentrator with a 10 kDa MWCO (2.1.3).

Purification of $G_{s\alpha}$

The protein was expressed with a hexahistidine tag at the C-terminus. After cell lysis supernatant was therefore first purified by affinity chromatography using 2 tandemly arranged HisTrap 5 ml columns. The columns were washed with 100 ml H_2O_{dest}, followed by equilibration with $G_{s\alpha}$ lysis buffer. The lysis buffer contains high concentration of reducing agent β-ME, and therefore, the columns turn their colour from blue to light violet. We also used 10 ml Profinity IMAC Ni-charged resin that was more resistant against β-ME (compatible up to 30 mM concentration) which did not show any change in colour. However, both columns showed sufficient binding affinity. The supernatant was applied to the columns with a 2 ml/min flow rate and afterwards the columns were washed with 100 ml Wash buffer to remove non-specific bound contaminants. Elution of his-tagged protein was started by slow gradient elution from 0 to 150 mM imidazole for 200 ml, using Buffer A and B. Compositions of the buffers are shown below:

Wash buffer	pH 8.0
Imidazole	10 mM
NaCl	500 mM
Tris-HCl	50 mM
β-ME	20 mM
Glycerol	10% (v/v)
GDP	25 µM
NaF	10 mM
$AlCl_3$	30 µM
$MgCl_2$	4 mM
PTT	1x
H_2O_{dest}	ad 400 ml

Elute buffer A	pH 8.0
Tris-HCl	50 mM
β-ME	20 mM
Glycerol	10% (v/v)
PTT	1x
H_2O_{dest}	ad 400 ml

Elute buffer B	pH 8.0
Tris-HCl	50 mM
β-ME	20 mM
Glycerol	10% (v/v)
PTT	1x
Imidazole	150 mM
H_2O_{dest}	ad 400 ml

The protein solution was collected in 5 ml fractions, run on SDS-PAGE (2.2.1.9), and the fractions containing $G_{s\alpha}$ were further used for anion exchange chromatography using a HiTrapQ 5ml column. The column was equilibrated with 50 ml buffer C. The protein solution was diluted with buffer C in a 1:1 ratio to decrease the β-ME concentration and then loaded

onto the HiTrapQ column with a flow rate of 2 ml/min. The column was then washed using 2x CV of buffer C.

Buffer C*	pH 8.0
Tris, pH 8.0 (RT pH 7.7)	50 mM
DTT	1 mM
Glycerol	10% (v/v)
H_2O_{dest}	ad 250 ml

Buffer D*	pH 8.0
Buffer C + 1 M NaCl	250 ml

*buffers were filtered (0.22 µm filter)

A gradient from 0 – 250 mM NaCl was run for 10x CV, followed by a gradient to 1 M NaCl for 10x CV, using buffer C and D and 3.5 ml fractions were collected.

Fractions were used for SDS-PAGE analysis (2.2.1.9) and the $G_{s\alpha}$-containing fractions were pooled together. KH_2PO_4/ K_2HPO_4 = KPO_4-buffer 1 M (pH 8.0) and GDP were added to the solution in a final concentration of 10 mM and 5 µM, respectively. The protein solution was then loaded onto a 50 ml HAP column (2.1.1) that was preequilibrated with 50 ml buffer E. The flow rate was set at 2 ml/min and after a wash for 2x CV, elution was started by first running a gradient from 10 – 250 mM KPO_4-buffer for 10x CV and then to 500 mM KPO_4 for 5x CV.

Buffer E*	pH 8.0
NaCl	100 mM
Tris, pH 8.0 (RT pH 7.7)	100 mM
DTT	2 mM
GDP	5 µM
Glycerol	10% (v/v)
KH_2PO_4/ K_2HPO_4	10 mM
H_2O_{dest}	ad 500 ml

*buffers were filtered (0.22 µm filter)

Buffer F*	pH 8.0
NaCl	100 mM
Tris, pH 8.0 (RT pH 7.7)	100 mM
DTT	2 mM
GDP	5 µM
Glycerol	10% (v/v)
KH_2PO_4/ K_2HPO_4	500 mM
H_2O_{dest}	ad 500 ml

Samples of the 3 ml fractions were run on SDS-PAGE (2.2.1.9); the important fractions were pooled together and concentrated using a centrifugal filter device with a 10 kDa MWCO.

To remove KPO_4 the protein solution was placed in a dialysis membrane with a 10 kDa MWCO and 3x dialysed in 1.0 L buffer G.

Buffer G	pH 8.0
NaCl	50 mM
HEPES	20 mM
β-ME	1 mM
EDTA	1 mM
$MgCl_2$	5 mM
H_2O_{dest}	ad 1.0 L

For crystallization, $G_{s\alpha}$ had to be activated by GTPγS and digested to a smaller protein fragment of ~ 37 kDa in order to remove floppy ends that may prevent formation of a stable heterotrimeric complex. For this purpose dialysed and concentrated protein was diluted with an equal volume of activation buffer (HEPES 40 mM, pH 8.0; $MgCl_2$ 4 mM, β-ME 1 mM, NaCl 200 mM) and GTPγS was added at a concentration of 500 µM. The protein was incubated for 2 h at 30°C and afterwards, digestion was started by addition of 1 mg/ml trypsin (TPCK-treated) to make a final concentration of 5 µg/ml. To control digestion, the solution was incubated for 2 h on ice. Imidazole and PTT was added to a final concentration of 5 mM and 1x PTT, and the protein solution was loaded onto a preequilibrated 0.8 ml Ni-NTA or Talon gravity column. The pass-through was collected and then the column was washed with 5 ml wash buffer (Tris-HCl 50 mM, pH 8.0; NaCl 120 mM, Imidazole 8 mM). Pass-through and the wash were pooled together, diluted to 50 ml with buffer A and purified using anionic exchange chromatography. A MonoQ 5/50 GL column was equilibrated with buffer A and after protein loading; a gradient to 300 mM NaCl for 25 ml was run. Isocratic elution at 300 mM followed for 5 ml and at the end gradient elution to 1 M NaCl for 10 ml.

Buffer A*	pH 8.0
HEPES	20 mM
$MgCl_2$	2 mM
EDTA pH 8.0	1 mM
DTT	2 mM
H_2O_{dest}	ad 500 ml

Buffer B*	pH 8.0
Buffer A + 1 M NaCl	250 ml

*buffers were filtered (0.22 µm filter)

The fractions (1 ml) were collected and further characterized on SDS-PAGE (2.2.1.9) and concentrated with a Vivaspin 10 kDa MWCO.

2.2.1.9. Protein biochemical methods

SDS polyacrylamide gel electrophoresis (SDS-PAGE)

Purification quality was assessed using SDS polyacrylamide gel electrophoresis. A complex protein sample can be characterized and separated into protein fractions dependent on their size due to their electrophoretic mobility (Laemmli, 1970). SDS is added to the solutions and gels and binds to the proteins to denature the protein structure and to achieve an identical (negative) charge to mass relationship of the proteins. Therefore, protein mobility, in theory, depends on the size of the protein and the pore diameter of the gel. The pore diameter is influenced by the polymerization degree of acrylamide to bis-acrylamide. Pore size decreases with increasing amount of acrylamide. We used either 4-20% (m/v) Ready Gel Tris-HCl, Bio-Rad (precast gels) or 15% (m/v) separating gel (hand-casted gels).

Hand-casting of the gels and subsequent gel electrophoresis was achieved using the casting stands and vertical electrophoresis system Mini-PROTEAN® Tetra Cell (Bio-Rad). First the separating gel was loaded into the casting stands, leaving a 2 ml gap on top that was filled with isopropanol. After ~ 45 min the separating gel was polymerized and the gap was filled, after removal of isopropanol, with loading gel plus a pocket forming comb. Gels were inserted into the vertical electrophoresis chamber.

15% m/v separating gel	**2 small gels**
Buffer A*, pH 8.8	4 ml
Acrylamide 30% (m/v)	8 ml
APS 10% (m/v) (in water)	66.7 µl
TEMED	6.7 µl
Glycerol 50% (v/v)	1.06 ml
H_2O_{dest}	2.8 ml

loading gel	**2 small gels**
Buffer B*, pH 6.8	2.5 ml
Acrylamide 30% (m/v)	1 ml
APS 10% (m/v)	100 µl
TEMED	6.7 µl
H_2O_{dest}	6.5 ml

Buffer A*:	
Tris-HCl, pH 8.8	1.5 M
SDS 10% (m/v)	4 ml
H_2O_{dest}	100 ml

Buffer B*:	
Tris-HCl, pH 6.8	0.5 M
SDS 10% (m/v)	4 ml
H_2O_{dest}	100 ml

The protein sample was mixed with 2x Laemmli buffer at a 1:1 ratio to a final volume of 20 µl and then heated for 3 min at 95°C. The samples and a protein standard were applied to the gel pockets and separated at 150 V in 1x running buffer. After gel electrophoresis the gels were stained with Coomassie or blotted on nitrocellulose membrane for Western Blot.

10 x running buffer	**pH 8.3**
Tris-HCl, pH 8.3	250 mM
Glycine	1.92 M
SDS	1% (m/v)
H_2O_{dest}	ad 10.0 L

2x Laemmli buffer	**pH 8.0**
Tris-HCl, pH 8.0	25 mM
DTT	200 mM
SDS	2.5% (m/v)
Glycerol	5% (v/v)
Bromphenolblue	0.01% (m/v)
Urea	8 M
H_2O_{dest}	ad 60 ml

Coomassie blue - staining

To detect seperated proteins on the SDS-PAGE gel, Coomassie staining was used. The gels were shaken for ~ 30 min in Coomassie staining solution and afterwards a destaining solution was used to remove the blue background color from the gel.

Coomassie staining solution	
Coomassie Blue R 250	1.5 g
Methanol	455 ml
Acetic acid	90 ml
H_2O_{bidest}	ad 1.0 L

Destaining solution	
Acetic acid	100 ml
Methanol	300 ml
H_2O_{dest}	ad 1.0 L

The destaining solution was changed every 20 min until a good detection of protein bands could be seen. The gels were dried on filter paper at 80°C under vacuum or between two cellophane sheets using a Gel Air Drying system (Bio-Rad).

Western Blot

Proteins, separated *via* SDS-PAGE can be further analyzed by transfer to a nitrocellulose or polyvinylidene difluoride (PVDF) membrane. The blotting of proteins to a membrane is referred to as Western Blot. The protein bands on the gel were transferred to a nitrocellulose membrane (2.1.3) using a tank transfer system (Mini Trans-Blot® Cell, Bio-Rad), filled with blotting buffer. The transfer was achieved after 120 min at 0.15 A current and can be checked by application of Ponceau S, a dye that stains the protein bands on membranes in a reversible manner. The membrane was then incubated with a specific primary antibody (2.1.2), followed by a horseradish peroxidase secondary antibody (2.1.2) that binds to the primary antibody and can be photocemically detected - showing only “the protein of interest”. TBS buffer (1x) substituted with Tween 20 (TBS-T buffer) and with or without addition of skimmed milk (5% m/v) was used for the application of the antibodies and during the wash of the membranes. In our case, we used a hexahistidine antibody as primary antibody to control expression levels of the hexahistidine tagged proteins in the protein solutions.

Blotting buffer	
Tris	3 g
Glycin	14 g
Methanol	200 ml
H_2O_{dest}	800 ml

10x TBS buffer	**pH 7.6**
Tris-HCl, pH 7.6	200 mM
NaCl	1.37 M
H_2O_{dest}	ad 1.0 L

TBS-T buffer	**pH 7.6**
Tween 20	1 ml
TBS buffer 1x	ad 1.0 L

The exact procedure is explained in detail in the supplementary data (8.1).

Bradford protein assay

For quantification of the pure protein after protein purification we used the colorimetric Bradford protein assay (Bradford, 1976). In principle, the protein was detected *via* interaction of positively charged amino acids with the negatively charged Coomassie dye. By binding to the protein the originally red form of Coomassie changes to Coomassie blue, shifting the absorption maximum from 465 to 595 nm. Protein concentration was detected by measuring the extinction at 595 nm (Biophotometer, Eppendorf), using BSA as calibration standard.

Either 100 µl protein sample, or BSA standard (1-10 µg BSA/100 µl H_2O_{bidest}) or buffer (as blank) were mixed with 1 ml Bradford dye (Bio-Rad), incubated for 5 min and then measured at 595 nm.

2.2.2. Crystallization

All crystallization work was done at the University of Montana under supervision by Drs. Steve Sprang (Ph.D.) and Tung-Chung Mou (Ph.D.).

2.2.2.1. Complex formation

A ternary complex of H6-VC1 (580), IIC2 or IIC2 mutant (K1014N) and $G_{s\alpha}$-GTPγS was formed by mixing the three purified proteins in the following order (no specific time interval): C1 + C2 → $G_{s\alpha}$.

An excess amount of C1 (~ 37.5 µmole) was used relative to C2 and $G_{s\alpha}$ (~ 25 µmole each). The higher concentration of C1 and the order of mixing prevented that C2 and $G_{s\alpha}$ form a complex in the absence of C1. The formed complex was then incubated on ice for 30 min, with or without the addition of 200 µM FS or FS analog. Afterwards the complex was isolated from the single proteins in the absence or presence of FS by tandem gel filtration. The sample was first applied to a Superdex 75 gel filtration column to which a Superdex 200 had been attached.

gel filtration buffer pH 8.0	(mM)
HEPES	20
$MgCl_2$	2
EDTA pH 8.0	1
DTT	2
NaCl	100
GTPγS	0.01
(FS/FS analog	0.025)

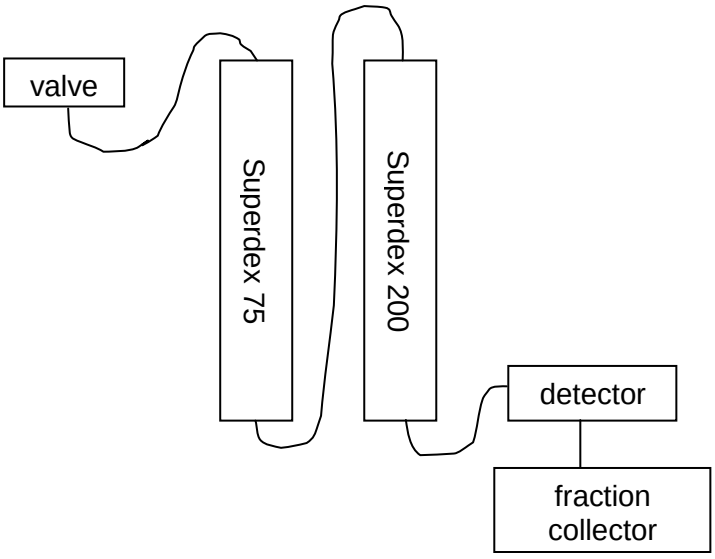

The FPLC fraction collector collected 300 µl fractions that were resolved on a 4-20% (m/v) TRIS-glycine precast gel. Fractions containing only ternary complex were pooled together and after adding 5 mM DTT, 500 µM GTPγS, with or without FS or FS analog, the protein complex was concentrated to ~ 8 mg/ml with Vivaspin 30K.

2.2.2.2. Crystal growth

To grow crystals, we set up 24-well crystallization plates. We used either VDX plates for a hanging drop setup or Cryschem plates for a sitting drop setup (2.1.3). Figure 5 illustrates the different crystallization setups.

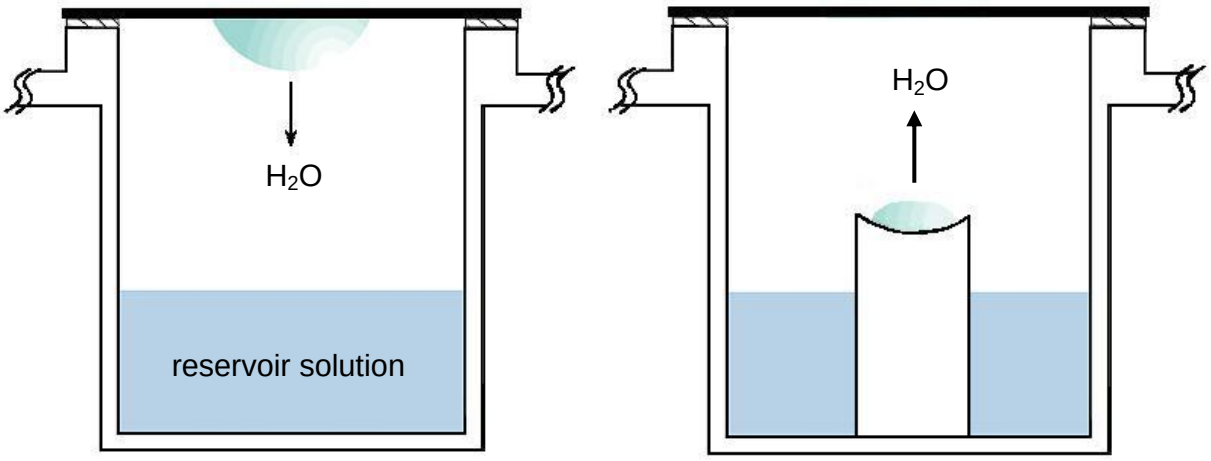

Figure 5. Crystallization setup. In the hanging drop crystallization plates, the protein solution (1 µl) is hanging on the cover lid. In contrast, the protein solution can also "sit" on a concave drop post using sitting drop plates.

The reservoir solution contained a mixture of:

- polyethylene glycol (PEG) 8000, in different concentrations (7.0 – 8.0% v/v)
- NaCl 0.5 M and
- 0.1 M MES, with different pH (5.3 – 5.7).

See section G4 for a better understanding of the reservoir solution preparation where a protocol for the setup of a crystal try is shown. The reservoir solution was freshly prepared and directly mixed inside one well. The 24 well plates had to be prepared before applying the reservoir solution. With a hand syringe vacuum grease was applied to the rim of the 24 wells. The grease is used to form a closed environment inside the well. As soon as 1 µl of protein solution was applied to the lid (hanging drop version) or to the drop post (sitting drop version), the lid is tightly pushed onto the greased crystal tray to prevent any water loss. The trays were incubated at 16°C in a special temperature controlled incubator. To prevent strong movement of the trays inside the incubator, they were placed in special racks. Formation of micro crystals and large crystals were monitored by light microscopy.

2.2.2.3. Crystal collection and soaking

After optimal crystal growth, crystals were picked using a cryo loop (2.1.3) with a diameter of 100 - 200 µm and cryoprotectant. To measure nucleotide – crystal interactions large crystals were soaked with 2 mM MANT-ITP/TNP-GTP and 3 mM $MnCl_2$ (in cryoprotectant) for at least 2 h at room temperature and then harvested and stored in liquid nitrogen.

Cryoprotectant	
PEG 8000	9% (v/v)
PEG 400	30% (v/v)
MES pH 5.4	100 mM
NaCl	500 mM
HEPES (NaOH) pH 8.0	20 mM
EDTA	1 mM
DTT	2 mM
MP-FS	200 µM
GTPγS	100 µM
MANT-ITP	2 mM
$MnCl_2$	3 mM

2.2.2.4. Structure determination and model refinement

Diffraction data sets were collected at the Stanford Synchrotron Radiation Lightsource SSRL-SMB-MC 9-1 beamline by oscillation method (1°/frame, 60 s/frame). The incident beam wavelength was 0.9795 Å. The images were processed using HKL2000 package (Otwinowski and Minor, 1997). Due to anisotropy of the plate-type crystal, data with *I* index > 21 were excluded from the data set. Structures were determined by molecular replacement using the structure of the $G_{s\alpha}$-GTPγS:VC1:IIC2 complex (PDB code: 1AZS) as the initial phasing model (Tesmer *et al.*, 1997). Atomic positions and thermal parameters of the mAC structure were refined by Refmac5.5 using the CCP4 program suite (Collaborative Computational Project, 1994). MANT-ITP/TNP-GTP and Mn^{2+} ions in the structure were located in the weighted $|F_o|-|F_c|$ omit map computed with phases from the refined model. The model was iteratively improved by manual refitting into weighted $2|F_o|-|F_c|$map using the computer graphics program Coot (Emsley and Cowtan, 2004) and subsequent refinement cycles with CCP4. The visualization of the refined crystal structure was created with Pymol (DeLano, 2002).

2.2.3. Molecular modelling

For evaluation of AC inhibition, as well as fluorescence and crystallographic measurements, structure models for the complex of VC1/IIC2 with MANT-ITP and MANT-GTP were generated *via* docking studies and subsequently refined by molecular dynamics simulations. The computer models for the two MANT nucleotides were constructed using the crystal structures of VC1/IIC2:$G_{s\alpha}$:FS inhibited by MANT-ITP (PDB 3G82) and MANT-GTP (PDB 1TL7) as template. In both cases, the new complex was constructed by editing the structure of co-crystallized ligand in SYBYL to represent the desired ligand (Tripos, 2008). Only the isomer resolved as a co-crystallized component in the crystal structure was used for structure determination. Conformational predictions were conducted using the whole C1/C2 molecule. All atoms were frozen except for the ligand and any residue with at least one atom within 8 Å of the ligand to examine the ligand conformational variation. The full complex was then protonated in SYBYL: both ligands were assumed to have a fully anionic triphosphate tail (net charge = -4), while the receptor valences were assumed to correspond to physiological pH, with cationic lysine and arginine residues, anionic aspartates and glutamates and all other atoms saturated to neutrality. Unrealistic atomic contacts were alleviated by energetically minimizing all hydrogen atom coordinates *via* the AMBER ´89 force field and corresponding charges as implemented in the MOE software suite. Based on the assumed valences, Gasteiger-Marsili partial charges were assigned to all atoms (Gasteiger and Marsili, 1978). The system was permitted some modest relaxation *via* an 11 ps molecular dynamics simulation in SYBYL (1 ps warming from 0 to 300 K, followed by 10 ps thermal equilibration) in which the ligand and all receptor residues within 8.0 Å of the ligand were left conformationally mobile. The resulting relaxed complex structures were then optimized within SYBYL default convergence thresholds *via* molecular mechanics.

2.2.4. Electrophysiology

The electrophysiological measurements on cardiomyocytes were carried out at the Department of Pharmacology, University of Cologne, under supervision of Prof. Dr. Stefan Herzig. We studied the effect of different MANT nucleotides on basal L-type calcium current. Cardiomyocytes were freshly isolated from a common WT mouse line C57BL/6 mice on the day of WC measurement.

2.2.4.1. Animals

The following materials were used for the breeding of WT C57BL/6 mice:

- Makrolon cages with wire lids and water bottles, Tecniplast, Italy
- sterile standard diet and animal bedding fiber, Altromin, Lage

All experiments with animals complied with respective laws and local regulations regarding animal care. Due to the fact that mice were also used for transgenic breeding their WT background was checked *via* genotyping, using standard PCR technique.

2.2.4.2. Isolation of murine cardiomyocytes

The isolation of murine ventricular myocytes was performed using enzymatic dissociation (Wolska and Solaro, 1996; Beetz *et al.*, 2009). The heart was perfused through the coronary arteries to digest the myocardium. We used 3-9 months old mice that were sacrificed by cervical dislocation. To prevent thrombus formation in the aorta we injected heparin (final concentration 500 I.E./ml in sterile 0.9% m/v NaCl) intraperitoneally 30 min before the mice were sacrificed (7.5 I.E./g body weight). The heart was immediately excised, rinsed in solution A and the aorta ascendens was cleaned from fat and connective tissue before canulation with a blunt injection needle. The aorta was attached to the injection needle with a sewing thread. Afterwards the canulated heart was mounted on a Langendorff apparatus and perfused with solution B.

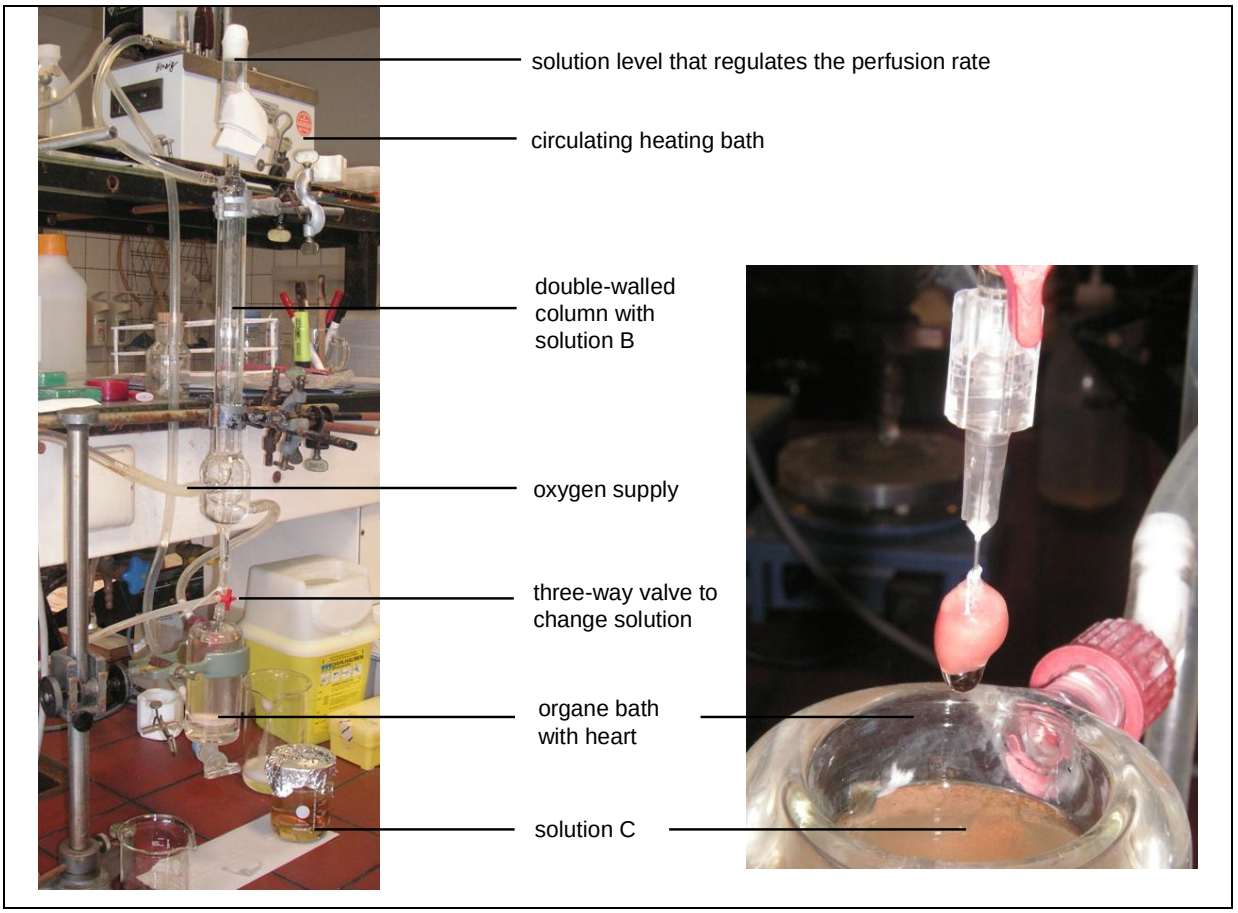

Figure 6. Langendorff setup. On the left picture a Langendorff column and an organ bath, filled with solution B is illustrated. The right picture shows the canulated heart, hanging on a three-way valve.

The Langendorff apparatus is a double-walled column that is regulated by a water bath and can be supplied with oxygen (Figure 6). Therefore, the heart can be perfused and oxygenated at 37°C. The flow rate was controlled by the height of the column. After 5 min of perfusion, solution B was removed through a three-way valve and exchanged with solution C. Solution C contains collagenase type 1 and 2 that starts the enzymatic digestion of the connective tissue in the heart. The heart was perfused with solution C for 10-15 min, depending on the appearance of the heart and the perfusion rate. Due to increased digestion over time, the perfusion rate increased and the heart became discolored. The heart was removed from the Langendorff apparatus and the ventricles were separated from atrial tissue in 10 ml solution D. With a scalpel, the ventricles were cut into small pieces. In order to separate single cells from the tissue, the small pieces were homogenized with a transfer pipette by gentle agitation for 2 min. The large tissue chunks were separated from the single cells using nylon cheesecloth with a pore diameter of 250 µm. Single cells were incubated in solution D (100 µM $CaCl_2$ in solution B) for 20 min at room temperature to adjust the cells to a calcium rich solution. Step-wise, the calcium concentration was increased by removal of 5 ml solution D and addition of 10 ml solution E (200 µM $CaCl_2$ in solution B). After an additional 20 min of incubation, solution E was exchanged for solution F (400 µM $CaCl_2$ in solution B). Afterwards, the cells are ready for electrophysiological measurements and can be used 5-6 hours, when stored at room temperature.

Solution A (with NaOH) pH 7.4	
NaCl	133 mM
KCl	4 mM
NaH_2PO_4 x $1H_2O$	1.2 mM
$MgSO_4$ x $7H_2O$	1.2 mM
HEPES	10 mM
glucose	12 mM
H_2O_{dest}	ad 1.0 L

Solution B	
BSA	500 mg
solution A	ad 500 ml

Solution C	
Collagenase type 1	75 U/ml
Collagenase type 2	75 U/ml
solution B	ad 200 ml

2.2.4.3. Patch clamp

A valuable tool in the analysis of excitable membranes is the patch-clamp technique (Numberger and Draguhn, 1996). It is used to measure membrane currents and membrane capacitance. Already in 1791, Luigi Galvani postulated that muscles work *via* electrical signals. However, it took almost a century until electrophysiological measurements were established by using zinc electrodes to detect nerve and muscle current. At the end of the 1930s, Cole and Curtis established the voltage-clamp technique to measure the conductivity of membranes. This technique was later used by Hodgkin and Huxley to show the formation

of an ion induced action potential in the giant axon of squid (Hodgkin and Huxley, 1952b; Hodgkin and Huxley, 1952a). But to identify single channels it took an additional 20 years until Neher and Sakmann developed the patch clamp technique (Hamill *et al.*, 1981). They were awarded the Nobel Prize in Physiology and Medicine in 1991 “for their discoveries concerning the function of single ion channels in cells”. The idea is that a membrane patch is shielded from the environment by a tightly bound glass pipette expressing a high resistance on the cell surface. A very close seal of the pipette to the membrane is reached when the electrical resistance is > 1 GΩ, referred to as gigaseal. With the development of tight seals, the electrical noise could be diminished and the development of more sensitive amplifier technology made it possible to measure even picoampere (pA) currents. Different patch clamp configurations are used nowadays; the most important are cell-attached, inside-out, outside-out and whole cell (WC) (Hamill *et al.*, 1981). In our case we used the cell-attached configuration followed by WC configuration.

The following figure shows a schematic WC patch clamp setup.

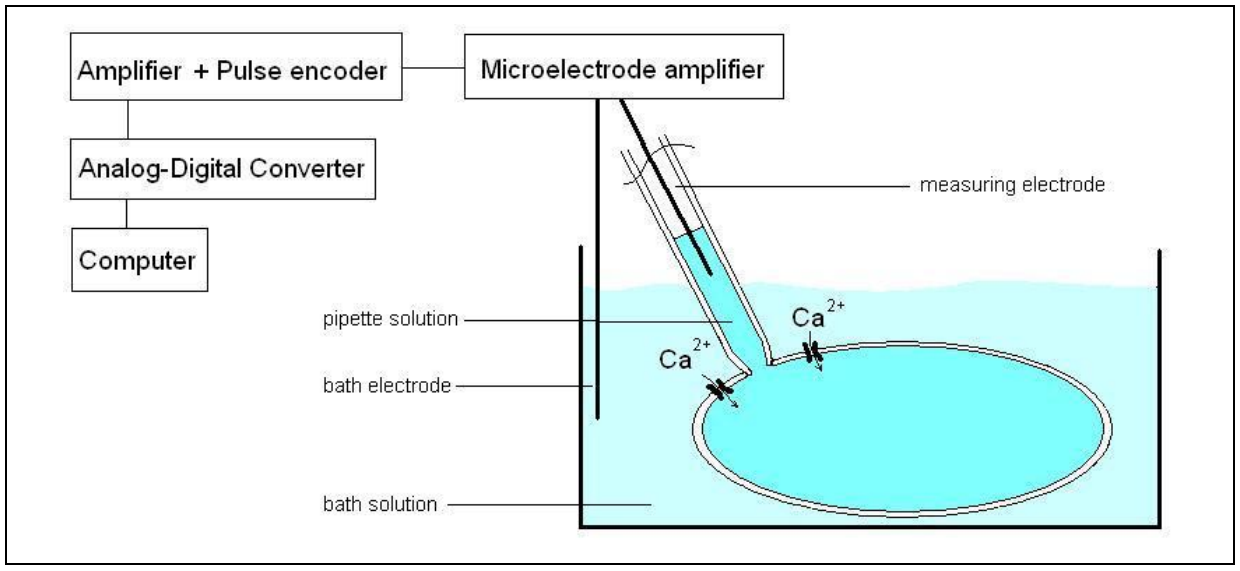

Figure 7. Scheme of Patch clamp setup in WC configuration. An action potential can be initiated by application of a depolarizing pulse from the pulse encoder and computer, respectively. In our case this opens Ca^{2+} channels and the change in membrane potential is detected by the bath and pipette electrode of the preamplifier, further transmitted to the amplifier and converted into digital data *via* the AD converter. The computer records these digital data.

2.2.4.4. Whole cell configuration

Whole cell recordings were performed at room temperature (22-25°C) using the WC configuration as shown in Figure 7. Optical control of the cells during the entire experiment was carried out with an inverse microscope (2.1.1) using a 100-fold and 400-fold magnification. The experiment was conducted within a Faraday cage and the microscope was operated with a battery to prevent any interference by electromagnetic noise.

Cells (300 µl, in solution F) were placed in disposable Petri-dishes and superfused with an external bath solution (ad 3 ml). The bath electrode connected to the microelectrode amplifier is a reference electrode that was placed into the bath solution. The measuring electrode was also connected to the preamplifier and positioned in the glass pipette. Pipettes (2-3 MΩ) were filled with pipette solution. The solutions were prepared freshly on the day of measurement.

MANT nucleotides were added directly to the pipette solution in a concentration of 1 µM. The advantage of the whole-cell configuration was the application of impermeable substances into the cells *via* the pipette solution. In our case, it was possible to apply a specific concentration of MANT nucleotides directly into the cytoplasm.

Bath solution	pH 7.4
NaCl	137 mM
CsCl	5.4 mM
$CaCl_2$	2 mM
$MgCl_2$	1.25 mM
glucose	10 mM
HEPES (with NaOH)	10 mM

Pipette solution*	pH 7.2
CsCl	120 mM
$MgCl_2$	1 mM
Mg^{2+}-ATP	4 mM
HEPES (with CsOH)	5 mM

*was filtered through a 0.22 µm filter

Positioning of the glass pipette was achieved using a micromanipulator (2.1.1) that was adjustable in 3 directions. Any offset potential in consequence of differences between the pipette and bath solution were corrected by the main amplifier as soon as the pipette touched the bath solution. It is important that these fluctuations are eliminated before seal formation.

The pipette was placed very close to the cardiomyocyte. As soon as the pipette resistance increased and a light reflection on the cell surface was visible, soaking through a flexible tube connected to the pipette holder was accomplished. The previously applied over-pressure inside the pipette (2.2.4.5) was reduced, the pipette resistance further increased and the cell membrane was slowly soaked onto the pipette tip and a gigaseal (2-5 GΩ) was established. The pipette was then in the cell-attached configuration and allowed single-channel measurements, if the membrane patch covered a very small area. It is very important that the membrane is not ruptured during this procedure. Capacitive transients caused by the pipette and the membrane patch have to be compensated with the main amplifier. A negative holding potential of -80 mV was applied to the cell to keep the cell in an unexcited state before switching to the WC configuration.

To measure the entity of ion current in the cell we had to penetrate the membrane. Whole cell configuration was achieved by gentle suction with a syringe. Thereby, it was necessary to keep a tight seal of the pipette to the membrane, expressed by high resistance. If this was

not the case, the cell became leaky and lost cytoplasmic constituents. It was then impossible to keep a patch for long time. After penetration through the cell membrane, the pipette solution was released into the cytoplasm. The volume of the pipette solution is much bigger and "dilutes" the cytoplasm reducing essential cytoplasmic factors, like ATP (O'Rourke *et al.*, 1992; Yazawa *et al.*, 1997). Loss in functional components leads to inactivation of ion channels, resulting in "run-down" of ion currents. Another factor that influences "run-down" of the cells is an increasing Ca^{2+} concentration (Belles *et al.*, 1988). Therefore, it was necessary to reduce "run-down" of the cells to facilitate long-term whole cell measurements. In our case, the pipette solution was optimized by addition of 4 mM Mg^{2+}-ATP and EGTA as Ca^{2+} chelator.

As soon as a stable WC configuration was achieved, the cells were ready for Ca^{2+} current measurements. Membrane currents were measured with a low-pass filter of 2 kHz. The cell remained unexcited as long as a holding potential of -80 mV was applied *via* the electrode. Application of a prepulse to -40 mV for 45 ms was used to depolarize the cell. The prepulse inactivates Na^{+} and T-type Ca^{2+} channels. Over a time period of at least 15 min, whole cell calcium currents were recorded using a protocol that started at a holding potential of -80 mV, followed by the depolarizing voltage step to -40 mV for 45 ms and $I_{Ca,L}$ was subsequently measured using a 200 ms-lasting voltage step to +10 mV. The stimulation frequency was 0.3 Hz, leaving 3 s between single stimulations. The protocol measured 30 subsequent stimulations (sweeps). To identify the voltage that induces the maximal Ca^{2+} signal in each cell and to assure that $I_{Ca,L}$ signals are detected, we determined a current - voltage (I-V) curve. Therefore, 10 depolarizing pulses from -40 to +50 mV that lasted 140 ms were applied after prepulsing from -80 to -40 mV. The current - voltage relationship was assessed after 30 sweeps at the test potential (+10 mV), i.e. every 2 minutes throughout the experiment. Membrane capacitance was measured using a fast depolarizing pulse protocol for 5 ms from -40 to -35 mV. The newer pClamp10.2 software was able to calculate membrane capacitance (Axon Instruments, Molecular Devices, USA).

2.2.4.5. Preparation of glass pipettes

The glass pipettes used for WC experiments were prepared on the day of use. Borosilicate glass tubes were cut into ~ 8 cm long capillaries and then fixed in a horizontal pipette puller (2.1.1). The shape and the diameter of the pipette tip can be varied to achieve a specific pipette resistance of 2-3 MΩ. Therefore, different parameters on the puller were changed: heat, the tension of the puller, as well as the time and the speed of the tension. A square shaped filament was placed around the middle of the capillary and heated. It melted the glass and at the same time the glass was dragged at both sides until it ripped into two glass pipettes. The pipettes could not immediately be used after pulling because the tips were edged and would damage the cell during sealing. They had to be "polished" and this

was achieved by fixing the glass pipette in close distance to a heated filament (custom-made microforge). The heat partially melted the tip of the pipette which made the cut smooth and even. The ready-to-use glass pipettes were stored in a special, closed jar and were filled with pipette solution immediately before use. At the beginning, the pipettes had to be filled from the back due to the fact that the tips have a very small diameter ("tip-filling"). A tube with a syringe was connected to the back of the pipette and the tip was placed into the pipette solution. *Via* soaking, the tip was filled with solution and through a thin custom-made plastic cannula the rest of the pipette solution was filled into the pipette from the back ("back filling"). Strong tapping against the side of the pipette removed any air bubbles. The pipette was fixed to a pipette holder and located around the measuring electrode. The solution in the pipette should cover the tip of the measuring electrode and not exceed a certain level. Otherwise liquid can leak into the flexible tube. With the aid of the flexible tube, a connecting valve and a syringe a high pressure was created on the pipette. The over-pressure maintained a continuous outflow of pipette solution which helped to prevent the pipette tip from becoming clogged by any particles in the bath solution. As soon as the pipette is placed into the bath solution, pipette resistance was calculated. It was calculated by the pClamp software, but can be also calculated using Ohm's law (application of a 5 mV pulse).

2.2.4.6. Electrodes

We used silver chloride (AgCl) electrodes as bath and measuring electrodes. Before the first use and as soon as AgCl electrodes appear polished, they have to be chlorinated. Chlorination was achieved by electrolysis. $Ag + Cl^- \leftrightarrow AgCl + e^-$

A clean electrode was connected to an anode of a DC voltage source and placed into 1 mM KCl. On the electrode surface silver was oxidized to Ag^+ and this reacted with the Cl^- ions to AgCl. We applied a current of 1 mA for chlorination.

2.2.4.7. Electrophysiology - Data analysis

The pClamp6 and pClamp10.2.software (2.1.4) were used for data acquisition. Current amplitudes were determined by using the difference between the peak current (I_{peak}) and the lowest current after 200 ms test potential (I_{low}). To exclude variability of cell size, current density was calculated using current amplitudes in picoamperes (pA) divided by cell capacitance in picofarads (pF). To show the reaction of the cell to different MANT nucleotides, data was plotted as current density over a 15 min time interval. Statistics and data analysis was achieved using GraphPad prism version 5.0.

3. Interaction of MANT-ITP with VC1/IIC2

3.1. Protein purification and crystallization

3.1.1. Protein purification of VC1

A substantial drawback of the VC1 protein purification was the low expression level of the protein. Initially, we tested several *E.coli* cell lines (JM109, Origami), but expression with BL 21 (DE3) yielded the best expression levels. The protein has a molecular mass of ~ 25 kDa. The first lysis did not liberate much protein. Therefore, second lysis was very important, but the VC1 protein amount was really low and not detectable in a Coomassie stained SDS-gel. To ensure that protein expression worked out well, a Western Blot with HIS-antibody was carried out at the beginning (8.1). After application of the supernatant to Talon column the protein was eluted using an imidazole gradient. As soon as ~3 ml of elution buffer had been applied to the column, the protein was eluted as shown in Figure 8.

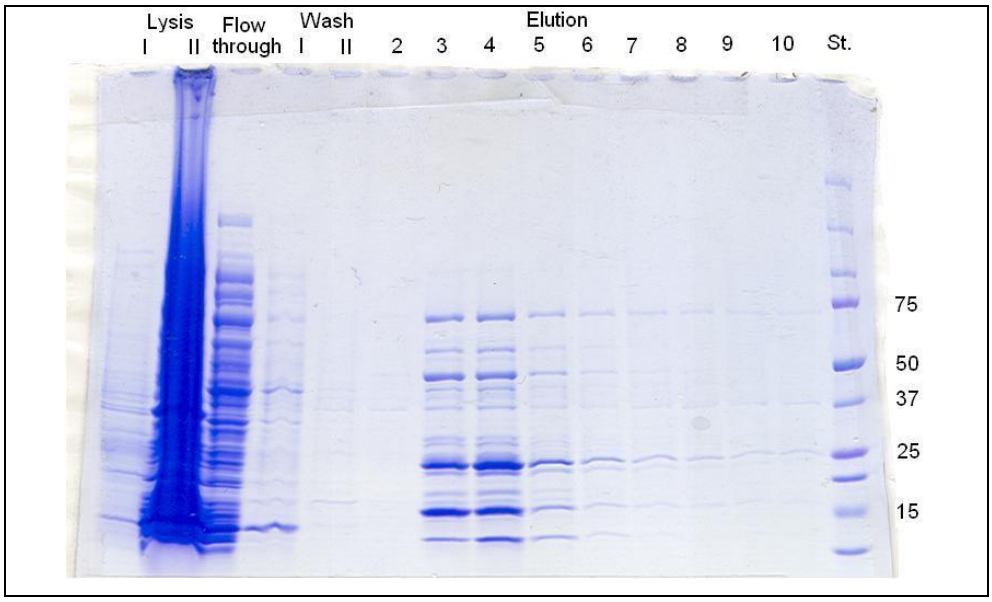

Figure 8. Lysis and Talon chromatography. The SDS-PAGE shows the cell lysis and the first step of protein purification. The second lysis step was necessary, because the first lysis did not extract a lot of protein. The elution fractions 3-6 were pooled together and applied to the second purification column. Unit for protein marker in kDa.

The Talon resin still binds many contaminants that are eluted together with VC1. They can be separated by using a cationic exchange column (Mono S 5/50 GL). Figure 9 shows that the protein band at ~ 23 kDa was eluted first, followed by pure VC1 protein. It is very important that the whole purification procedure was conducted under cold room-conditions (4°C) and in a short time interval of ~ 24 h. The purified protein was never frozen, but used immediately for making complex.

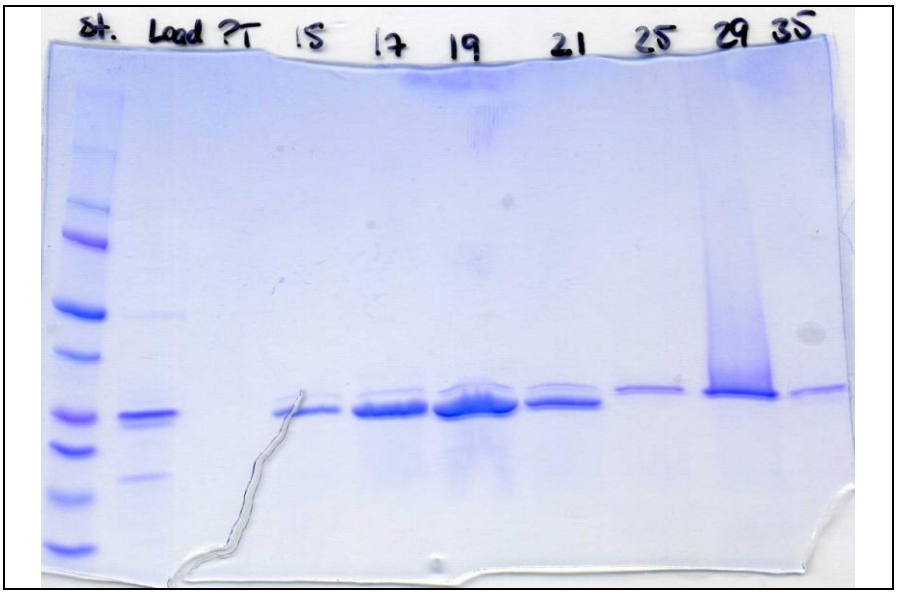

Figure 9. Ion exchange chromatography using a HiTrap Q/ Mono S column. The gel shows only fractions that were eluted from the Mono S column. The HiTrap Q column was bypassed. The last three lanes (fractions 25, 29, 35) show the pure VC1 protein separated from any contaminants (fractions 15-21).

3.1.2. Protein purification of IIC2

The tagless protein IIC2 is well expressed in BL21-pREP4 cells and can be detected at ~ 23 kDa using SDS-PAGE (Figure 10). Again, a lot of protein is still captured in the cells after the first lysis step. At the beginning, protein expression did not work and no protein could be detected in the crude cell lysate. Sequencing of the pQE60-ArgC-IIC2 plasmid identified a mutation in the promoter region that prevented the expression of the protein, but we could obtain new plasmid that did not carry this mutation.

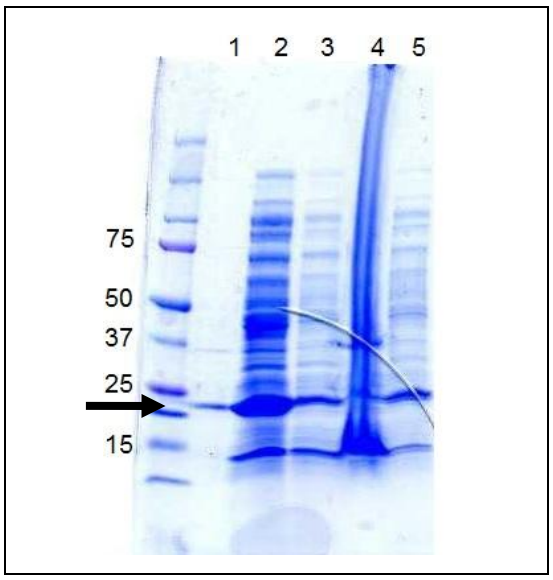

Figure 10. Lysis of IIC2.
IIC2, indicated by a black arrow, was well expressed and the second lysis step still released a big amount of protein.

Lane:
1 after homogenization
2 Lysis I
3 Lysis II
4 pellet
5 Loading of 1st column

Figure 11 shows that after 3 purification steps (anionic exchange, hydroxyapatite column and hydrophobic interaction) the protein was still contaminated.

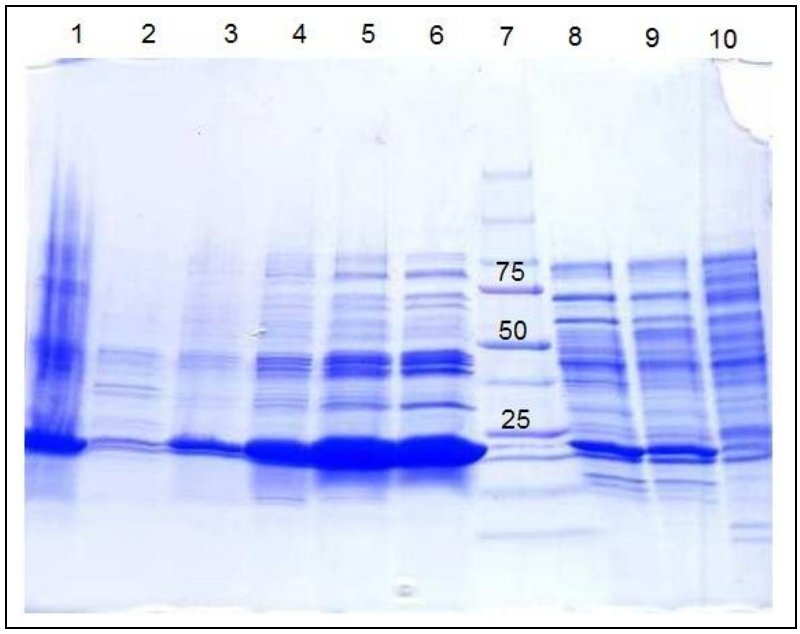

Figure 11. Chromatography with Phenyl column.
After three purification steps protein is still not totally pure.
Lane:

1	Loading
2	Pass through
3	Fraction #3
4	Fraction #5
5	Fraction #7
6	Fraction #9
7	Standard
8	Fraction #15
9	Fraction #16
10	Fraction #19

Therefore, anionic exchange chromatography was applied a second time and the purification quality was assessed by SDS Page (Figure 12). It was not possible to totally liberate the protein from all the contaminants, but the protein could be used ultimately for crystallization, because the contaminants do not disturb the formation of the complex and can be avoided by application of the complex to size exclusion chromatography.

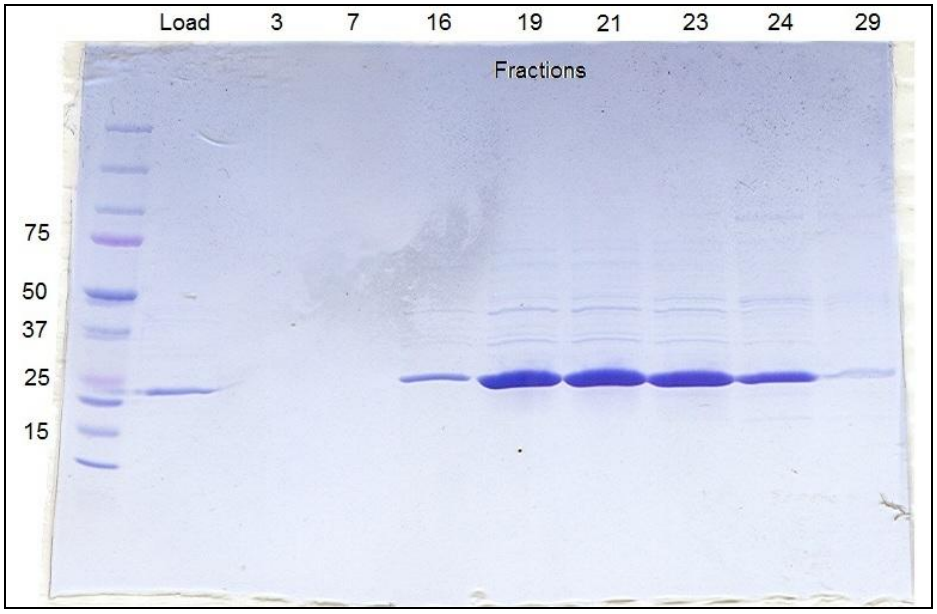

Figure 12. 2nd time Q Sepharose FF column 50 ml. Fractions 16 - 24 contain almost pure protein. The protein can be used for crystal growth, because the contaminants are insignificant.

3.1.3. Purification of $G_{s\alpha}$

Due to the fact that the crude lysate contained many contaminants besides $G_{s\alpha}$, not all of the protein was bound to the Ni-IMAC column. Therefore, pass-through and also the wash of the Ni-IMAC were applied a second time onto the Ni-IMAC column. The protein was already quite pure, when Ni-IMAC column was used as indicated by Figure 13.

To obtain a pure protein for trypsinization, anionic exchange and hydroxyapatite chromatography were additionally applied. The protein was loaded onto anionic exchange column after trypsinization and a pure GTPγS-activated $G_{s\alpha}$ (Gs_{tryp}) was obtained as shown in the last lane of Figure 13.

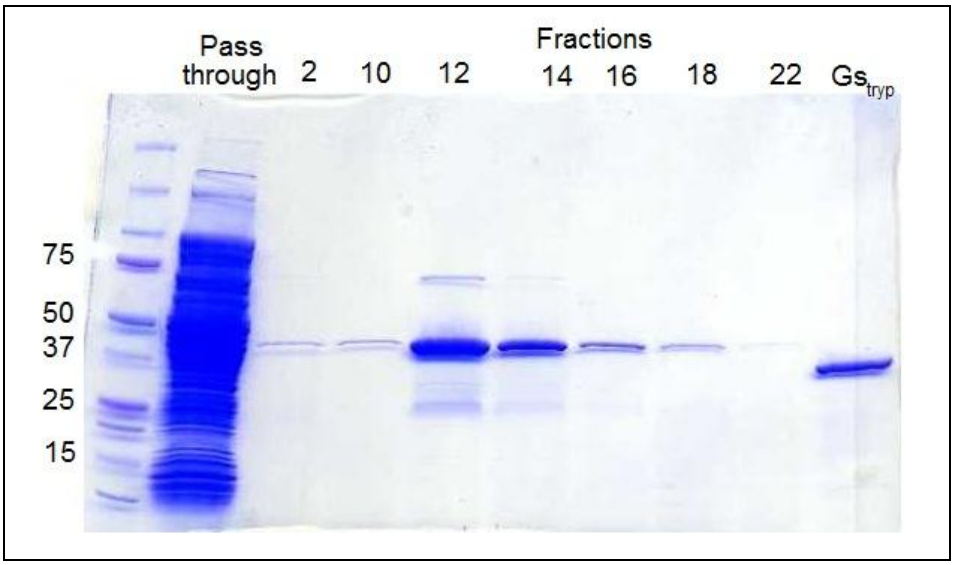

Figure 13. Ni-IMAC purification. The first purification step was repeated several times, because a lot of protein still stayed in the pass through and was not bound to the column. The protein was already quite pure (fractions 2-22). The last lane shows the trypsinized form of $G_{s\alpha}$.

Like VC1, protein expression and purification was also evaluated using Western Blot (8.1). These proteins were then used to setup the ternary complex for crystallization.

3.1.4. Crystallization of FS-stimulated AC complex

The ternary complex was formed as explained in Materials and Methods (2.2.2.1) and applied to gel filtration to separate the complex from single proteins. Figure 14 shows that some fractions (23-32) contain equal amounts of the 3 proteins, indicating the formation of the ternary structure. The chromatogram shows a clear peak at a time point that corresponds to the MW of the protein complex (~ 85 kDa).

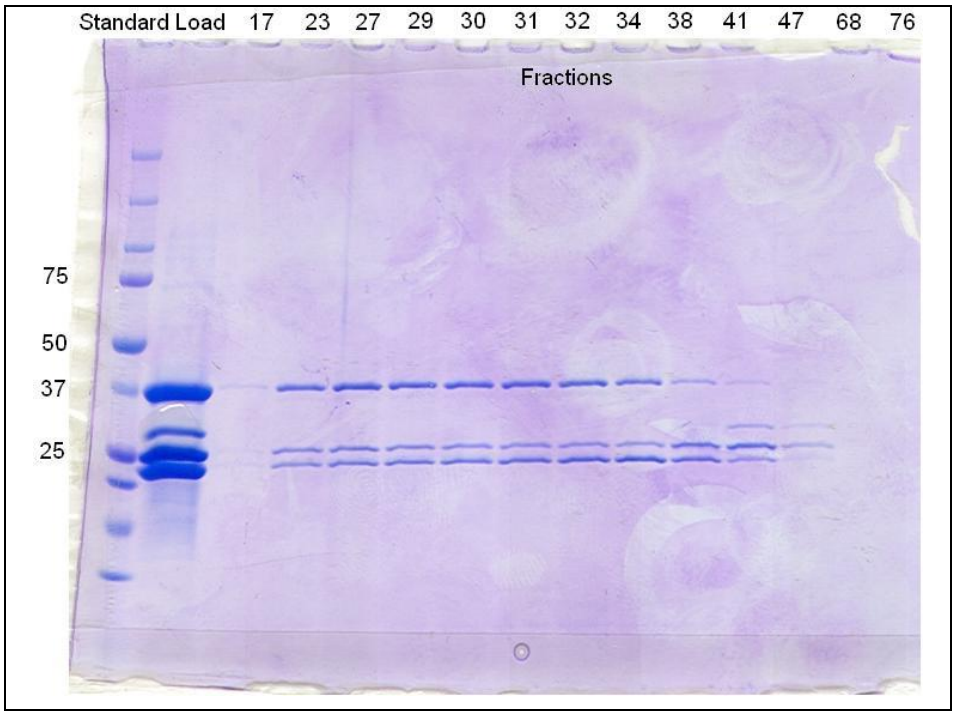

Figure 14. Gel filtration of ternary complex. The ternary complex of FS stimulated VC1-IIC2-$G_{s\alpha}$-GTPγS was formed and purified by size exclusion chromatography. Fractions 23 to 32 were pooled together. The concentrated complex was used to prepare crystal trays.

The protein complex was concentrated to ~ 8 mg/ml and used to setup crystal trays. After 3-4 weeks large crystals were obtained (Figure 15) that were soaked with MANT-ITP and TNP-GTP to study nucleotide-protein interaction. The crystals were plate-like and had a diameter of ~ 100 µm in the first two directions, but only 5-10 µm in c-axis. In order to gain structural information from the plate-like structure, we sent the crystals to the high-intensity X-ray beam light of the Stanford Synchrotron Radiation Lightsource (SSRL).

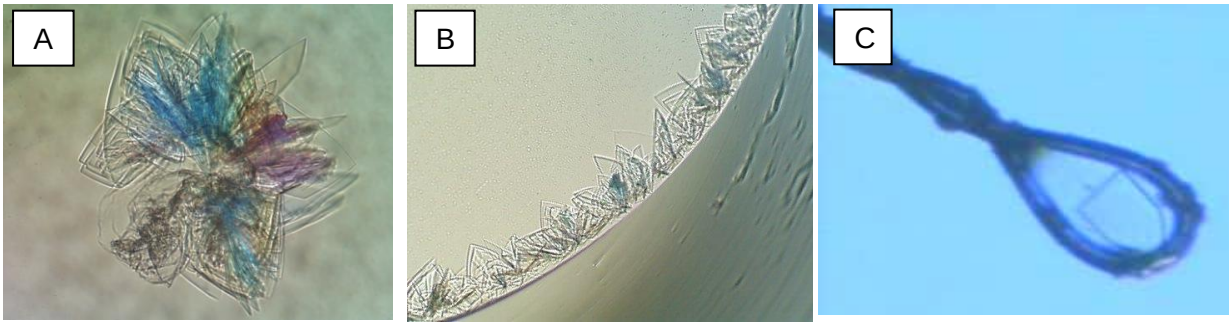

Figure 15. Crystals used for MANT-ITP-mAC-complex. Panel A shows a bunch of AC crystals in a hanging drop. B displays several crystals that grow on the surface of a sitting drop and panel C shows one crystal that was soaked with MANT-ITP, situated on a cryoloop and used for X-ray measurement in the SSRL.

Due to the fact that we also aimed at growing crystals with other FS analogs we tried several other crystallization options. Furthermore, we tried to apply MANT-ITP directly to the

protein solution, instead of soaking experiments with already crystallized FS-AC-complexes. One IIC2 mutant (K1014N) is known to stabilize the protein complex. Therefore, we prepared complexes with VC1-IIC2 K1014N-$G_{s\alpha}$, with and without FS. With FS we also obtained very large crystals that were used for X-ray measurements. However, when we mixed these three proteins together without FS and used MANT-ITP for co-crystallization, most of the protein complex precipitated. In contrast to FS, MANT-ITP did not stabilize the ternary complex. Therefore, we tried the crystallization of the FS-free complex without the addition of MANT-ITP. Several times the complex did not form properly, because a lot of protein precipitated and the SDS-PAGE after gel filtration did not show an equal ratio of the 3 proteins. But once, a ternary complex was formed and after 3 weeks some microcrystals were obtained. However, these crystals were too small for structure determination using the SSRL beam light.

We also tried to add FS analogs (1-deoxy-FS, 1,9-dideoxy-FS and 6-acetyl-7-deacetyl-FS) to identify the interactions of different FS analogs with the catalytic domains (Pinto *et al.*, 2009). All crystallization trials were unsuccessful, even though we obtained a pure protein complex (8.2). Due to the fact that FS analogs are very hydrophobic we had to add the FS analogs in DMSO or ethanol yielding a final solvent concentration of 2%. The procedure was the same as for obtained crystals that contain FS. It is possible that the solvent composition prevented the crystallization of the protein complex or that the complex with “inactive” FS analogs was not stable enough for crystallization.

The soaking experiments with TNP-GTP were successful and we could send some crystals for structure determination to the SSRL. TNP nucleotides are excited in the visible light range (λ = 405 nm) and have an orange color. The crystals showed an intensive orange color after 2 h of soaking at 25°C, confirming the presence of TNP-GTP (Figure 16).

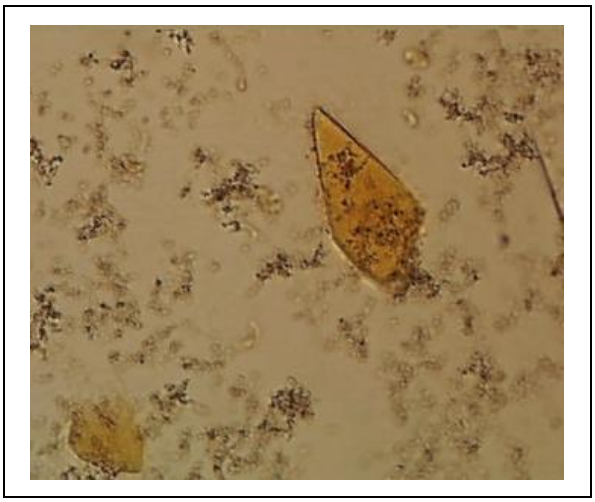

Figure 16. Crystal of FS/$G_{s\alpha}$ stimulated AC after soaking with TNP-GTP. The orange color was evidence for the presence of TNP-GTP in crystal.

However, even though analysis of the diffraction data gave us a resolution of 3.0 Å and completeness of 78%, we could only achieve partial electron densities around the phosphate groups of TNP-GTP in the AC binding pocket (Figure 17).

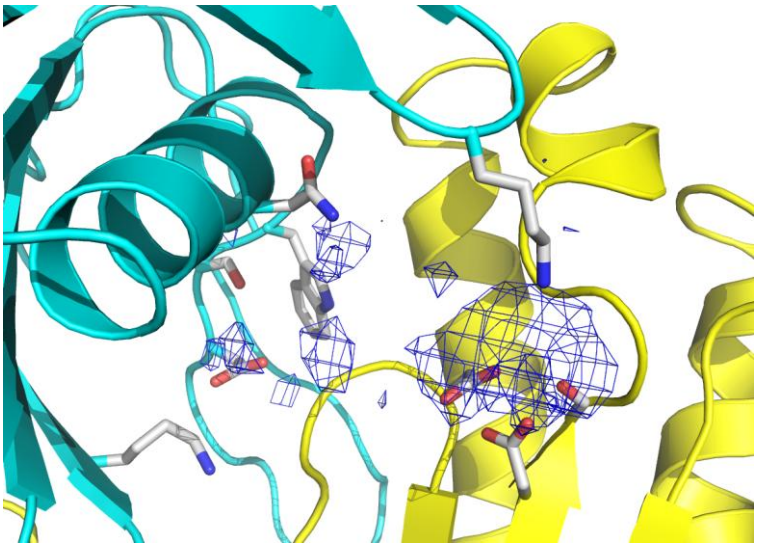

Figure 17. Difference electron density for TNP-GTP and Mn^{2+}. The *blue* wire represents the $|F_o|-|F_c|$ electron density for TNP-GTP and Mn^{2+} contoured at 2.5 σ. VC1 and IIC2 are shown as *yellow* and *cyan* helical structures. Important protein residues are shown as stick model (C-atoms *grey*, oxygen atoms *red* and nitrogen atoms are colored *darkblue*, respectively). The difference electron density is not sufficient for structure determination of TNP-GTP in the active site.

3.2. Crystal structure of FS-/$G_{s\alpha}$ activated VC1-IIC2 with MANT-ITP

For a better understanding of the high inhibitory potency of MANT-ITP at ACs 1, 2 and 5 as well as at the catalytic domains VC1/IIC2 (Table 2, 1.5.1.1), crystallographic studies were conducted. The structure was determined by X-ray diffraction using the VC1-IIC2-$G_{s\alpha}$-GTPγS crystals soaked with 2 mM MANT-ITP and 3 mM $MnCl_2$ (2.2.2.3). The crystal structure of MANT-ITP:Mn^{2+} was determined up to a resolution of 3.1 Å. The crystallographic data collection and refinement statistics are summarized in Table 3. The coordinates for the MANT-ITP:Mn^{2+} structure were deposited in the Protein Data Bank with the code 3G82.

Parameters	MANT-ITP:Mn^{2+}
Cell constants (Å)	
a	117.6
b	133.4
c	70.6
No. of crystals	1
D_{min} (Å)	3.1
Average redundancy	3.0 (1.8)[a]
R_{sym} (%)[b]	17.9 (34.5)
Completeness (%)	81.4 (55.1)
‹I›/‹σ›	4.5 (1.7)
Resolution range for refinement (Å)[c]	15-3.1
Total reflections used	15824
No.of protein atoms	5645
No. water molecules	5
No. ligand atoms	106
rmsd bond length (Å)	0.007
rmsd bond angle (°)	1.21
R_{work} (%)[d]	24.1
R_{free} (%)[e]	29.4
Average B-factor (Å^2)	45.2

Table 3. Summary of crystallography data collection and refinement statistics.

[a] numbers in parentheses correspond to the statistic data from the highest resolution shell.
[b] $R_{sym} = \sum_h \sum_i | I(h) - I(h)_i | / \sum_h \sum_i I(h)_i$, where $I(h)$ is the mean intensity after rejections.
[c] Due to anisotropy, data with an *I* index greater than 21 were omitted from refinement.
[d] $R_{work} = \sum_h ||F_o(h)| - |F_c(h)|| / \sum_h |F_o(h)|$, $F_o(h)$ and $F_c(h)$ are the observed and calculated structure factors, respectively.
[e] 5.1% of the complete data set was excluded from refinement to calculate R_{free}

The statistics show that only 5 water molecules could be detected, based on the resolution of 3.1 Å. The structure shows $G_{s\alpha}$ protein that carries GTPγS in the nucleotide binding pocket and interacts primarily with the IIC2-subunit. The catalytic domains VC1 and IIC2 have the already mentioned pseudo-symmetric arrangement (Tesmer *et al.*, 1997). The two subunits form a very large interface between each other, facilitating the binding of FS and MANT-ITP. FS is situated at the end of the cleft between VC1 and IIC2 that is closer to $G_{s\alpha}$. Meanwhile MANT-ITP is bound to the catalytic site that converts ATP to cAMP, located

on the other site of the VC1:IIC2 interface. Figure 18 illustrates an overview of the ternary complex.

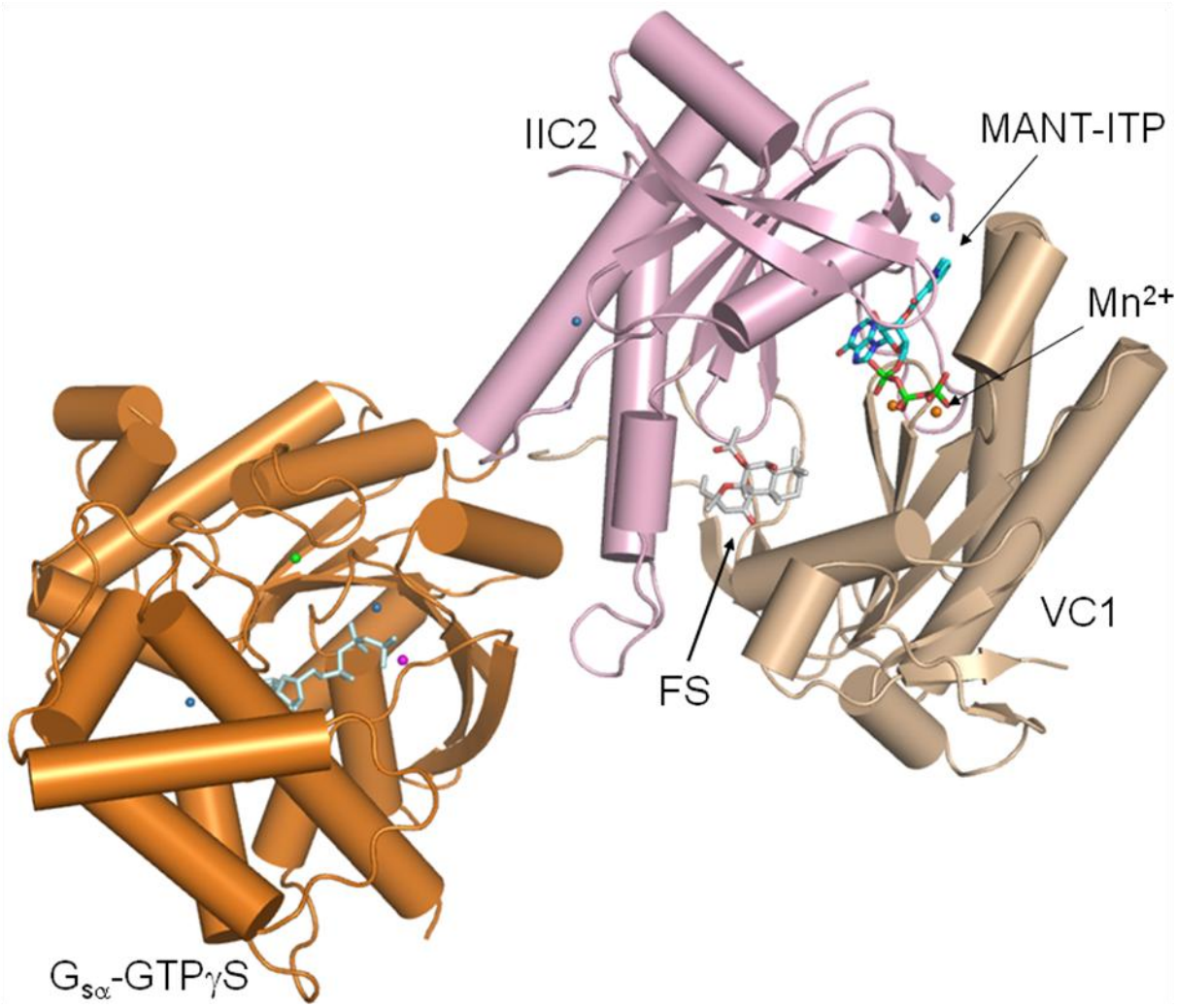

Figure 18. Structure of $G_{s\alpha}$-GTPγS and FS-activated catalytic domains VC1:IIC2.

VC1 and IIC2 are colored *wheat* and *lightpink*, respectively. The $G_{s\alpha}$-domain is colored *orange* and carries GTPγS. GTPγS, FS and MANT-ITP are shown as stick models. The former two ligands are colored in *grey*, the oxygen atoms of FS are shown in *red*. MANT-ITP carbon atoms are *cyan*, nitrogen atoms are *darkblue*, oxygen atoms are *red*, and phosphorus atoms are *green*. The two Mn^{2+} ions are shown as *orange* spheres. Water molecules are drawn as *blue* spheres, Mg^{2+} ion interacting with the phosphate group of GTPγS is shown as *pink* sphere and one chloride ion is shown as *green* sphere.

MANT-ITP was modeled into the continuous $|F_o|-|F_c|$ map in the binding pocket using the structure of the $G_{s\alpha}$-GTPγS:VC1:IIC2 complex as the initial phasing model (Tesmer *et al.*, 1997) (PDB code: 1AZS). The conformation of the 3'-O-MANT-ITP is more in agreement with the electron density than that of the 2'-O-MANT-ITP (Figure 19 A). The two diffuse blue colored lattices in the difference electron density map are corresponding to the two Mn^{2+} ions where the A-site is weaker than that for the B-site suggesting the Mn^{2+} ion at the B-site is more stable than that at the A-site, similar to other ligands observed in mAC crystal structures (Mou *et al.*, 2005; Mou *et al.*, 2006).

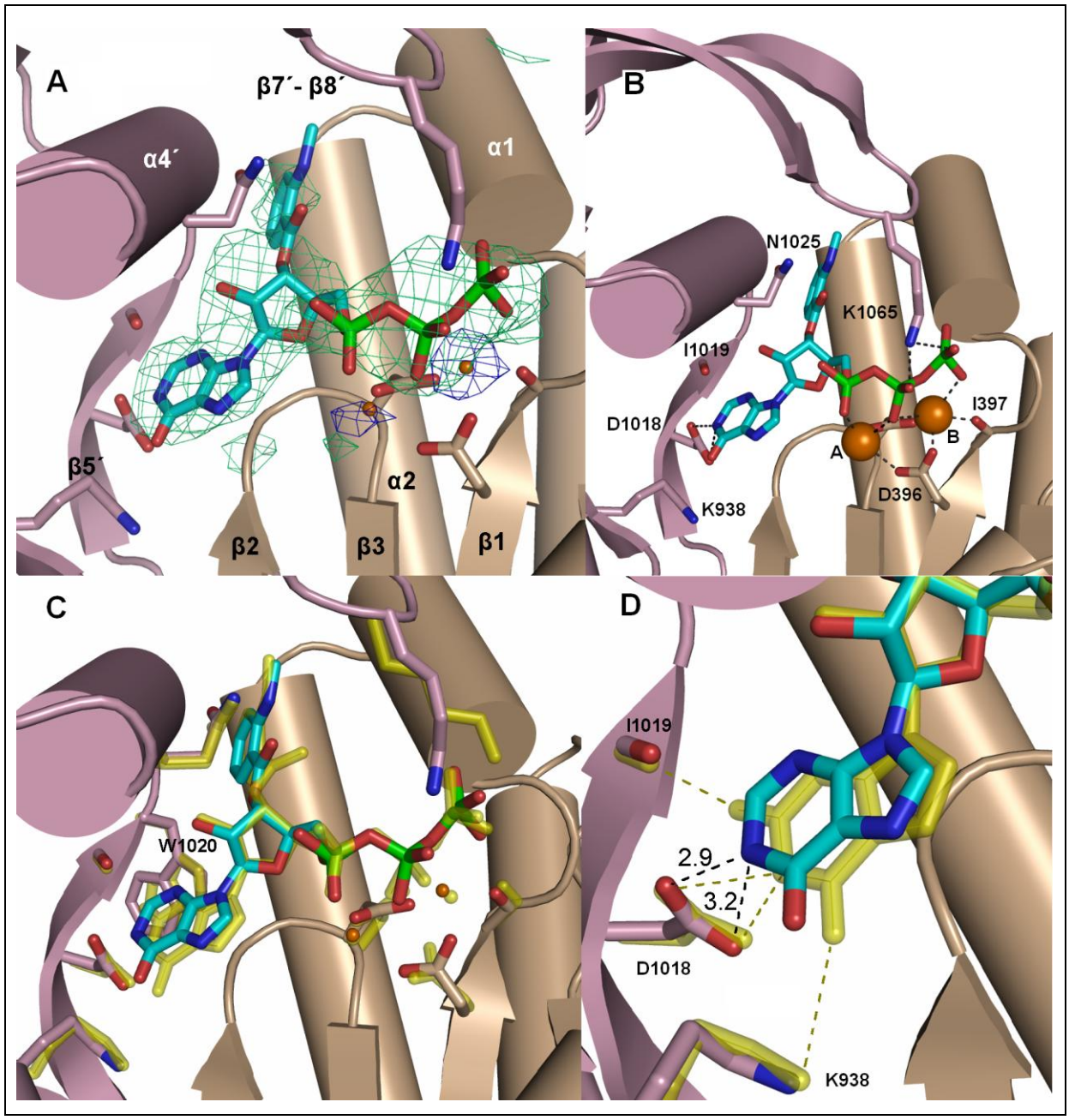

Figure 19. Crystal structure of $G_{s\alpha}$/FS-activated mAC with MANT-ITP and two Mn^{2+} ions in the catalytic site. MANT-ITP and two metal ions are bound in the cleft between the soluble domains C1a and C2a. The coloring scheme of figures A-D is: VC1 and IIC2 are colored *wheat* and *violet*, respectively. MANT-ITP is shown as stick model, carbon atoms are *cyan*, nitrogen atoms are *darkblue*, oxygen atoms are *red*, and phosphorus atoms are *green*. The two Mn^{2+} ions are shown as *orange* spheres. **A, *Difference electron density for 3´-O-MANT-ITP and Mn^{2+}***. The *lime green* wire represents the $|F_o|-|F_c|$ electron density for MANT-ITP contoured at 2.5 σ. The *blue* wire corresponds to the $|F_o|-|F_c|$ electron density for the two Mn^{2+} ions contoured at 5 σ. The coordinates for the ligands were omitted from the phasing model. The secondary structure elements of the complex are labeled as defined previously (Tesmer *et al.*, 1997). **B, *Detailed view of substrate-binding site of VC1:IIC2 with MANT-ITP:Mn^{2+}***. The catalytic site of VC1:IIC2 shows MANT-ITP, A- and B- site of two Mn^{2+} ions and the protein residues that are responsible for ligand interaction. The interaction among protein residues and MANT-ITP, Mn^{2+} are shown as *gray dashed lines.* **C, *Superimposed crystal structures of 3´-O-MANT-ITP and 3´-O-MANT-GTP.*** The derived MANT-ITP crystal structure was superimposed and compared with the crystal

structure of MANT-GTP, shown as a transparent *yellow* stick model (Protein Data Bank code 1TL7) (Mou *et al.*, 2005). The protein residues are in almost identical conformation and the inhibitors are situated in the substrate-binding pocket in a similar fashion. **D, *Superimposed purine binding site of 3´-O-MANT-ITP and 3´-O-MANT-GTP.*** The interaction of the hypoxanthine ring and guanine ring of MANT-ITP and MANT-GTP are shown as *black* and *olive green* dashed lines, respectively. The distances of hydrogen bond between the hypoxanthine ring and surrounding protein residues of MANT-ITP are indicated in Å. The hydrogen bond between I1019 and the amino group of MANT-GTP is missing in the MANT-ITP structure. K938 and the oxygen of the hypoxanthine ring are further apart (3.77 Å *versus* 3.4 Å). The hypoxanthine ring has less binding constraint in the purine binding pocket in comparison to the guanine ring of MANT-GTP.

The structure was compared to the crystal structure of mAC with MANT-GTP for differences in binding mode because these two analogs are structurally very similar (Mou *et al.*, 2005) (PDB code 1TL7). Superimposing both structures the overall placement of VC1 and IIC2 did not differ greatly from each other with the RMSD less than 0.5 Å (Figure 19 C).

The overall MANT-ITP conformation was similar to the MANT-GTP in the mAC structure having similar H-bond interactions as well as metal ion coordination with the protein residues (Figure 19 B and D). The $|F_o|$-$|F_c|$ electron density map for MANT-ITP was well defined and showed clearly that there is no obvious conformational difference between the two ligands. Therefore we looked for minor differences in the very similar binding mode of MANT-ITP and MANT-GTP. One noticeable difference is that the hypoxanthine ring of MANT-ITP lacks an amino group that could form a hydrogen bond with the side chain of I1019 of IIC2-domain (MANT-GTP 2.6 Å; Figure 19 D). We checked if a conformational inversion of the hypoxanthine ring in the base binding pocket, which would lead to a stronger interaction with D1018 and W1020, could explain the higher affinity of MANT-ITP. However, this conformation was not favored by the ligand, because the ribose moiety was sterically hindered. The decreased interaction in the purine binding site for MANT-ITP would apparently lead to lower binding strength between the MANT-ITP and mAC protein. However, the observed difference in the purine binding pocket between MANT-ITP and MANT-GTP structures are contradictory because we observed a higher inhibitory potency of MANT-ITP on mAC compared to MANT-GTP (Table 2, 1.5.1.1).

Thus, it appears that other interaction sites of MANT-ITP with the mAC are more important for the high affinity. The average temperature factor (B-factor) of the bound FS and GTPγS between these two structures is similar, but the B-factor of MANT-GTP is higher than that of MANT-ITP (the B-factor of MANT-GTP and MANT-ITP is 55 and 41, respectively), indicating a more restricted degree of freedom of MANT-ITP and a well predicted location of the molecule in the binding pocket. The high inhibitory potency of MANT-ITP may, therefore, be related to a more complicated binding energy distribution. The binding affinity of the MANT nucleotide is dependent on the three binding groups in the catalytic pocket –

interacting with base-binding site, phosphate-binding site and MANT-binding site. The lower binding constraint of MANT-ITP in the purine binding pocket could lead to a higher affinity of the molecule for the hydrophobic MANT-binding site and the phosphate binding site.

The stronger hydrophobic interaction of MANT-ITP can be assessed by fluorescence spectroscopy, both basal direct fluorescence and FRET of MANT-ITP are increased at least 50% compared to MANT-GTP. If we compare these results with another very similar MANT nucleotide, MANT-XTP, we see almost no increase in direct fluorescence or FRET (Figure 4, 1.5.1.2). Compared to MANT-ITP and MANT-GTP, MANT-XTP is at least 60-fold less potent on VC1/IIC2 (Table 2, 1.5.1.1). It has oxygen on the C2-position of the purine ring that introduces a repulsion force on D1018 in the base-binding pocket and may move the MANT-group away from the hydrophobic pocket, leading to strong decrease in inhibitory potency and fluorescence properties.

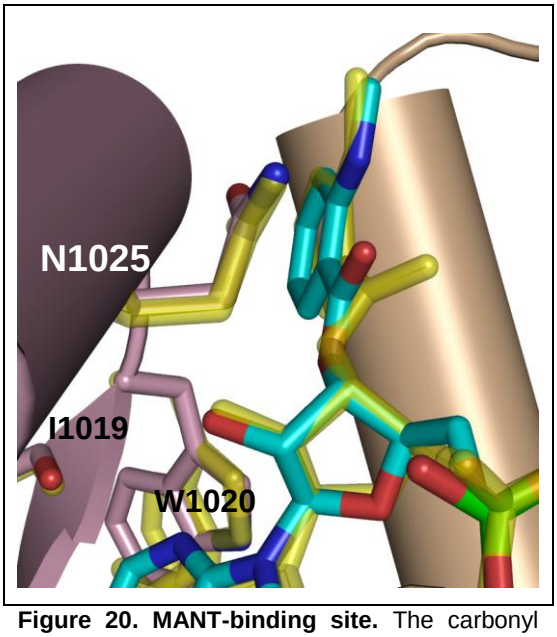

Figure 20. MANT-binding site. The carbonyl group of MANT-ITP is in closer contact to N1025. Apart from that no conformational differences between MANT-ITP and MANT-GTP are detected.

In the crystal structure the location of the MANT-group of MANT-ITP and MANT-GTP form similar interactions at the interface of α4'-α1-domain. The aryl function of MANT has hydrophobic interaction with A409, L412, V413, V1024, V1026 and W1020. The oxygen of the carbonyl group of MANT-ITP moved in closer proximity to N1025 compared to MANT-GTP (Figure 20). Interestingly, this oxygen is very close to the carbonyl oxygen of the N1025 side chain (2.77 Å), introducing a repulsion force. A 180° rotation of the amide group of N1025 (NH_2-C=O instead of O=C-NH_2) would form much better interactions between the MANT-group and N1025 (hydrogen bond between amino group of N1025 and oxygen of MANT-ITP as well as with the carbonyl oxygen of G1021). We tried to reverse the obtained conformation to achieve H-bonding between MANT-ITP and N1025. However, after every round of refinement the amide of N1025 flipped back to its original, entropically favored location. The same event happened during Molecular Dynamics (MD) simulations. It has to be mentioned that the $|F_o|$-$|F_c|$ electron density is not very strong for the MANT-moiety, suggesting that it is poorly ordered within the binding site (Figure 19 A).

A stronger interaction of MANT-ITP with the phosphate binding site is supported by two observations. The side chain K1065 of IIC2 interacts with the β- and γ-phosphate of MANT-ITP, whereas the amino group of K1065 in the MANT-GTP structure is only orientated

towards the γ-phosphate (Figure 19 C). The amino group of K1065 is also significantly closer to the oxygen of the β-phosphate of MANT-ITP (2.86 Å) in comparison to the oxygen of the γ-phosphate of MANT-GTP (3.06 Å). However, we have to be careful about the interpretation of the interaction of the K1065 side chain with the phosphate group. Unfortunately, the resolution of the MANT-ITP structure is below 3 Å, and this can introduce errors in structure determination (up to +/-0.3 Å). Furthermore, the electron density of K1065 side chain was not well defined and we showed the energetically most favorable conformation after several rounds of structure refinements. It is, therefore, possible that the side chain does not differ as much as is expected by our model. MD simulations support the crystallographic data. During the 10 ps simulation the distance between the amino group of K1065 and the gamma phosphate is effectively identical with 3.04 ± 0.11 Å and 3.05 ± 0.12 Å for MANT-GTP and MANT-ITP, respectively. In contrast, the distance of the β-phosphate of MANT-ITP and K1065 (3.69 ± 0.14 Å) is significantly smaller than for MANT-GTP (4.15 ± 0.28 Å).

Another interesting interaction in the phosphate binding site is visible between MANT-ITP phosphate groups and D396. On first glance, it looks contradictory that the carboxyl group of D396 does have closer interaction to the phosphate oxygen group of MANT-ITP (2.73 Å) in comparison to MANT-GTP (3.2 Å), introducing electrostatic repulsion. But this amino acid is also important to coordinate the two metal ions that are important for phosphate interaction with the protein residues of VC1 (D396, I397 and D440) (Figure 19 B). Due to the fact that D396 and MANT-ITP are in closer proximity to each other they introduce differences in metal coordination for MANT-ITP and MANT-GTP. With the different arrangement of the two metal ions to the phosphate groups we recognize that the Mn^{2+} ions in the MANT-ITP structure have more interaction with the α- and γ-phosphate whereas in the MANT-GTP structure the Mn^{2+} ions seem to focus on the β-phosphate (Figure 21).

It also appears that the gap between the phosphate groups and the important VC1-residues is much smaller in the MANT-ITP structure, because there is also a closer proximity between I397 and the γ-phosphate of MANT-ITP (2.86 Å) in comparison to MANT-GTP (3.38 Å). The phosphate site plays a crucial role for binding affinity. This is further assessed by changes in potency due to differences in the phosphate moiety. As soon as a phosphate group is missing there is a strong decrease in potency; MANT-GTP has ~ 70-fold higher affinity at VC1/IIC2 in comparison to MANT-GDP (Gille *et al.*, 2004). Furthermore, affinities are influenced by substitution of oxygen for sulfur at the γ-phosphate. MANT-ITPγS has a decreased potency at recombinant ACs in comparison to MANT-ITP, maybe because sulfur introduces a repulsion force. In contrast, MANT-GTPγS and MANT-ATPγS have a higher affinity in comparison to the corresponding MANT-NTPs (Table 2, 1.5.1.1).

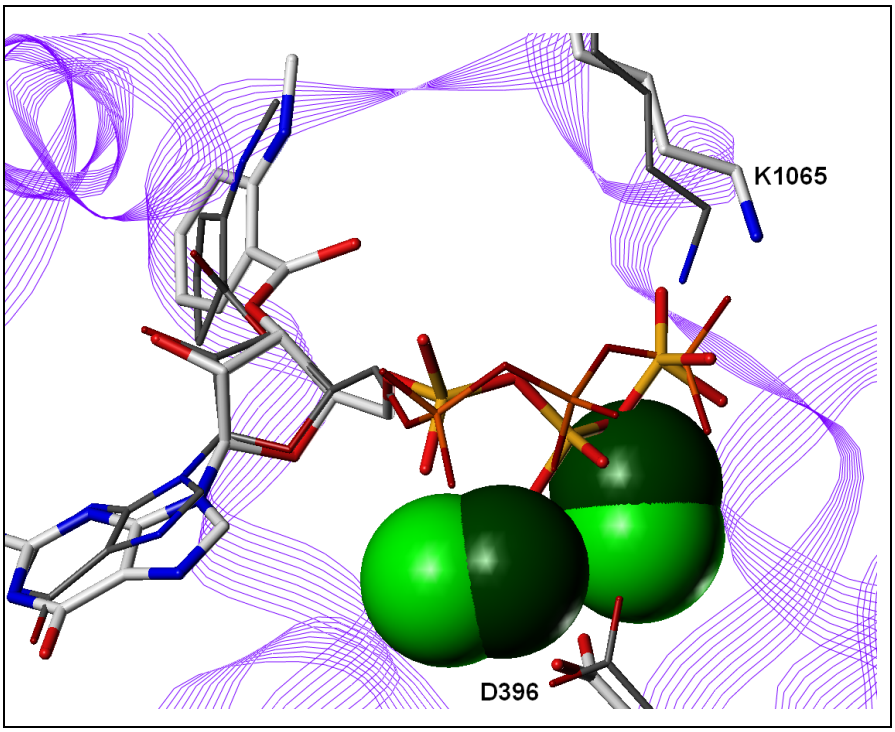

Figure 21. Phosphate binding site of mAC. The graphic is based on the two crystal structures and shows the relative positions of K1065 and the kinking in the phosphate chain. Note that MANT-ITP is represented by thinner, darker sticks than MANT-GTP. The phosphate chain of MANT-GTP is more bended in comparison to MANT-ITP. The Mn^{2+} ions are shown as large spheres to illustrate the differences between MANT-GTP (*light green* spheres) and MANT-ITP (*dark green* spheres). The Mn^{2+} ions of MANT-ITP are distributed between the phosphate groups.

3.3. Discussion

We have resolved the mAC crystal structure with the most potent competitive inhibitor known so far and assume that a balance of binding energies among the three pharmacophores in the mAC binding site considerably affects ligand potency. First of all, we could show that the MANT-ITP structure shares the common features with previously published mAC structures in complex with 2',3'–substituted purine and pyrimidine nucleotide inhibitors, where the base, triphosphates and 2',3'-ribose substituents reside in three distinct grooves of the substrate-binding site (Mou *et al.*, 2006). The overall conformations of MANT-ITP and MANT-GTP show minimal differences. This result is not surprising. The crystal structures were derived with a racemic mixture of 2'-O- and 3'-O-MANT-ITP. Both structures favor the 3'-O-MANT-conformation for binding to the catalytic center as shown with the MANT-GTP crystal (Mou *et al.*, 2005). The strong $|F_o|-|F_c|$ electron density in the gap of N1025 and the 2'-OH-group of MANT-ITP could indicate that it can also bear the 2'-O-MANT isomer. However, the orientation of the other functional groups cannot be accommodated in

the experimental electron density with the same good quality. The better fit of the 3'-O-MANT isomer is further explained by the better fit of the 2'-OH group at the interface of IIC2.

A very intriguing finding was the subtle difference in binding mode of MANT-ITP at the purine-binding site in comparison to the high inhibitory potency of the nucleotide. Usually, high inhibitory potency is accomplished through strong binding of the inhibitor to the active site of the enzyme. Hence, there have to be strong protein-ligand interactions. In our case, there was actually less protein-ligand interaction due to a missing hydrogen bond. Nonetheless, it was already shown in several publications that a gain in affinity is not only related to the number of hydrogen bonds, but also to hydrophobic interactions, residual mobility of the ligand and partial solvation of the binding pocket (Gohlke and Klebe, 2002). The loss of hydrogen bonds does not necessarily lead to a decrease in binding affinity of a ligand to a protein as assessed by molecular thermodynamic and crystallographic studies of thermolysin inhibitors (Morgan *et al.*, 1991). Binding of those inhibitors is, therefore, not only dependent on hydrogen bonding, but also on metal coordination and higher ligand basicity (Grobelny *et al.*, 1989). In the MANT-ITP structure, the loss of hydrogen bonding is negligible for an increase in affinity.

Comparing three different MANT/TNP inhibitors and their structural variations in the binding pocket already revealed that hydrogen bonds to the base seem to have small contribution to interaction strength (Mou *et al.*, 2006). SVD (Singular value decomposition) calculation was used to compare the contribution of the three different pharmacophores for inhibitory potency and it showed that the 2',3'-ribosyl substituent contributes much more to inhibitory potency than the phosphate groups and the least contribution was made by the base variations (Figure 22). However, hypoxanthine substitution increases ligand affinity by 10-fold compared to guanine substitution and improves interaction with the catalytic site as assessed by fluorescence spectroscopy. The base substitution plays a role in inhibitory potency, as soon as repulsion forces in the purine binding pocket lead to a strong decrease of the nucleotide potency which also affects hydrophobic interactions, as shown with MANT-XTP (Figure 4, 1.5.1.2) and MANT-ATP (Mou *et al.*, 2006). The fluorescence data support our hypothesis that between the various MANT nucleotides there are subtle differences in binding of the MANT-group to the hydrophobic pocket. If MANT-ITP is subjected to less binding constraints in the purine-binding pocket compared to MANT-GTP, it can better move into the hydrophobic regions of the MANT-binding site, which is associated with higher fluorescence signals.

Besides of the strong hydrophobic interactions, MANT-ITP seems to bind more tightly into the phosphate binding pocket. The metal coordination of the phosphate groups in the

phosphate binding site of VC1 is very important for the high inhibitory potency of MANT-ITP. The relative electrostatic energies of the triphosphate - metal complex, ignoring all the other substituents (such as base, sugar, MANT-group) are almost identical for MANT-ITP and MANT-GTP with -254 kcal/mol and -253.9 kcal/mol, respectively. However, the bond/angle strain in the MANT-GTP β-phosphate is much higher (64.9 kcal/mol) than in the MANT-ITP one (49.5 kcal/mol). This indicates that the MANT-GTP phosphate groups are significantly kinked in comparison to MANT-ITP (Figure 21). The average temperature factor of MANT-ITP:Mn^{2+} is lower than that of MANT-GTP:Mn^{2+} and also much lower than MANT-ATP and TNP-ATP:Mn^{2+}, which indicates that MANT-ITP is much more ordered in the crystal structure than the other three ligands. It is also possible that the high B-values reflect only partial occupancy of the catalytic site of VC1:IIC2, especially by the latter two ligands (Mou *et al.*, 2005; Mou *et al.*, 2006).

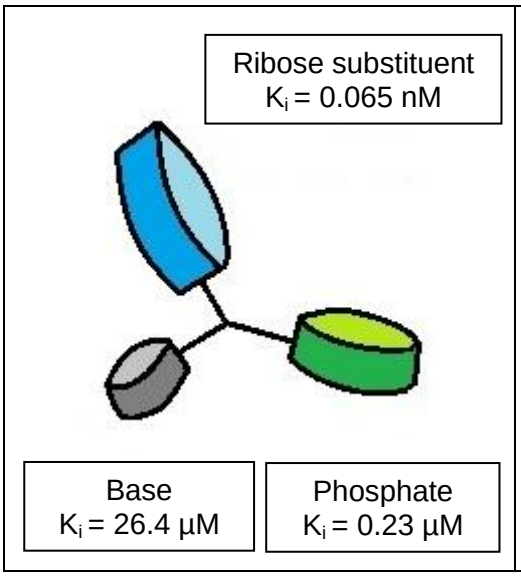

Pharmacophore	Component	K_i* (µM)
Base	Adenine	2.9
	Guanine	48.9
	Cytidine	175
	Uracil	110
	Hypoxanthine	4.6
	Xanthine	247,000
Ribose substituent	MANT	(0.014 ± 0.001)
	TNP	0.003
Phosphate	Monophosphate	371,000
	Diphosphate	443
	Triphosphate	0.06
	[γ-Thio]-triphosphate	0.45

Figure 22. General pharmacophore model of 2',3'-ribose-substituted mAC inhibitors. The model shows the three functional groups, nucleotide base (*grey*), phosphate group (*green*) and 2', 3'-ribose substituent (*blue*). SVD analysis calculated overall K_i values that represent the contribution of each functional group (on the left side) and K_i* values (on the right side) that indicate the contribution of individual components (Mou *et al.*, 2006).

Finally, we compared the MANT-ITP crystal structure with the MANT-ATP crystal structure, PDB code 2GVZ. SVD analysis calculated a high contribution of the adenine group; hence MANT-ATP was first expected to be the most potent MANT nucleotide (Mou *et al.*, 2006). However, exchange of hypoxanthine by adenine caused a decrease in potency by at least 60-fold (Table 2, 1.5.1.1). Superimposing both crystal structures showed that MANT-ITP and MANT-ATP adopt the same conformation in the binding pocket between the C1:C2 interface. However, one obvious difference is visible in the purine binding site: The hypoxanthine ring of 3'-O-MANT-ITP adopts an *anti* conformation with respect to the ribosyl

residue that allows interaction with K938 and D1018 (Figure 19 D and 23 A). Meanwhile, MANT-ATP does not form hydrogen bonds in the purine binding pocket and interacts with mAC by weak hydrophobic interactions (F889, L438 and I940). In contrast to MANT-ITP, the adenine ring is situated in the purine binding pocket in *syn* conformation and introduces electrostatic repulsion on D1018 leading to a strong decrease in potency (Figure 23 B).

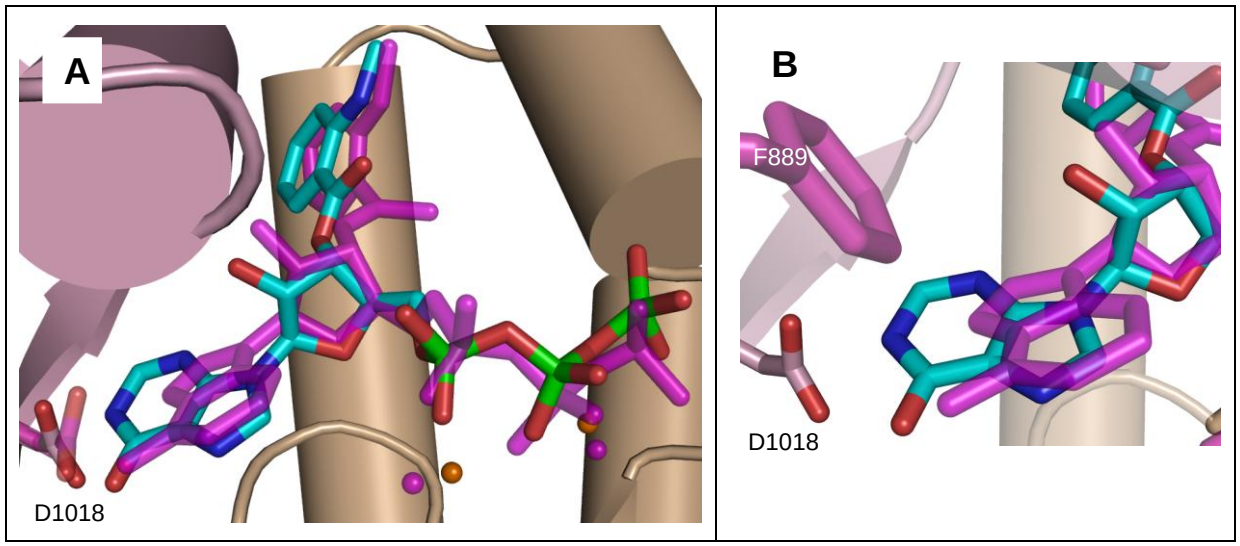

Figure 23. 3'-O-MANT-ITP *versus* *3'-O*-MANT-ATP crystal structure (PDB 3G82 and 2GVZ). Coloring scheme of VC1, IIC2 and MANT-ITP adopted from Figure 19. MANT-ATP is shown as *magenta* stick model. Figure 22 B shows the *anti* and *syn* conformation of the purine rings of MANT-ITP and MANT-ATP, respectively and the important proteins residues within 3 Å that interact with the ligands.

It should be mentioned that differences in inhibitory potency are not only restricted to direct protein-ligand interaction, but also to interaction with bound water molecules. Unfortunately, the resolutions of MANT-ITP and MANT-GTP crystal structures are not sensitive enough and, therefore, the detection of water molecules is poor. Another explanation for the higher inhibitory potency of MANT-ITP could be the possibility of another ligand conformation in the purine binding site that is not resolved with the obtained X-ray data.

In conclusion, our data could corroborate the three-site pharmacophore model (Figure 22) already postulated in previous studies (Mou *et al.*, 2005; Mou *et al.*, 2006). The contribution for binding differences could be assessed with very accurate structural information of the complex, however, sometimes further evaluation of catalytic activity and fluorescence are necessary to understand contradictory binding affinities.

4. Effects of MANT nucleotides in cardiomyocytes

4.1. Cardiomyocyte preparation

The cardiomyocyte preparation is influenced by many parameters, like temperature of the Langendorff apparatus, composition of the solution and digestion with collagenases. Especially the collagenases (CLS) can vary in their activity as indicated in Table 4.

Set	Composition	Batch	CLS Activity (U/mg)	Caseinase activ. (U/mg)	Clostripain activ. (U/mg)	Tryptic activ. (U/mg)	Cell yield
I	Collagenase 1 Collagenase 2	X6C8693 46H8900	191 200	392 545	3.4 4.3	0.3 0.3	**Good**
II	Collagenase 1 Collagenase 2	S5K8219 S9H11286	230 240	350 360	2.31 4.37	0.35 0.81	NON
III	Collagenase 1 Collagenase 2	S9C11129 S8P10943	250 360	275 560	1.86 4.23	0.44 0.67	NON
IV	Collagenase 1 Collagenase 2	S5P8401 M8B10274	172 210	204 440	1.5 4.0	0.26 0.22	**Good**
V	Collagenase 1 Collagenase 2	S8B10327 S8N10850	210 230	370 515	2.2 4.21	0.18 0.29	FEW

Table 4. Collagenase sampling. Because of lot-to-lot variations it was necessary to pre-test particular enzyme lots. Different collagenase batches were tested at least two times under equal assay conditions to select the best combination for cardiomyocyte preparation. Collagenase lots with a high tryptic activity showed only small cell yields or no living cell at all.

We carefully examined the cardiomyocytes after digestion and used only freshly isolated cells for electrophysiological measurements that were rod-shaped and showed a clear striation as shown in the following figure (Figure 24).

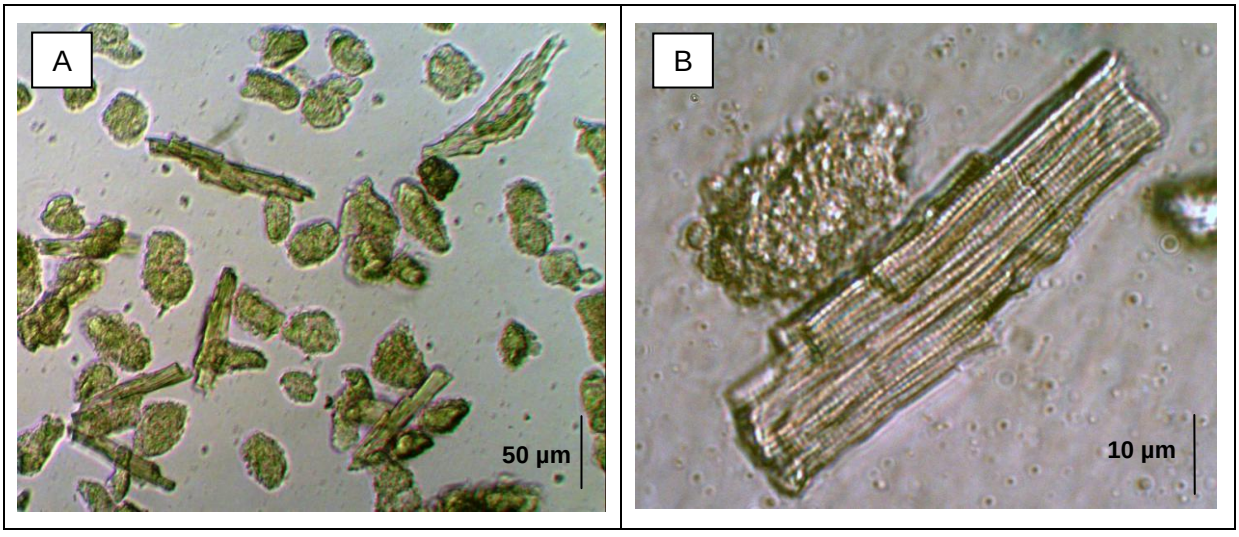

Figure 24. Cardiomyocyte micrographs. These pictured cardiomyocytes were taken for measurements. Micrograph A shows several cells in 200-fold magnification, B shows one single cardiomyocyte that has clear striation and a "log"-kind shape. C illustrates a cell shortly before seal formation. The light reflection from the pipette tip is clearly visible in the middle of the cell. Pictures taken with a DMC 510 microscope camera.

4.2. Effect of MANT nucleotides on basal L-type Ca^{2+} current

It was already shown in cardiomyocytes that MANT-GTPγS elicited an inhibitory effect on basal as well as isoprenaline-stimulated L-type Ca^{2+} current in murine cardiomyocytes of WT mice. Studies on AC $5^{-/-}$ mice showed that inhibition of L-type Ca^{2+} current was indirectly accomplished mainly *via* AC 5, because lack of this AC isoform attenuated the cardiomyocyte effect (Rottländer *et al.*, 2007). Therefore, we wished to study the effect of an even more potent AC inhibitor, MANT-ITP, in intact cardiomyocytes to support the previous findings. We used the same strain of WT mice (C57BL/6) to isolate the cardiomyocytes and we applied a very similar patch clamp protocol. The only difference was a different holding potential and the recovery time between single measurements was shorter. We started at a holding potential of -80 mV that was more physiological than the previously applied -60 mV holding potential (Rottländer *et al.*, 2007). Furthermore, we measured every 3 s the $I_{Ca,L}$ signal depolarized at +10 mV. The previous study applied every 10 s current measurements during the 15 min time interval. Additionally, I-V measurements were conducted every 2 min during one patch clamp measurement and not only at the beginning and at the end. The 15 minute time interval was chosen because MANT-GTPγS showed significant changes in $I_{Ca,L}$ after ~ 10 min. Due to the fact that good results were achieved with 1 µM MANT-GTPγS, we kept the concentration for all the other tested MANT nucleotides at 1 µM for a direct comparison of the data.

4.2.1. Basal L-type Ca^{2+} current

First of all, we measured basal $I_{Ca,L}$ current of ventricular cardiomyocytes of WT mice to evaluate the influence of MANT nucleotides on basal current. During the first measurements of basal L-type Ca^{2+} current with and without MANT-ITP in the patch pipette, the old amplifier (Axopatch 200A) broke down and we had to build up a new setup (Axopatch 200B). Figure 25 shows a comparison of basal $I_{Ca,L}$ current data from the old and new setup. The difference

between both traces was negligible. The summarized data of basal $I_{Ca,L}$ current without any MANT nucleotide and with MANT-ITP are, therefore, a combination of data collection with the old and new setup. Data collection of MANT-ITPγS, MANT-GTPγS and MANT-ATP measurements was later achieved by using the new setup.

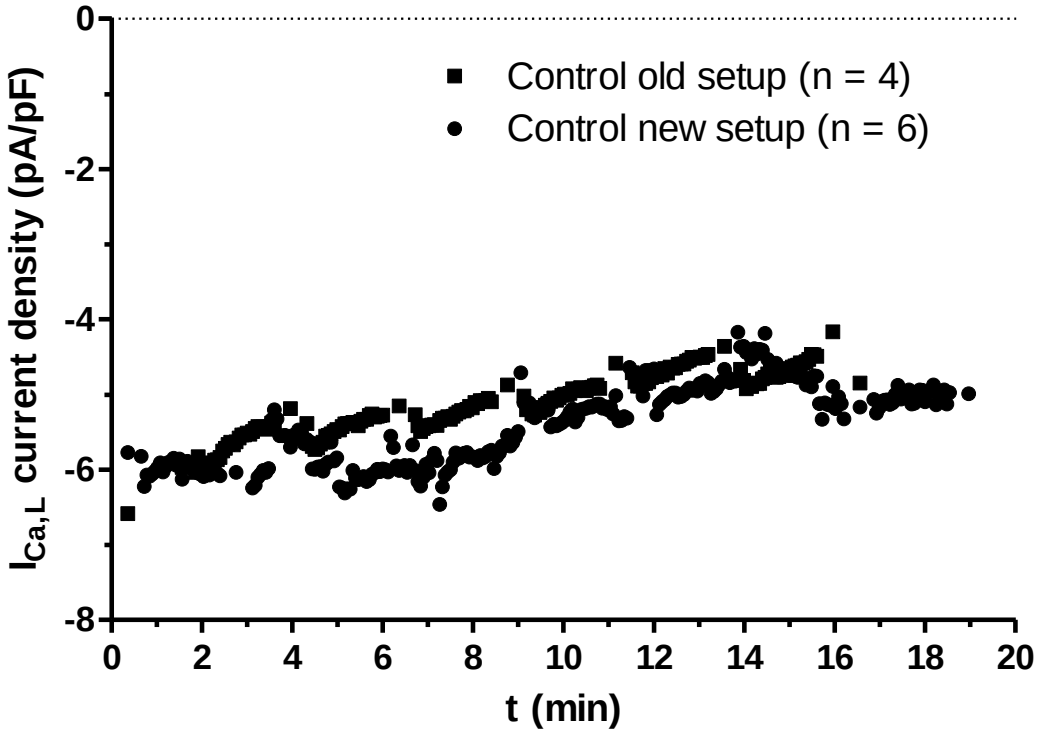

Figure 25. Control measurements with the old and new patch-clamp setup. The picture shows $I_{Ca,L}$ current normalized to the capacitance of single cells as current density in pA/pF to eradicate any variability in cell size. Patch clamp measurements are illustrated with filled squares, when done with the old patch-clamp setup. Filled circles show the measurements with the new patch clamp setup. Differences in Ca^{2+} current density between the two patch clamp setups are not visible and demonstrate that current measurements are not influenced by those changes. S.E.M. is not illustrated in this graph, because of better visualization, but is shown in Figure 26 B.

Figures 25 and 26 B show that basal $I_{Ca,L}$ current decreased during 15 min due to a "run-down" effect of the cardiomyocyte that can not totally be eliminated, even though Mg-ATP and EGTA were added to the patch pipette (2.2.4.4). The basal "run-down" was quite pronounced, because after 15 min we had a reduction in $I_{Ca,L}$ of 18.4 ± 3.3% (Figure 26 B). In the following chapters, the effects of MANT nucleotides added to the pipette solution are evaluated and compared to control.

4.2.2. Effect of MANT-ITP in comparison to control

After addition of MANT-ITP to the pipette solution we observed within the first 2.5 min a current increase of basal Ca^{2+} current that was not detected in the control measurements (Figure 26). It seems that MANT-ITP immediately expressed an effect in cardiomyocytes that

was not correlated to the expected AC inhibition. After 2.5 min $I_{Ca,L}$ current decreased to a higher extent compared to control. The inhibition of $I_{Ca,L}$ current by MANT-ITP reached a steady-state level after ~ 12 min, because Ca^{2+} current decrease approached current decrease of basal "run-down".

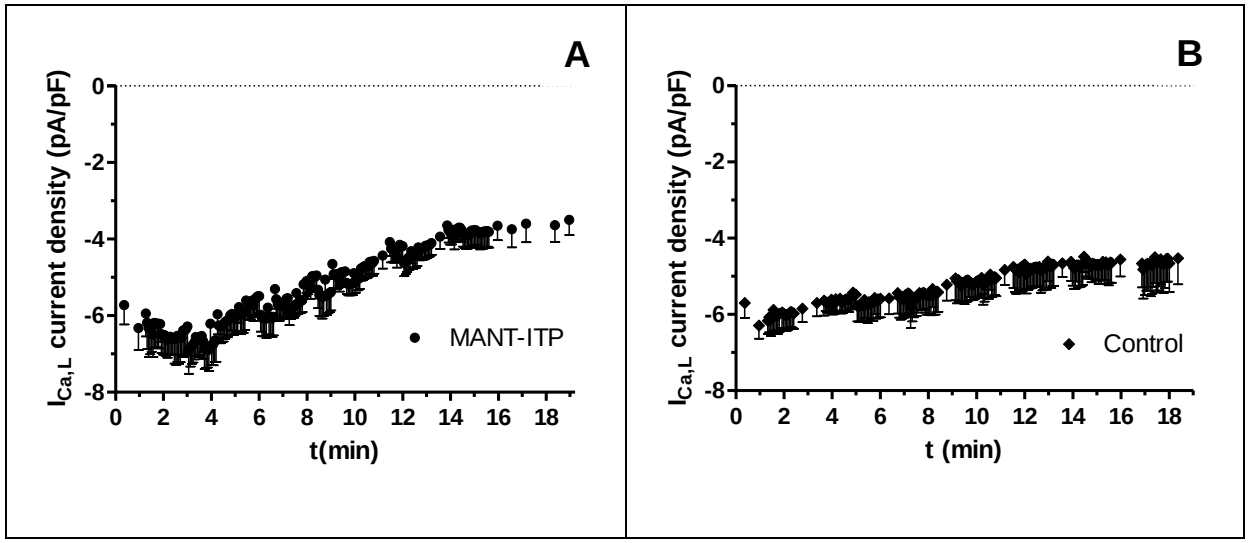

Figure 26. Basal MANT-ITP (A) *versus* control measurements (B). Mean and S.E.M. of basal $I_{Ca,L}$ current with MANT-ITP (n=8) or no inhibitor (n=10) in the patch pipette. Both graphs illustrate that measurements start at similar current densities (MANT-ITP = -5.67 ± 0.50 pA/pF *versus* control = -5.7 ± 0.35 pA/pF). During the first 2.5 min, MANT-ITP showed a substantial current increase that was not visible without MANT nucleotide. Afterwards, a stronger decrease of basal $I_{Ca,L}$ was detected with MANT-ITP in comparison to control experiments.

4.2.3. Replication of MANT-GTPγS experiments

Due to the fact that we observed an initial current increase with MANT-ITP, we repeated the measurements with MANT-GTPγS. On the one hand, we were specifically interested in reevaluation of the first 5 min, when MANT-GTPγS is present in the patch pipette to verify if previous experiments with MANT-GTPγS did not observe the initial current increase. On the other hand, we wanted to replicate the data obtained by Rottländer *et al.*, because we already observed strong differences in basal $I_{Ca,L}$ "run-down" (Rottländer *et al.*, 2007). Figure 27 shows a continuous reduction of $I_{Ca,L}$ by MANT-GTPγS over the 15 min time course, but the current inhibition was much smaller compared to MANT-ITP (Figure 26 A). At the beginning a slight current increase could be detected that is not significantly different, compared to control. Thus, it could be verified that MANT-GTPγS does not exhibit a characteristic stimulating effect on L-type Ca^{2+} channels. This was also confirmed by evaluation of the I-V relationship during the 15 min run, because we could not observe a strong difference in peak current at +10 mV during the first 2.5 min and the I-V curve did not express a horizontal shift over time (Figure 27 B). Furthermore, after 15 min $I_{Ca,L}$ was

decreased by 38.9 ± 5.3%, which is comparable to the already published data. Again, we observed that the MANT-GTPγS effect reaches steady-state levels after ~ 12 min.

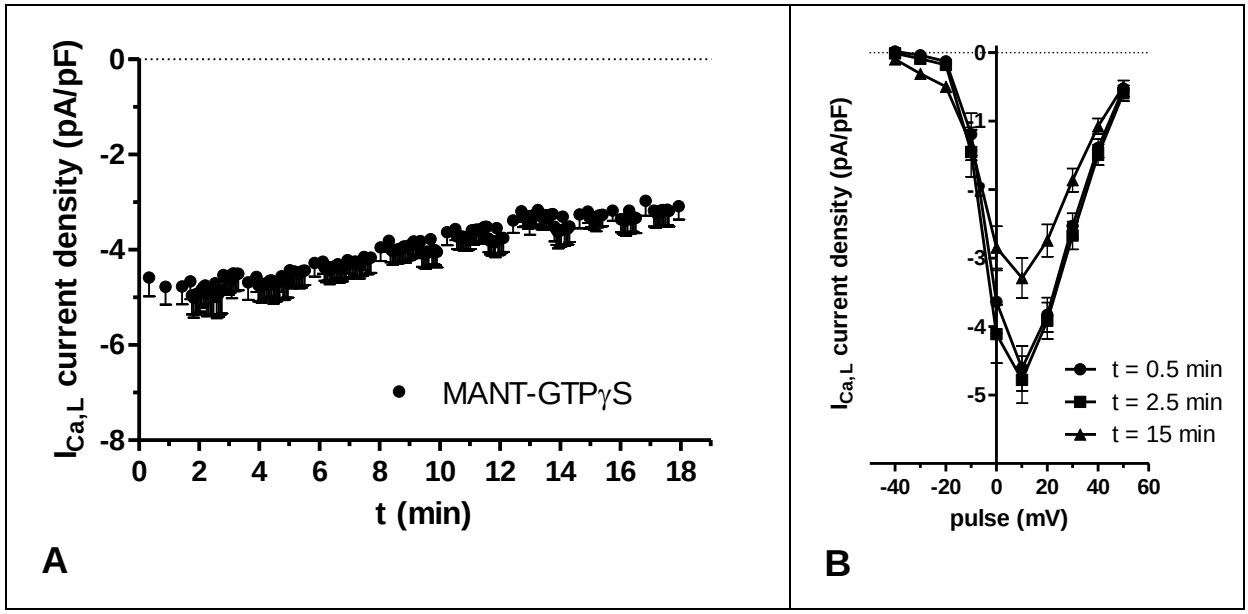

Figure 27. Basal MANT-GTPγS experiments. A, Mean and S.E.M. of basal $I_{Ca,L}$ current with MANT-GTPγS (n=10) and **B,** I-V relationship of MANT-GTPγS over time. An initial current density increase with MANT-GTPγS was not detected. The highest current density was accomplished with a test pulse of +10 mV, affirming the detection of L-type Ca^{2+} current. The current-voltage curve did not show a horizontal shift, suggesting that the MANT nucleotide did not directly affect Ca^{2+} channel phosphorylation.

4.2.4. Effect of MANT-ITPγS

MANT-ITP and MANT-ITPγS showed very similar inhibition on AC, especially on cardiac AC membrane preparations (1.5.1.1). Therefore, we applied the hydrolysis resistant analog of MANT-ITP, to evaluate the stability of MANT-ITP in intact cells. Interestingly, we detected an even higher current increase with MANT-ITPγS compared to MANT-ITP and this effect started immediately after the beginning of the WC measurement, because the first current density measurement after ~ 0.5 min (-9.19 ± 0.8 pA/pF) showed already higher values than MANT-ITP or control (-5.67 ± 0.50 pA/pF and -5.7 ± 0.35 pA/pF, respectively). The current density increased to -11.75 ± 0.4 pA/pF within the first 2.5 min (+106% increase compared to control). Figure 28 A illustrates five single WC measurements that reflect the significant initial current increase. The experiments were performed on several independent days. Therefore, we can exclude the possibility that the effects are related to the cardiomyocyte preparation. This must be also applied to the current decrease that starts after ~ 2.5 min. Two of five experiments showed a more pronounced current decrease than the other 3 experiments (MIγS1 and MIγS4). However, they are obtained from different cardiomyocyte preparations and the slope of the curves decreased to the same extent. Due to the fact that no difference

in the accomplishment of the patch was detected for any of the 5 experiments, we combined all the measurements with each other.

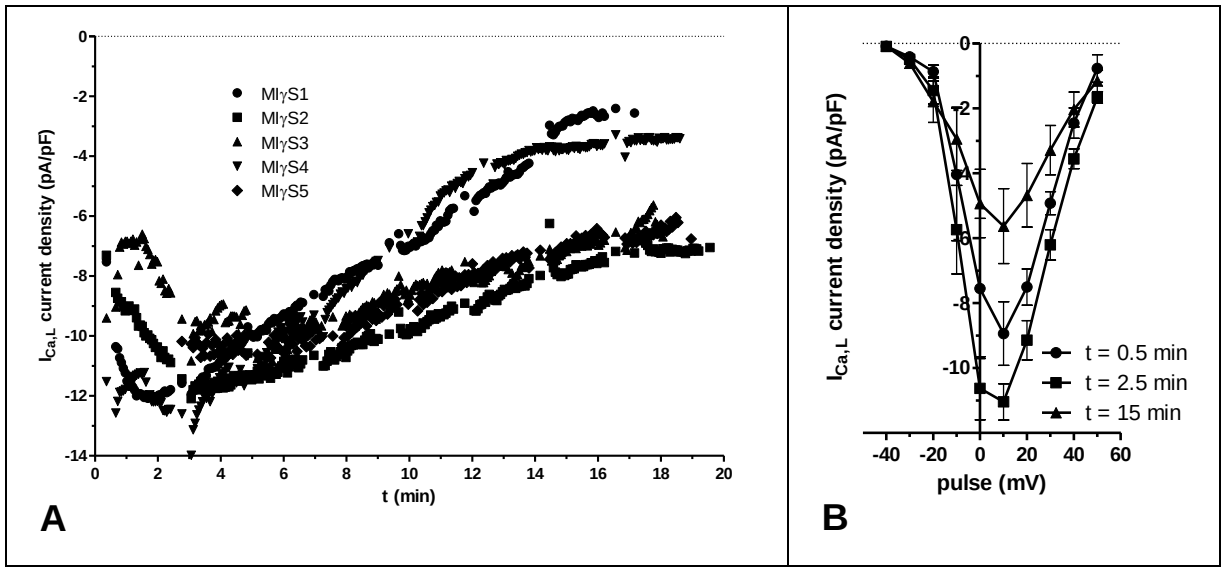

Figure 28. Single experiments (A) and I-V curves (B) of MANT-ITPγS (MIγS). The five single WC measurements (MIγS 1-5) show clearly that there was a pronounced current increase at the beginning that exceeded MANT-ITP effects. Two of the five experiments showed a stronger current decrease (MIγS 1 and 4), but the inhibition was to a similar extent. Therefore all of the five experiments were taken for evaluation. I-V curves show clearly the current increase during the first 2.5 min, but no horizontal peak shift.

4.2.5. Effect of MANT-ATP

Based on the contradictory findings of stimulating effects with MANT-ITP and MANT-ITPγS we also investigated the effects of MANT-ATP on cardiomyocytes. MANT-ATP inhibits AC 5 with 200-fold lower potency than MANT-ITP (K_i 200 nM). Therefore, we expected no significant effect of MANT-ATP on basal $I_{Ca,L}$ ("negative control"). However, in contrast, we found an even larger initial current increase than with MANT-ITP and the subsequent current decrease was comparable to MANT-ITP (Figure 29). Again, basal $I_{Ca,L}$ current density reached a steady-state plateau after ~ 13 min.

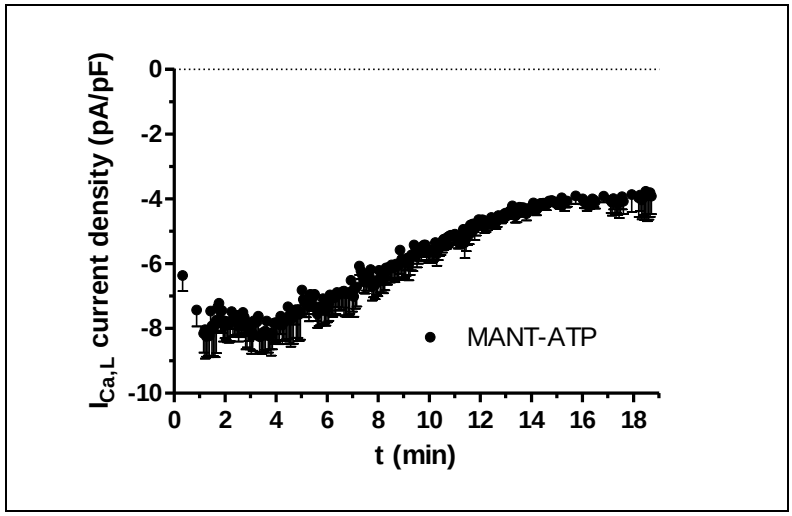

Figure 29. Basal effect of MANT-ATP on cardiomyocytes.
Mean and S.E.M. of basal $I_{Ca,L}$ current density with MANT-ATP (n=6). MANT-ATP showed an initial current increase that exceeded MANT-ITP effects. After 2.5 min Ca^{2+} current is inhibited by MANT-ATP. The inhibitory MANT-ATP effect vanished after ~ 13 min.

4.2.6. Comparison of MANT nucleotides

Figure 30 shows single original traces of basal L-type Ca^{2+} current and the effect of different MANT nucleotides. As expected, basal $I_{Ca,L}$ decreased during the 15 min time interval triggered by a "run-down" of the cell (Figure 30 A). The $I_{Ca,L}$ peak was at the beginning higher when MANT-ITPγS and MANT-ATP were present in the patch pipette, compared to control (Figure 30 C and E). Furthermore, we observed a more pronounced decrease of $I_{Ca,L}$ with these two nucleotides, but the overall inhibition of $I_{Ca,L}$ was not very large, because it reached only basal current levels after ~15 min. The $I_{Ca,L}$ peak of MANT-ITP was also higher than control, but not as pronounced as for the other two nucleotides (Figure 30 B). MANT-GTPγS did not show an increased peak current, but the $I_{Ca,L}$ peak at the end was smaller than control (Figure 30 D).

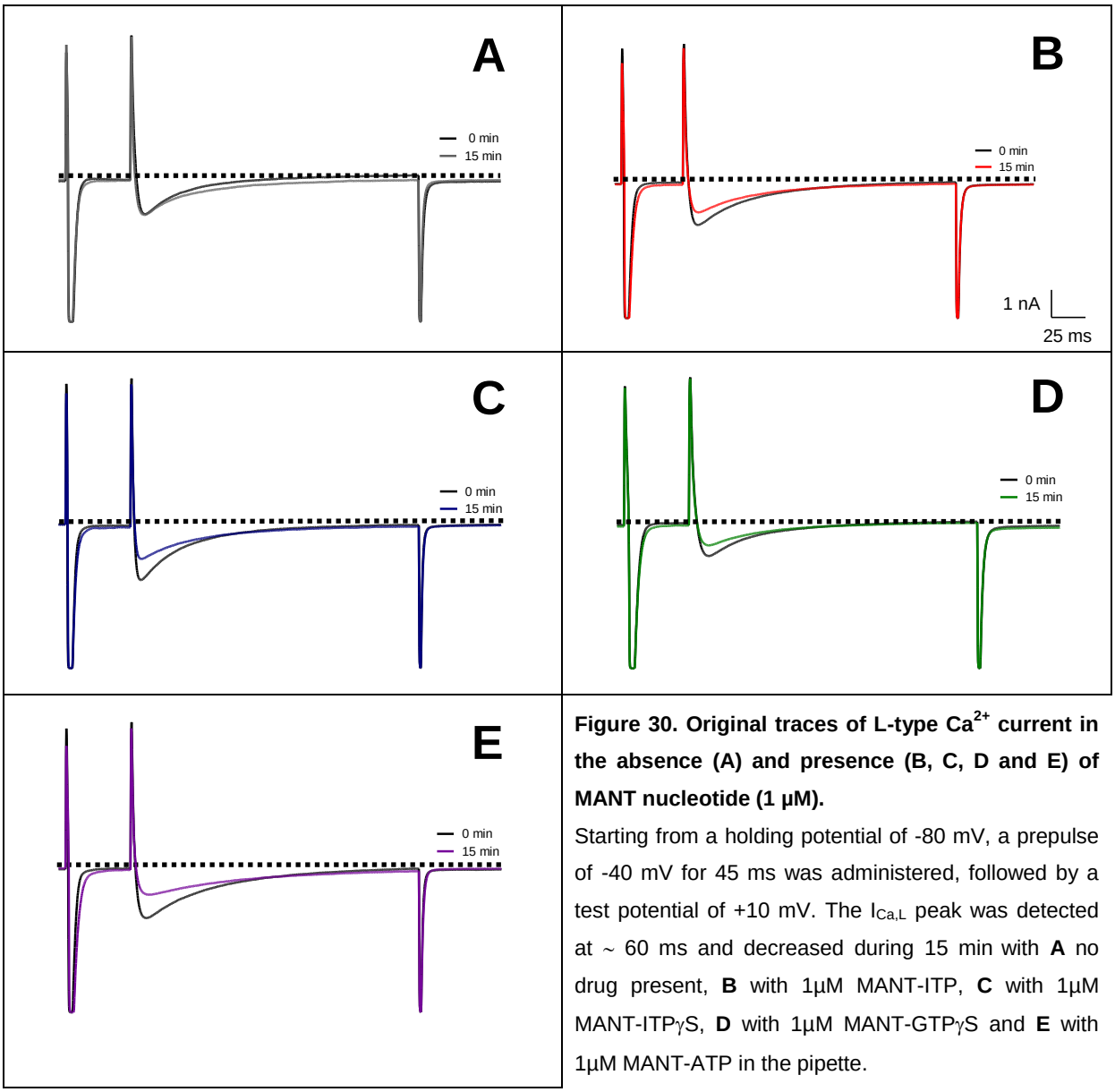

Figure 30. Original traces of L-type Ca^{2+} current in the absence (A) and presence (B, C, D and E) of MANT nucleotide (1 µM).

Starting from a holding potential of -80 mV, a prepulse of -40 mV for 45 ms was administered, followed by a test potential of +10 mV. The $I_{Ca,L}$ peak was detected at ~ 60 ms and decreased during 15 min with **A** no drug present, **B** with 1µM MANT-ITP, **C** with 1µM MANT-ITPγS, **D** with 1µM MANT-GTPγS and **E** with 1µM MANT-ATP in the pipette.

To summarize the effects of MANT nucleotides over the 15 min time interval, Figure 31 incorporates all measurements taken at +10 mV with the two pulse protocols. The time course is now averaged to specific time points to superimpose and better illustrate single I-V measurements and peak $I_{Ca,L}$ current measurements.

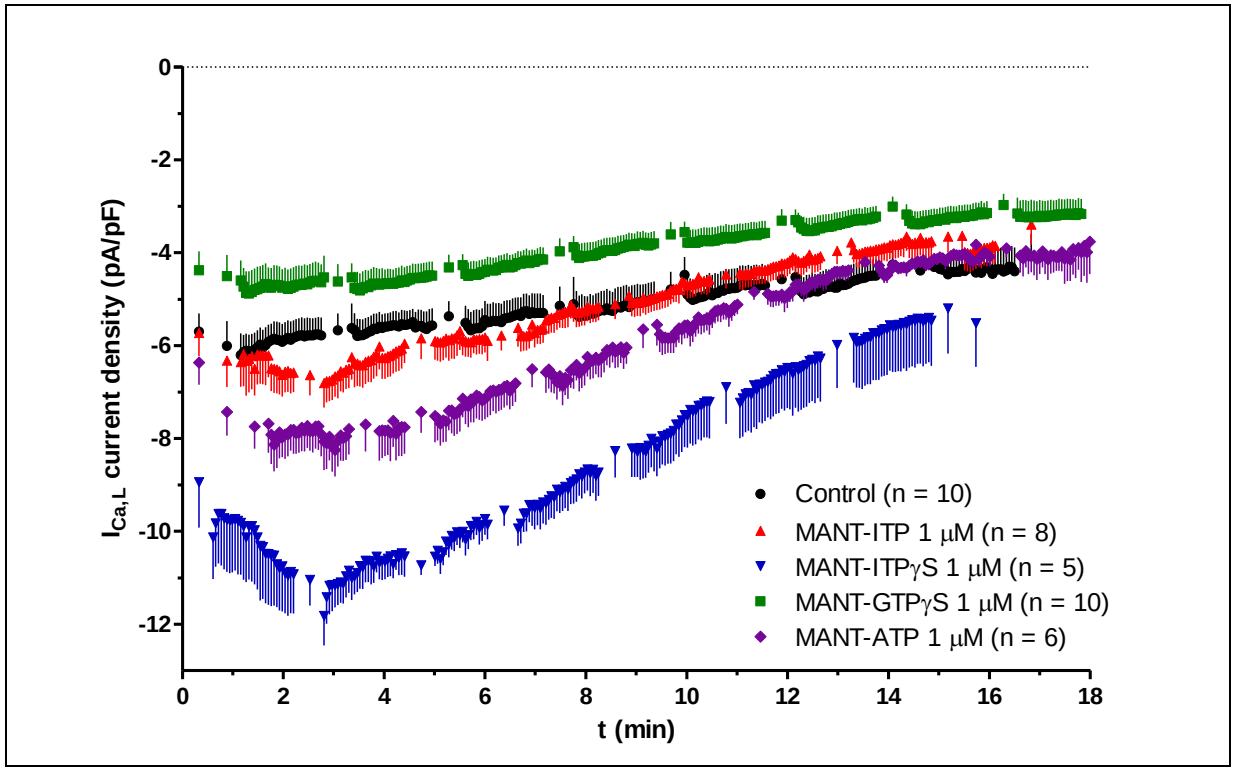

Figure 31. Effect of MANT nucleotides (1 µM) on basal L-type Ca^{2+} current in WT cardiomyocytes.
Averaged time course of whole cell L-type Ca^{2+} current density in the absence and in the presence of MANT nucleotide (1 µM). Note that only in the presence of MANT-ITPγS, MANT-ITP and MANT-ATP we observed an initial current increase.

Figure 31 illustrates that MANT-ITP and control experiments start at the same $I_{Ca,L}$ current density, but MANT-ITP current density increased during the first 2.5 min to a higher extent than control. During the subsequent decrease it exceeded the "run-down" of control experiments, but not to a very large extent. In contrast, MANT-ITPγS and also MANT-ATP showed a very pronounced current increase at the beginning that started immediately and thus suggests that the diffusion of the MANT nucleotide was achieved within the first 30 seconds. MANT-ITPγS was able to inhibit $I_{Ca,L}$ after the initial current increase and the inhibition was much stronger compared to control, but the overall effect after 15 min did not exceed the basal "run-down". MANT-ATP did not show such a strong current increase as MANT-ITPγS and also expressed a current inhibition after 2.5 min. Therefore $I_{Ca,L}$ is decreased after 15 min, exceeding control measurements and interestingly, the overall effect was similar to MANT-ITP. MANT-GTPγS started at a smaller $I_{Ca,L}$ current density than control experiments, but the difference was not significant (-4.5 ± 0.4 *versus* -5.7 ± 0.4 pA/pF,

respectively) and might be related to an instantaneous current inhibition. The $I_{Ca,L}$ current density values for MANT-GTPγS resembled already published data and also showed a lower starting point for MANT-GTPγS (Rottländer *et al.*, 2007). MANT-GTPγS did not show the initial current increase and the current inhibition did not approach the inhibitory effects seen with the other MANT nucleotides. However, the overall effect might be even higher than for the other MANT nucleotides, because $I_{Ca,L}$ current density was much lower for MANT-GTPγS compared to control experiments and the other MANT nucleotides after 15 min. Table 5 provides a statistical summary of all these findings.

Parameters	Control	MANT-ITP	MANT-ITPγS	MANT-GTPγS	MANT-ATP
Initial current increase (%)[1]	13.9 ± 2.9	28.75 ± 8.2	106.2 ± 7.02 ***, +++, ###	18.6 ± 4.6[(a)]	48.2 ± 8.3**, #
Relative current decrease (%)[1]	18.4 ± 3.3	30.8 ± 7.8	8.34 ± 16.8#	43.2 ± 5*	27.1 ± 2.2
Inhibition based on max. $I_{Ca,L}$ (%)	28.0 ± 3.4	49.2 ± 3.5**	54.5 ± 9.2**	38.9 ± 5.3*	47.1 ± 5*
$I_{Ca,L}$ current density (pA/pF) at beginning	-5.7 ± 0.4	-5.67 ± 0.5	-9.2 ± 0.8 ***, +++, ###	-4.5 ± 0.4	-6.4 ± 0.5
Maximum $I_{Ca,L}$ current density (pA/pF)	-6.5 ± 0.4	-7.34 ± 0.5#	-11.75 ± 0.4 ***, +++, ###	-5.3 ± 0.4	-8.45 ± 0.5*,###
n	10	8	5	10	6

Table 5. Summary of WC experiments with and without MANT nucleotides. Mean and S.E.M. of initial current increase, current decrease and current densities at beginning and after ~ 2.5 min of n experiments. After 15 min MANT-ITPγS did not achieve a current inhibition, compared to control, due to a strong initial current increase. Overall, MANT-GTPγS showed the highest current decrease compared to control, but the other MANT nucleotides showed stronger inhibitory effects after the initial current increase.

[1] Values based on first control measurement, with no MANT nucleotide in the patch pipette.

[a] Value is based on first WC measurement of MANT-GTPγS, because current density at beginning was smaller than control.

The results were compared using one-way ANOVA, followed by Bonferroni's/Dunnett's multiple comparison tests. Parameters are significantly different to: *control, +MANT-ITP and #MANT-GTPγS. One symbol: $p < 0.05$; two symbols: $p < 0.01$; three symbols: $p < 0.001$; confidence interval 95%.

Comparison of the cardiomyocyte effects with the inhibitory profile of MANT nucleotides on AC membrane preparations (ACs 1, 2, 5, 6 and cardiac AC) clearly revealed that the obtained current decrease was not correlated to AC inhibition (Table 2; 1.5.1.1, Table 5,

Figure 32 B). MANT-ATP possesses a 200-fold lower potency than MANT-ITP in AC 5 membrane preparations, but the overall decrease of $I_{Ca,L}$ current was not significantly different. Additionally, current decrease based on maximum $I_{Ca,L}$ current density was also comparable for both AC inhibitors. Furthermore, MANT-GTPγS effects should be lower compared to MANT-ITP and MANT-ITPγS, because it is a less potent AC inhibitor on cardiac and AC 5 membrane preparations under Mg^{2+} conditions. This could be detected for the subsequent current decrease after 2.5 min, because the slope of current inhibition was steeper for MANT-ITP and MANT-ITPγS. However, overall current inhibition was much smaller for MANT-ITPγS and also less pronounced for MANT-ITP, due to the initial current increase.

The current increase was not related to AC inhibition. MANT-ITP, MANT-ATP and MANT-ITPγS expressed a strong current increase, even though they should be inhibitors on $I_{Ca,L}$ current, due to their strong inhibitory potency on cardiac ACs. This stimulating effect on $I_{Ca,L}$ was, therefore, not initiated *via* AC, but may be due to activation of another nucleotide binding protein that phosphorylates the L-type Ca^{2+} channel. An initial activation of AC that may increase $I_{Ca,L}$ current can be also excluded, because, on the one hand we did not see a correlation between the affinity of MANT nucleotides for cardiac AC in membrane preparations and the indirect stimulating effects on L-type Ca^{2+} channels (Figure 32 A). On the other hand, AC activity assays with MANT nucleotides were carried out for 1-2 min, i.e. in the time of current increase and showed clearly AC inhibition in this time frame.

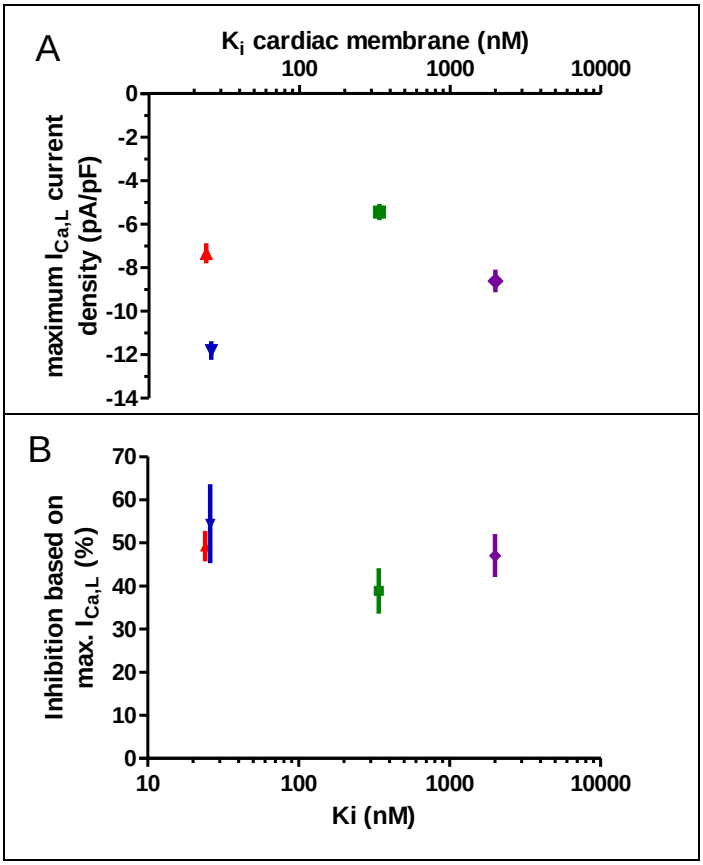

Figure 32. Correlations of WC patch clamp effect with inhibitory AC-activity.

A. Maximum $I_{Ca,L}$ density in intact cells *versus* inhibitory affinity (K_i) on cardiac mice membrane preparations did not show that the detected effects are correlated to AC inhibition, because MANT-ATP showed stronger current increase than MANT-ITP and MANT-GTPγS and MANT-ITPγS showed larger effects than MANT-ITP.

B. Absolute current inhibition of MANT nucleotides *versus* K_i on cardiac AC. We observed a stronger inhibition after initial current increase with MANT-ATP compared to MANT-GTPγS and the effect was similar to MANT-ITP, although MANT-GTPγS and MANT-ITP are more potent than MANT-ATP. Figure legend:

- MANT-ITP
- MANT-ITPγS
- MANT-GTPγS
- MANT-ATP

To evaluate if the MANT nucleotides have a direct effect on L-type Ca^{2+} channels we measured the current-voltage (I-V) relationship of all MANT nucleotides during the WC experiment. Isoproterenol, a β-AR agonist, enhances $I_{Ca,L}$ and induces a shift of the I-V curve by about 10 mV toward more negative potential, because it indirectly activates AC *via* $G_{s\alpha}$ and increases the phosphorylation of the Ca^{2+} channel *via* PKA. This leftward shift can be also detected with FS, a direct AC activator. Interestingly, we did not detect any leftward shift of the I-V curve during the whole experiment, even though we observed a current increase (Figure 33). This finding further strengthens our hypothesis that current increase is not elicited by AC. The following I-V curves show the current increase of MANT-ITP, MANT-ATP and MANT-ITPγS during the first 2.5 min. The subsequent decrease thereafter lead to a slight inhibitory effect of MANT-ITP and MANT-ATP after ~15 min, but MANT-ITPγS did not exceed "run-down" levels of control.

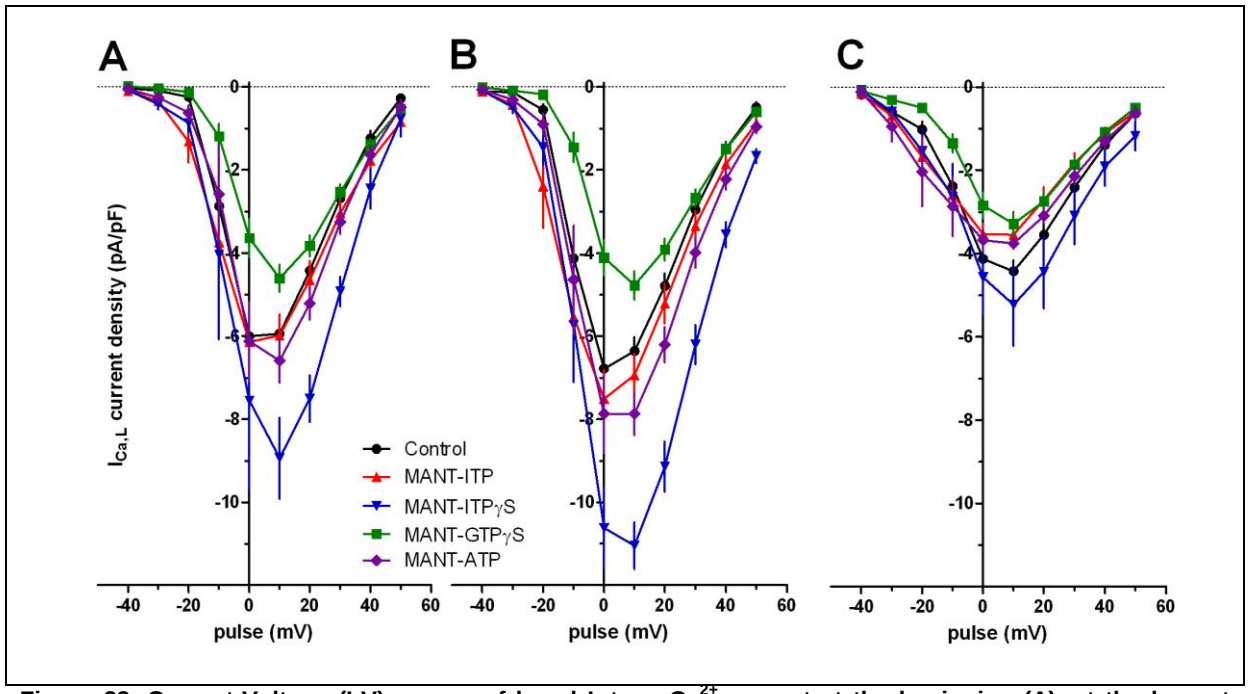

Figure 33. Current-Voltage (I-V) curves of basal L-type Ca^{2+} current at the beginning (A), at the largest current density (B) and at the end (C, t = 15min) of the experiment. The mean values of at least 5 independent experiments with or without MANT nucleotide are shown. MANT nucleotides did not cause a voltage shift of the I-V curve.

4.3. Discussion

We characterized a class of potent AC inhibitors – MANT nucleotides – for their indirect effect and potency on basal L-type Ca^{2+} current in cardiomyocytes. We could confirm that MANT nucleotides influence the constant basal $I_{Ca,L}$. However, in contrast to previous experiments, MANT nucleotides show not only inhibitory effects on $I_{Ca,L}$, but have inconsistent impact on L-type Ca^{2+} channel activity. Until now, all the data about potency and selectivity of MANT nucleotides was gained in recombinant AC membrane preparations, providing information about direct AC inhibition by these nucleotides. However, we did not have data about the effects of MANT nucleotides in intact cells. Only one MANT nucleotide, MANT-GTPγS, was subsequently tested in WC patch clamp experiments. It showed inhibition of Ca^{2+} current in cardiomyocytes *via* AC, with a strong impact on AC 5, because the inhibitory effect of MANT-GTPγS was reduced in cardiomyocytes of AC $5^{-/-}$ mice (Rottländer *et al.*, 2007). Therefore, we expected that even higher inhibitory effects on basal $I_{Ca,L}$ can be detected with more potent MANT nucleotides. Due to the fact that MANT-ITP as well as MANT-ITPγS did not show a more pronounced current inhibition and meanwhile even increased $I_{Ca,L}$, we expect that the initial increase and subsequent decrease of basal $I_{Ca,L}$ may be related to unspecific interactions of MANT nucleotides with other proteins or other AC isoforms that were not extensively monitored yet. The physiological role of other AC isoforms in heart such as 2, 3, 4, 7 and 9 is not clarified until now (Okumura *et al.*, 2009). However, it is possible that the entity of ACs have an important influence on basal $I_{Ca,L}$. The MANT nucleotides used in our experiments were not tested on the other AC isoforms apart from AC 2. It is possible that those MANT nucleotides might also express a diverse, relevant effect on ACs 3, 4, 7 and 9 and that the effect superimposes the inhibition of ACs 2 and 5.

Most probably, however, is the possibility that MANT nucleotides undergo many intracellular interactions in cardiomyocytes. The intracellular signaling cascade is very complex and an appreciation of all protein interrelations with MANT nucleotides is currently missing. GPCRs, G proteins, mACs, phosphodiesterases, adenylate kinases and protein kinases influence the cAMP levels that regulate L-type Ca^{2+} channel activity. An unspecific effect of MANT nucleotides in this complex signaling cascade may not be eradicated by our findings. Studies with ANT- and MANT-ATP showed substrate activity for adenylate kinase, guanylate kinase, glutamine synthetase, myosin ATPase and Na^+/K^+-ATPase. MANT- and ANT-ADP are substrates for creatine kinase and the GMP- and adenosine derivatives are substrates for guanylate kinase and adenosine deaminase, respectively. On adenylate kinase, MANT-ATP showed the same K_m values as ATP and even higher affinity for guanylate kinase (Hiratsuka, 1983). Many of these enzymes regulate ATP synthesis and hydrolysis. It is, therefore, possible that the MANT nucleotides change the physiological ATP

homeostasis by competition for the substrate-binding site of ATP binding proteins and that these effects lead to an initial increase in cAMP and $I_{Ca,L}$ before AC inhibition is achieved.

Especially the effects detected with MANT-ATP support the hypothesis that many other nucleotide binding proteins can use MANT-ATP and probably other MANT-NTPs instead of ATP as substrate (Figure 32). In one study, MANT-ATP, -ADP and the two deoxy substances MANT-2'deoxy-ATP and MANT 3'deoxy-ATP were tested for their affinity to the catalytic subunit of PKA (Ni *et al.*, 2000). Binding to PKA was assessed by fluorescence resonance energy transfer, showing a large increase in FRET at 440 nm. Reversed-phase chromatography was used to measure PKA-induced phosphorylation of a small peptide substrate. It was found that MANT-ATP served as a phosphorylating agent in this PKA-catalyzed reaction and both isomers of MANT-ATP are substrates for PKA. The rate for peptide phosphorylation is ~ 20-fold lower than that for ATP. Additionally, MANT-GTPγS and MANT-GppNHp are also known as inhibitors of G proteins and showed relatively high affinity and changes in fluorescence upon G protein binding (Remmers and Neubig, 1996; Remmers, 1998). The affinity of MANT-GTPγS to recombinant $G_{s\alpha}/G_{i\alpha}$ fusion proteins with the formyl peptide receptor or the β_2-adrenergic receptor was 30- to 300-fold lower compared to GTPγS (Gille and Seifert, 2003a). The stronger relative inhibition of $I_{Ca,L}$ with MANT-GTPγS in comparison with the other MANT nucleotides could therefore be explained by a combined inhibition of both, AC and $G_{s\alpha}$.

Another explanation for the diverse effects of the different MANT nucleotides could be that they interact not only with proteins of the AC pathway, but also *via* the cGMP-mediated pathway. Cardiac L-type Ca^{2+} current can be modulated by cGMP *via* activation of cGMP-dependent protein kinase or regulation of cGMP-inhibited and activated cAMP phosphodiesterases (Lohmann *et al.*, 1991). In frog ventricular cardiomyocytes, it was reported that cGMP can decrease isoprenaline- or cAMP-stimulated $I_{Ca,L}$ by stimulation of cyclic nucleotide phosphodiesterases that increase cAMP hydrolysis (Hartzell and Fischmeister, 1986). Furthermore, in mammalian cells cGMP potentiates the stimulation of $I_{Ca,L}$ by isoprenaline *via* cGMP-inhibited phosphodiesterases (Ono and Trautwein, 1991). Just recently, it was published, that MANT-GTP can also be a substrate and fluorescent probe for the detection of soluble guanylyl cyclase (sGC) activity. Stimulation of sGC with NO lead to a complete conversion of MANT-GTP to MANT-cGMP, confirmed by HPLC and fluorescence measurements. The K_m of sGC for MANT-GTP was 35.7 ± 9.37 µM and showed a similar enzyme affinity as the physiological substrate GTP (Newton *et al.*, 2010). However, another study rather expects an enzyme inhibition. MANT-ATP and MANT-GTP showed effectual inhibitory potency on sGC with a K_i of 430 and 710 nM, respectively (Gille *et al.*, 2004). The effects of MANT nucleotides on sGC are, therefore, quite controversial. MANT-cGMP was also tested on rabbit brain phosphodiesterase and showed substrate affinity. Interestingly, it

exhibits similar kinetic parameters than cGMP (Johnson *et al.*, 1987). Therefore, interaction of MANT nucleotides with regulators of cGMP homeostasis could be also responsible for the complex electrophysiological results.

MANT nucleotides directly enter the cell through the pipette solution. It was expected that intracellular dialysis requires some time. However, our findings showed that there is an immediate reaction, because MANT-ITPγS showed right from the beginning a very strong $I_{Ca,L}$ signal that is significantly different from control and other MANT nucleotides and is not related to any changes in the WC setup or cardiomyocyte preparation. Already published results with MANT-GTPγS confirm that the intracellular dialysis is achieved in a short time, because MANT-GTPγS expresses the strongest effect within the first 5 min and $I_{Ca,L}$ decreases immediately to a higher extent than control (Rottländer *et al.*, 2007). A steady-state level is reached after ~ 10 min and is compliant to the inhibitory profile of MANT-ITP, MANT-ITPγS and MANT-ATP that reach steady state levels after ~ 12-13 min.

Comparison of our data with previous studies show that basal “run-down” after 10 min is increased with ~ 13% *versus* ~ 8%, respectively. This can be explained by differences in the patch clamp protocols, because in our protocol the cardiomyocytes are more stressed by a higher, but more physiological, holding potential of -80 mV *versus* -60 mV and by a 3-fold higher rate of WC measurements during the same time interval. In contrast, MANT-GTPγS did not show a more tremendous reduction of $I_{Ca,L}$. Rottländer *et al.* already detected a reduction of $I_{Ca,L}$ by 39.5 ± 6.8% after 10 min. Anyway, the results are comparable, because we detected a reduction by 38.9 ± 5.3% after 15 min, but $I_{Ca,L}$ decreases constantly, whereas in the previous study it reached steady-state levels after 10 min and reduction was not further enhanced anymore.

We also evaluated the stability of MANT-NTPs *versus* MANT-NTPγS. The differences in initial current increase and subsequent current decrease between MANT-ITP and MANT-ITPγS suggest that the hydrolysis-resistant MANT nucleotides are more stable (Figure 32 A, Table 5). This may be the fact, if these findings are correlated to the inhibitory potency on mAC, because MANT-ITP and MANT-ITPγS show comparable affinity for cardiac AC. Therefore, we would have expected similar effects. However, the overall inhibitory effect for MANT-ITP after 15 min was still stronger than for MANT-ITPγS, when compared to control. Furthermore, MANT-ATP also shows a continuous and strong decrease during the 15 min, although it is a less potent AC inhibitor and should also immediately hydrolyze. It has to be considered that the MANT-NTPs are also enzyme substrates. HPLC analysis of 5 µM MANT-GTP and 8 µM MANT-cGMP showed that substrate conversion starts immediately, but a complete turnover is achieved after ~1h with sGC and phosphodiesterase of rabbit brain

(Johnson *et al.*, 1987; Newton *et al.*, 2010). Therefore, a clear assertion about the nucleotide stability in cardiomyocytes is not possible and further investigation with other MANT-NTPs (e.g. MANT-GTP) and MANT-NTPγS (e.g. MANT-ATPγS) or investigations of the degradation products *via* HPLC analysis are necessary to clarify the stability of those nucleotides in cell assays.

During the patch-clamp experiment, all the tested MANT nucleotides did not change cell viability monitored by visual observation. This is in agreement with previous measurements and indicates that the MANT nucleotides do not express a toxic intracellular effect.

In summary, the effects of MANT nucleotides on cardiomyocytes did not reflect the inhibitory profile obtained in recombinant and cardiac membrane preparations. Due to the fact, that a broad range of different MANT nucleotides were examined for their effects in intact cells and showed quite contradictory results, we observed that MANT nucleotides may influence a variety of proteins beside ACs and therefore, their selectivity for AC is quite equivocal. MANT nucleotides are suitable experimental tools for the analysis of recombinant ACs, purified catalytic mAC subunits and ACs in native cell membranes (Gille *et al.*, 2004; Göttle *et al.*, 2009; Pinto *et al.*, 2009). They can also be effectively used as fluorescence probes and ligands for crystallography (Remmers, 1998; Mou *et al.*, 2006). Unfortunately, MANT nucleotides also have various disadvantages. Due to their nucleotide structure, they have very poor membrane permeability and, hence, have to be injected into cells, limiting the type and number of experiments that can be conducted. Moreover, MANT nucleotides may bind to various nucleotide-binding proteins. The search for even more potent and selective non-nucleotidic mAC inhibitors that display higher membrane permeability may be established from our findings. A substantial advantage for the achievement of this ambitious goal is the fact that the substrate-binding pocket of AC is very flexible and can accommodate a broad range of inhibitors (Dessauer *et al.*, 1999; Mou *et al.*, 2006)

5. Summary

Adenylyl cyclases (ACs) play a crucial role in G protein-coupled receptor signaling, because they generate cyclic adenosine 3',5'-monophosphate (cAMP). AC inhibitors could be applied when pathophysiological high cAMP concentrations are predominant, such as in heart failure or neurodegenerative disorders. 2',3'-O-(N-Methylanthraniloyl)-nucleoside 5'-triphosphates (MANT-NTPs) are a new class of potent AC inhibitors with isoform selectivity for ACs 1, 5 and 6 in comparison to AC 2 and MANT-inosine-5'-triphosphat (MANT-ITP) is currently the most potent known AC inhibitor. The present work is, on the one hand, about the molecular interaction of MANT-ITP with the catalytic subdomains of membranous AC (mAC) to understand the structure-activity relationship of MANT-NTPs with the enzyme. On the other hand, the effect of different MANT-NTPs in murine cardiomyocytes was analyzed.

With the help of the crystal structure of MANT-ITP in complex with the VC1/IIC2-domains of mAC we could demonstrate that MANT-ITP has an almost identical conformation as MANT-GTP, when both crystal structures are superimposed. Based on a missing NH_2-group in the hypoxanthine ring of MANT-ITP the structure does not provide a hydrogen bond to I1019. The apparent decrease in affinity at the purine binding site is more than compensated by an increased interaction with the hydrophobic MANT-binding site, as assessed by fluorescence measurements that show already under basal conditions an intensified direct fluorescence and an increase in fluorescence resonance energy transfer (FRET). Additionally, the MANT-ITP structure shows a better triphosphate-metal ion coordination and stronger interaction with K1065 in the phosphate-binding site which was confirmed with MD simulations. The binding affinity of MANT nucleotides for mAC is regulated *via* a balance between the purine-, MANT- and phosphate binding site and corroborates a previously made 3-site-pharmacophore model.

AC 5 knockout (AC $5^{-/-}$) mice exhibited cardioprotective effects in a pressure-overload model, and cardiomyocytes were protected against apoptosis. Therefore, MANT nucleotides as potent AC inhibitors with a high selectivity for AC 5, such as MANT-ITP, MANT-ITPγS, and MANT-GTPγS were examined in ventricular wildtype (C57Bl/6) cardiomyocytes. MANT-ATP was used as a negative control, because it possesses a 200-fold lower affinity for AC 5. The substances were applied intracellularly and the indirect influence of ACs on L-type Ca^{2+} current ($I_{Ca,L}$) was detected *via* electrophysiological WC measurements. The effects of the MANT nucleotides on $I_{Ca,L}$ were unexpectedly complex. MANT-ITP, MANT-ATP und MANT-ITPγS showed an initial current increase of ~ 30, 106 and 48%, respectively, followed by a decrease of $I_{Ca,L}$ after ~ 2.5 minutes. The characteristics of MANT-GTPγS are very similar to

control and consistent with already published data. All MANT-NTPs show an inhibitory effect on basal $I_{Ca,L}$, but the overall inhibition in comparison to control is low or not existent, because of the initial current increase. An explanation could be that MANT-NTPs activate/inhibit other target proteins beside the AC inhibition.

Due to the complex, dually stimulatory and inhibitory effects in intact cells, the use of MANT nucleotides should be restricted as valuable fluorescent probes, crystallographic ligands and enzyme inhibitors to analyze recombinant and/or purified nucleotide-binding proteins. Hopefully, new inhibitors will exhibit greater selectivity for AC 5 and also membrane permeability.

6. Zusammenfassung

Adenylylzyklasen (ACs) spielen in der G-Protein-gekoppelten Rezeptor-Signalkaskade eine entscheidende Rolle, weil sie einen wichtigen intrazellulären Botenstoff, zyklisches Adenosinmonophosphat (cAMP), synthetisieren. AC-Inhibitoren könnten pharmakotherapeutisch bei pathophysiologisch erhöhten cAMP-Konzentrationen eingesetzt werden, die bei Herzinsuffizienz, aber auch bei neurodegenerativen Erkrankungen vorkommen. 2',3'-O-(N-Methylanthraniloyl)- (MANT-) Nukleotide stellen eine Klasse von AC-Inhibitoren dar, die eine Selektivität für ACs 1, 5 und 6 gegenüber AC 2 aufweisen. MANT-Inosin-5'-triphosphat (MANT-ITP) ist der potenteste Wirkstoff dieser Klasse. Die vorliegende Arbeit beschäftigt sich einerseits mit der molekularen Interaktion von MANT-ITP mit den aktivierten katalytischen Untereinheiten der membranären AC (mAC), um die Struktur-Wirkungsbeziehung von MANT-Nukleotiden besser zu verstehen. Andererseits wurde die Wirkung verschiedener MANT-Nukleotide in intakten Kardiomyozyten der Maus analysiert.

Anhand der Kristallstruktur von MANT-ITP im Komplex mit der VC1/IIC2 Untereinheit von mAC konnte gezeigt werden, daß MANT-ITP eine fast identische Konformation wie MANT-GTP aufweist, wenn beide Kristallstrukturen übereinandergelegt werden. Aufgrund einer fehlenden NH_2-Gruppe im Hypoxanthinring von MANT-ITP wird eine Wasserstoffbrückenbindung zu I1019 nicht ausgebildet. Die scheinbare Affinitätsminderung in der Purinbindungstasche wird durch eine verstärkte Interaktion mit der hydrophoben MANT-Bindungstasche mehr als ausgeglichen. Fluoreszenzmessungen bestätigten, dass sowohl die direkte Fluoreszenz als auch der Fluoreszenzresonanz-Energietransfer (FRET) mit MANT-ITP aufgrund der hydrophoben Wechselwirkung unter basalen Bedingungen erhöht sind. Außerdem zeigte die MANT-ITP-Struktur eine verbesserte Phosphat-Metallionen-Koordination und eine verstärkte Interaktion mit K1065 in der Phosphat-Bindungstasche, was durch MD-Simulationen bestätigt wurde. Die Bindungsaffinität von MANT-Nukleotiden für mAC wird durch ein Gleichgewicht zwischen Purin-, MANT- und Phosphat-Bindungstasche hervorgerufen und bestätigt ein bereits bestehendes trimeres Pharmakophor-Modell.

In AC 5 Knockout-Mäusen zeigte sich, dass das Fehlen der AC 5 eine kardioprotektive Wirkung im druckbelasteten Herzen hat und Apoptoseprozesse in Kardiomyozyten verhindert werden. Da MANT-Nukleotide potente AC-Inhibitoren sind und bereits gezeigt wurde, dass sie eine gewisse Selektivität für AC 5 aufweisen, wurden ausgewählte Substanzen (MANT-ITP, MANT-ITPγS und MANT-GTPγS) in ventrikulären Kardiomyozyten von C57Bl/6-Mäusen untersucht. MANT-ATP wurde aufgrund seiner 200-fach geringeren Affinität für AC 5 als Negativkontrolle eingesetzt. Dabei wurden die Substanzen anhand elektrophysiologischer Ganzzellmessung direkt intrazellulär appliziert und der indirekte

Einfluss von ACs auf den L-Typ Calciumkanalstrom ($I_{Ca,L}$) in Herzmuskelzellen von Mäusen vermessen. Die MANT-Nukleotide zeigten sehr komplexe Wirkungen auf $I_{Ca,L}$. MANT-ITP, MANT-ATP und MANT-ITPγS zeigten einen ungewöhnlichen initialen Stromanstieg von jeweils ~ 30, 106 und 48% bevor nach ~ 2,5 Minuten der stromhemmende Effekt eintrat. MANT-GTPγS entwickelte keinen signifikanten Stromanstieg und war den Kontroll-messungen ähnlich, was bisher publizierten Ergebnissen entspricht.

Alle MANT-Nukleotide haben eine hemmende Wirkung auf den basalen $I_{Ca,L}$, allerdings ist die Gesamtinhibition im Vergleich zur Kontrolle gering oder gar nicht erkennbar. Eine mögliche Erklärung wäre, dass MANT-Nukleotide neben der AC-Inhibition auch andere Zielproteine mehr oder weniger stark aktivieren bzw. inhibieren. Der Einsatz von MANT-Nukleotiden sollte sich auf die Nutzung als Fluoreszenssonden, Liganden zur kristallographischen Strukturanalyse, beziehungsweise als Enzyminhibitoren beschränken. Denn sie eignen sich gut zur Analyse molekularer Wechselwirkungen von rekombinanten und/oder aufgereinigten nukleotid-bindendenden Proteinen. Die bisherig gewonnenen Ergebnisse lassen sich aber durchaus für die Synthese von membrangängigen, selektiveren AC 5 - Inhibitoren für die Entwicklung neuer Arzneistoffe, z.B. zur Therapie der Herz-insuffizienz nutzen. In einem nächsten Schritt wäre es außerdem sehr wichtig, die unspezifischen Aktivierungs- bzw. Hemmeigenschaften der MANT-Nukleotide herauszu-arbeiten.

7. References

Antos CL, Frey N, Marx SO, Reiken S, Gaburjakova M, Richardson JA, Marks AR and Olson EN (2001) Dilated cardiomyopathy and sudden death resulting from constitutive activation of protein kinase A. *Circ Res* **89**:997-1004.

Beazely MA and Watts VJ (2006) Regulatory properties of adenylate cyclases type 5 and 6: A progress report. *Eur J Pharmacol* **535**:1-12.

Beetz N, Hein L, Meszaros J, Gilsbach R, Barreto F, Meissner M, Hoppe UC, Schwartz A, Herzig S and Matthes J (2009) Transgenic simulation of human heart failure-like L-type Ca^{2+}-channels: implications for fibrosis and heart rate in mice. *Cardiovasc Res* **84**:396-406.

Bellen HJ, Gregory BK, Olsson CL and Kiger JA, Jr. (1987) Two Drosophila learning mutants, dunce and rutabaga, provide evidence of a maternal role for cAMP on embryogenesis. *Dev Biol* **121**:432-444.

Belles B, Malecot CO, Hescheler J and Trautwein W (1988) "Run-down" of the Ca current during long whole-cell recordings in guinea pig heart cells: role of phosphorylation and intracellular calcium. *Pflüger's Arch* **411**:353-360.

Bradford MM (1976) A rapid and sensitive method for the quantitation of microgram quantities of protein utilizing the principle of protein-dye binding. *Anal Biochem* **72**:248-254.

Bristow MR, Hershberger RE, Port JD, Gilbert EM, Sandoval A, Rasmussen R, Cates AE and Feldman AM (1990) β-adrenergic pathways in nonfailing and failing human ventricular myocardium. *Circulation* **82**:I12-25.

Buck J, Sinclair ML, Schapal L, Cann MJ and Levin LR (1999) Cytosolic adenylyl cyclase defines a unique signaling molecule in mammals. *Proc Natl Acad Sci USA* **96**:79-84.

Chester JA and Watts VJ (2007) Adenylyl cyclase 5: a new clue in the search for the "fountain of youth"? *Sci STKE* **2007**:pe64.

Cohn JN, Levine TB, Olivari MT, Garberg V, Lura D, Francis GS, Simon AB and Rector T (1984) Plasma norepinephrine as a guide to prognosis in patients with chronic congestive heart failure. *N Engl J Med* **311**:819-823.

Collaborative Computational Project No. 4 (1994) The CCP4 suite: programs for protein crystallography. *Acta Crystallogr D Biol Crystallogr* **50**:760-763.

Dai S, Hall DD and Hell JW (2009) Supramolecular assemblies and localized regulation of voltage-gated ion channels. *Physiol Rev* **89**:411-452.

Defer N, Best-Belpomme M and Hanoune J (2000) Tissue specificity and physiological relevance of various isoforms of adenylyl cyclase. *Am J Physiol Renal Physiol* **279**:F400-416.

DeLano WL (2002) The PyMOL Molecular Graphics System, DeLano Scientific, San Carlos, CA, USA.

Desaubry L and Johnson RA (1998) Adenine nucleoside 3'-tetraphosphates are novel and potent inhibitors of adenylyl cyclases. *J Biol Chem* **273**:24972-24977.

Desaubry L, Shoshani I and Johnson RA (1996) Inhibition of adenylyl cyclase by a family of newly synthesized adenine nucleoside 3'-polyphosphates. *J Biol Chem* **271**:14028-14034.

Dessauer CW, Scully TT and Gilman AG (1997) Interactions of forskolin and ATP with the cytosolic domains of mammalian adenylyl cyclase. *J Biol Chem* **272**:22272-22277.

Dessauer CW, Tesmer JJ, Sprang SR and Gilman AG (1998) Identification of a $G_{i\alpha}$ binding site on type V adenylyl cyclase. *J Biol Chem* **273**:25831-25839.

Dessauer CW, Tesmer JJ, Sprang SR and Gilman AG (1999) The interactions of adenylate cyclases with P-site inhibitors. *Trends Pharmacol Sci* **20**:205-210.

Dyachok O, Idevall-Hagren O, Sagetorp J, Tian G, Wuttke A, Arrieumerlou C, Akusjarvi G, Gylfe E and Tengholm A (2008) Glucose-induced cyclic AMP oscillations regulate pulsatile insulin secretion. *Cell Metab* **8**:26-37.

El-Armouche A, Zolk O, Rau T and Eschenhagen T (2003) Inhibitory G-proteins and their role in desensitization of the adenylyl cyclase pathway in heart failure. *Cardiovasc Res* **60**:478-487.

Emsley P and Cowtan K (2004) Coot: model-building tools for molecular graphics. *Acta Crystallogr D Biol Crystallogr* **60**:2126-2132.

Engelhardt S, Bohm M, Erdmann E and Lohse MJ (1996) Analysis of β-adrenergic receptor mRNA levels in human ventricular biopsy specimens by quantitative polymerase chain reactions: progressive reduction of β_1-adrenergic receptor mRNA in heart failure. *J Am Coll Cardiol* **27**:146-154.

Engelhardt S, Hein L, Wiesmann F and Lohse MJ (1999) Progressive hypertrophy and heart failure in β_1-adrenergic receptor transgenic mice. *Proc Natl Acad Sci USA* **96**:7059-7064.

Ertel EA, Campbell KP, Harpold MM, Hofmann F, Mori Y, Perez-Reyes E, Schwartz A, Snutch TP, Tanabe T, Birnbaumer L, Tsien RW and Catterall WA (2000) Nomenclature of voltage-gated calcium channels. *Neuron* **25**:533-535.

Förster K, Groner F, Matthes J, Koch WJ, Birnbaumer L and Herzig S (2003) Cardioprotection specific for the G protein Gi_2 in chronic adrenergic signaling through β_2-adrenoceptors. *Proc Natl Acad Sci USA* **100**:14475-14480.

Gao MH, Lai NC, Roth DM, Zhou J, Zhu J, Anzai T, Dalton N and Hammond HK (1999) Adenylylcyclase increases responsiveness to catecholamine stimulation in transgenic mice. *Circulation* **99**:1618-1622.

Gasteiger J and Marsili MA (1978) A new model for calculating atomic charges in molecules. *Tetrahedron Letters* **19**:3181-3184.

Geduhn J (2009) Anthraniloyl-derived Nucleotides as potent and selective Adenylyl Cyclase Inhibitors, PhD thesis pp 1-181, University of Regensburg, Regensburg.

Gierschik P, Bouillon T and Jakobs KH (1994) Receptor-stimulated hydrolysis of guanosine 5'-triphosphate in membrane preparations. *Methods Enzymol* **237**:13-26.

Gille A, Lushington GH, Mou TC, Doughty MB, Johnson RA and Seifert R (2004) Differential inhibition of adenylyl cyclase isoforms and soluble guanylyl cyclase by purine and pyrimidine nucleotides. *J Biol Chem* **279**:19955-19969.

Gille A and Seifert R (2003a) 2'(3')-O-(N-methylanthraniloyl)-substituted GTP analogs: a novel class of potent competitive adenylyl cyclase inhibitors. *J Biol Chem* **278**:12672-12679.

Gille A and Seifert R (2003b) MANT-substituted guanine nucleotides: a novel class of potent adenylyl cyclase inhibitors. *Life Sci* **74**:271-279.

Gohlke H and Klebe G (2002) Approaches to the description and prediction of the binding affinity of small-molecule ligands to macromolecular receptors. *Angew Chem Int Ed Engl* **41**:2644-2676.

Göttle M, Geduhn J, König B, Gille A, Höcherl K and Seifert R (2009) Characterization of mouse heart adenylyl cyclase. *J Pharmacol Exp Ther* **329**:1156-1165.

Grobelny D, Goli UB and Galardy RE (1989) Binding energetics of phosphorus-containing inhibitors of thermolysin. *Biochemistry* **28**:4948-4951.

Hamill OP, Marty A, Neher E, Sakmann B and Sigworth FJ (1981) Improved patch-clamp techniques for high-resolution current recording from cells and cell-free membrane patches. *Pflüger's Arch* **391**:85-100.

Hanoune J and Defer N (2001) Regulation and role of adenylyl cyclase isoforms. *Annu Rev Pharmacol Toxicol* **41**:145-174.

Hardman JG (1984) Cyclic nucleotides and regulation of vascular smooth muscle. *J Cardiovasc Pharmacol* **6 Suppl 4**:S639-645.

Hartzell HC and Fischmeister R (1986) Opposite effects of cyclic GMP and cyclic AMP on Ca^{2+} current in single heart cells. *Nature* **323**:273-275.

Hatley ME, Gilman AG and Sunahara RK (2002) Expression, purification, and assay of cytosolic (catalytic) domains of membrane-bound mammalian adenylyl cyclases. *Methods Enzymol* **345**:127-140.

Hiratsuka T (1983) New ribose-modified fluorescent analogs of adenine and guanine nucleotides available as substrates for various enzymes. *Biochim Biophys Acta* **742**:496-508.

Hodgkin AL and Huxley AF (1952a) Currents carried by sodium and potassium ions through the membrane of the giant axon of Loligo. *J Physiol* **116**:449-472.

Hodgkin AL and Huxley AF (1952b) The dual effect of membrane potential on sodium conductance in the giant axon of Loligo. *J Physiol* **116**:497-506.

Hu CL, Chandra R, Ge H, Pain J, Yan L, Babu G, Depre C, Iwatsubo K, Ishikawa Y, Sadoshima J, Vatner SF and Vatner DE (2009) Adenylyl cyclase type 5 protein expression during cardiac development and stress. *Am J Physiol Heart Circ Physiol* **297**:H1776-1782.

Iwamoto T, Okumura S, Iwatsubo K, Kawabe J, Ohtsu K, Sakai I, Hashimoto Y, Izumitani A, Sango K, Ajiki K, Toya Y, Umemura S, Goshima Y, Arai N, Vatner SF and Ishikawa Y (2003) Motor dysfunction in type 5 adenylyl cyclase-null mice. *J Biol Chem* **278**:16936-16940.

Iwase M, Uechi M, Vatner DE, Asai K, Shannon RP, Kudej RK, Wagner TE, Wight DC, Patrick TA, Ishikawa Y, Homcy CJ and Vatner SF (1997) Cardiomyopathy induced by cardiac $G_{s\alpha}$ overexpression. *Am J Physiol* **272**:H585-589.

Iwatsubo K, Minamisawa S, Tsunematsu T, Nakagome M, Toya Y, Tomlinson JE, Umemura S, Scarborough RM, Levy DE and Ishikawa Y (2004) Direct inhibition of type 5 adenylyl cyclase prevents myocardial apoptosis without functional deterioration. *J Biol Chem* **279**:40938-40945.

Jameson DM and Eccleston JF (1997) Fluorescent nucleotide analogs: synthesis and applications. *Methods Enzymol* **278**:363-390.

Jessup M, Abraham WT, Casey DE, Feldman AM, Francis GS, Ganiats TG, Konstam MA, Mancini DM, Rahko PS, Silver MA, Stevenson LW and Yancy CW (2009) 2009 focused update: ACCF/AHA Guidelines for the Diagnosis and Management of Heart Failure in Adults: a report of the American College of Cardiology Foundation/American Heart Association Task Force on Practice Guidelines: developed in collaboration with the International Society for Heart and Lung Transplantation. *Circulation* **119**:1977-2016.

Johnson JD, Walters JD and Mills JS (1987) A continuous fluorescence assay for cyclic nucleotide phosphodiesterase hydrolysis of cyclic GMP. *Anal Biochem* **162**:291-295.

Johnson RA, Desaubry L, Bianchi G, Shoshani I, Lyons E, Jr., Taussig R, Watson PA, Cali JJ, Krupinski J, Pieroni JP and Iyengar R (1997) Isozyme-dependent sensitivity of adenylyl cyclases to P-site-mediated inhibition by adenine nucleosides and nucleoside 3'-polyphosphates. *J Biol Chem* **272**:8962-8966.

Johnson RA, Yeung SM, Stubner D, Bushfield M and Shoshani I (1989) Cation and structural requirements for P site-mediated inhibition of adenylate cyclase. *Mol Pharmacol* **35**:681-688.

Jones SW (1998) Overview of voltage-dependent calcium channels. *J Bioenerg Biomembr* **30**:299-312.

Kamenetsky M, Middelhaufe S, Bank EM, Levin LR, Buck J and Steegborn C (2006) Molecular details of cAMP generation in mammalian cells: a tale of two systems. *J Mol Biol* **362**:623-639.

Krupinski J, Coussen F, Bakalyar HA, Tang WJ, Feinstein PG, Orth K, Slaughter C, Reed RR and Gilman AG (1989) Adenylyl cyclase amino acid sequence: possible channel- or transporter-like structure. *Science* **244**:1558-1564.

Laemmli UK (1970) Cleavage of structural proteins during the assembly of the head of bacteriophage T4. *Nature* **227**:680-685.

Laugwitz KL, Spicher K, Schultz G and Offermanns S (1994) Identification of receptor-activated G proteins: selective immunoprecipitation of photolabeled G-protein α subunits. *Methods Enzymol* **237**:283-294.

Lechat P, Packer M, Chalon S, Cucherat M, Arab T and Boissel JP (1998) Clinical effects of β-adrenergic blockade in chronic heart failure: a meta-analysis of double-blind, placebo-controlled, randomized trials. *Circulation* **98**:1184-1191.

Lohmann SM, Fischmeister R and Walter U (1991) Signal transduction by cGMP in heart. *Basic Res Cardiol* **86**:503-514.

Lohse MJ, Engelhardt S, Danner S and Bohm M (1996) Mechanisms of β-adrenergic receptor desensitization: from molecular biology to heart failure. *Basic Res Cardiol* **91 Suppl 2**:29-34.

Lohse MJ, Engelhardt S and Eschenhagen T (2003) What is the role of β-adrenergic signaling in heart failure? *Circ Res* **93**:896-906.

Mikami A, Imoto K, Tanabe T, Niidome T, Mori Y, Takeshima H, Narumiya S and Numa S (1989) Primary structure and functional expression of the cardiac dihydropyridine-sensitive calcium channel. *Nature* **340**:230-233.

Morgan BP, Scholtz JM, Ballinger MD, Zipkin ID and Bartlett PA (1991) Differential binding energy: A detailed evaluation of the influence of hydrogen-bonding and hydrophobic groups on the inhibition of thermolysin by phosphorus-containing inhibitors. *J Am Chem Soc* **113**:297-307.

Mou TC, Gille A, Fancy DA, Seifert R and Sprang SR (2005) Structural basis for the inhibition of mammalian membrane adenylyl cyclase by 2'(3')-O-(N-Methyl-anthraniloyl)-guanosine 5 '-triphosphate. *J Biol Chem* **280**:7253-7261.

Mou TC, Gille A, Suryanarayana S, Richter M, Seifert R and Sprang SR (2006) Broad specificity of mammalian adenylyl cyclase for interaction with 2',3'-substituted purine- and pyrimidine nucleotide inhibitors. *Mol Pharmacol* **70**:878-886.

Neumann T, Biermann J, Erbel R, Neumann A, Wasem J, Ertl G and Dietz R (2009) Heart failure: the commonest reason for hospital admission in Germany: medical and economic perspectives. *Dtsch Arztebl Int* **106**:269-275.

Newton M, Niewczas I, Clark J and Bellamy TC (2010) A real-time fluorescent assay of the purified nitric oxide receptor, guanylyl cyclase. *Anal Biochem* **402**:129-136.

Ni Q, Shaffer J and Adams JA (2000) Insights into nucleotide binding in protein kinase A using fluorescent adenosine derivatives. *Protein Sci* **9**:1818-1827.

Numberger M and Draguhn A (1996) *Patch-Clamp-Technik*. Spektrum Akademischer Verlag GmbH, Heidelberg-Berlin-Oxford.

O'Rourke B, Backx PH and Marban E (1992) Phosphorylation-independent modulation of L-type calcium channels by magnesium-nucleotide complexes. *Science* **257**:245-248.

Okumura S, Kawabe J, Yatani A, Takagi G, Lee MC, Hong C, Liu J, Takagi I, Sadoshima J, Vatner DE, Vatner SF and Ishikawa Y (2003a) Type 5 adenylyl cyclase disruption alters not only sympathetic but also parasympathetic and calcium-mediated cardiac regulation. *Circ Res* **93**:364-371.

Okumura S, Suzuki S and Ishikawa Y (2009) New aspects for the treatment of cardiac diseases based on the diversity of functional controls on cardiac muscles: effects of targeted disruption of the type 5 adenylyl cyclase gene. *J Pharmacol Sci* **109**:354-359.

Okumura S, Takagi G, Kawabe J, Yang G, Lee MC, Hong C, Liu J, Vatner DE, Sadoshima J, Vatner SF and Ishikawa Y (2003b) Disruption of type 5 adenylyl cyclase gene preserves cardiac function against pressure overload. *Proc Natl Acad Sci USA* **100**:9986-9990.

Ono K and Trautwein W (1991) Potentiation by cyclic GMP of beta-adrenergic effect on Ca^{2+} current in guinea-pig ventricular cells. *J Physiol* **443**:387-404.

Otwinowski Z and Minor W (1997) Processing of X-ray diffraction data collected in oscillation mode. *Methods Enzymol* **276**:307-326.

Phan HM, Gao MH, Lai NC, Tang T and Hammond HK (2007) New signaling pathways associated with increased cardiac adenylyl cyclase 6 expression: implications for possible congestive heart failure therapy. *Trends Cardiovasc Med* **17**:215-221.

Pierre S, Eschenhagen T, Geisslinger G and Scholich K (2009) Capturing adenylyl cyclases as potential drug targets. *Nat Rev Drug Discov* **8**:321-335.

Pinto C, Hübner M, Gille A, Richter M, Mou TC, Sprang SR and Seifert R (2009) Differential interactions of the catalytic subunits of adenylyl cyclase with forskolin analogs. *Biochem Pharmacol* **78**:62-69.

Putnam WC, Swenson SM, Reif GA, Wallace DP, Helmkamp GM, Jr. and Grantham JJ (2007) Identification of a forskolin-like molecule in human renal cysts. *J Am Soc Nephrol* **18**:934-943.

Randall A and Benham CD (1999) Recent advances in the molecular understanding of voltage-gated Ca^{2+} channels. *Mol Cell Neurosci* **14**:255-272.

Remmers AE (1998) Detection and quantitation of heterotrimeric G proteins by fluorescence resonance energy transfer. *Anal Biochem* **257**:89-94.

Remmers AE and Neubig RR (1996) Partial G protein activation by fluorescent guanine nucleotide analogs. Evidence for a triphosphate-bound but inactive state. *J Biol Chem* **271**:4791-4797.

Reuter H (1983) Calcium channel modulation by neurotransmitters, enzymes and drugs. *Nature* **301**:569-574.

Roth DM, Gao MH, Lai NC, Drumm J, Dalton N, Zhou JY, Zhu J, Entrikin D and Hammond HK (1999) Cardiac-directed adenylyl cyclase expression improves heart function in murine cardiomyopathy. *Circulation* **99**:3099-3102.

Rottländer D, Matthes J, Vatner SF, Seifert R and Herzig S (2007) Functional adenylyl cyclase inhibition in murine cardiomyocytes by 2'(3')-O-(N-methylanthraniloyl)-guanosine 5'-[γ-thio]triphosphate. *J Pharmacol Exp Ther* **321**:608-615.

Sadana R and Dessauer CW (2009) Physiological roles for G protein-regulated adenylyl cyclase isoforms: insights from knockout and overexpression studies. *Neurosignals* **17**:5-22.

Schaefer ML, Wong ST, Wozniak DF, Muglia LM, Liauw JA, Zhuo M, Nardi A, Hartman RE, Vogt SK, Luedke CE, Storm DR and Muglia LJ (2000) Altered stress-induced anxiety in adenylyl cyclase type VIII-deficient mice. *J Neurosci* **20**:4809-4820.

Shoshani I, Boudou V, Pierra C, Gosselin G and Johnson RA (1999) Enzymatic synthesis of unlabeled and β-^{32}P-labeled β-L-2',3'-dideoxyadenosine-5'-triphosphate as a potent inhibitor of adenylyl cyclases and its use as reversible binding ligand. *J Biol Chem* **274**:34735-34741.

Steegborn C, Litvin TN, Levin LR, Buck J and Wu H (2005) Bicarbonate activation of adenylyl cyclase via promotion of catalytic active site closure and metal recruitment. *Nat Struct Mol Biol* **12**:32-37.

Sunahara RK, Dessauer CW and Gilman AG (1996) Complexity and diversity of mammalian adenylyl cyclases. *Annu Rev Pharmacol Toxicol* **36**:461-480.

Suryanarayana S, Göttle M, Hübner M, Gille A, Mou TC, Sprang SR, Richter M and Seifert R (2009) Differential inhibition of various adenylyl cyclase isoforms and soluble guanylyl cyclase by 2',3'-O-(2,4,6-trinitrophenyl)-substituted nucleoside 5'-triphosphates. *J Pharmacol Exp Ther* **330**:687-695.

Tang T, Gao MH, Lai NC, Firth AL, Takahashi T, Guo T, Yuan JX, Roth DM and Hammond HK (2008) Adenylyl cyclase type 6 deletion decreases left ventricular function via impaired calcium handling. *Circulation* **117**:61-69.

Tang T, Lai NC, Roth DM, Drumm J, Guo T, Lee KW, Han PL, Dalton N and Gao MH (2006) Adenylyl cyclase type V deletion increases basal left ventricular function and reduces left ventricular contractile responsiveness to beta-adrenergic stimulation. *Basic Res Cardiol* **101**:117-126.

Tepe NM and Liggett SB (1999) Transgenic replacement of type V adenylyl cyclase identifies a critical mechanism of β-adrenergic receptor dysfunction in the $G_{\alpha q}$ overexpressing mouse. *FEBS Lett* **458**:236-240.

Tepe NM, Lorenz JN, Yatani A, Dash R, Kranias EG, Dorn GW, 2nd and Liggett SB (1999) Altering the receptor-effector ratio by transgenic overexpression of type V adenylyl cyclase: enhanced basal catalytic activity and function without increased cardiomyocyte beta-adrenergic signalling. *Biochemistry* **38**:16706-16713.

Tesmer JJ, Sunahara RK, Gilman AG and Sprang SR (1997) Crystal structure of the catalytic domains of adenylyl cyclase in a complex with $G_{s\alpha}$.GTPγS. *Science* **278**:1907-1916.

Thomas JA and Marks BH (1978) Plasma norepinephrine in congestive heart failure. *Am J Cardiol* **41**:233-243.

Tobise K, Ishikawa Y, Holmer SR, Im MJ, Newell JB, Yoshie H, Fujita M, Susannie EE and Homcy CJ (1994) Changes in type VI adenylyl cyclase isoform expression correlate with a decreased capacity for cAMP generation in the aging ventricle. *Circ Res* **74**:596-603.

Treinys R and Jurevicius J (2008) L-type Ca^{2+} channels in the heart: structure and regulation. *Medicina (Kaunas)* **44**:491-499.

Tripos (2008) SYBYL 8.0, The Tripos Associates, St. Louis, MO.

Wang H, Gong B, Vadakkan KI, Toyoda H, Kaang BK and Zhuo M (2007) Genetic evidence for adenylyl cyclase 1 as a target for preventing neuronal excitotoxicity mediated by N-methyl-D-aspartate receptors. *J Biol Chem* **282**:1507-1517.

Wang H and Storm DR (2003) Calmodulin-regulated adenylyl cyclases: cross-talk and plasticity in the central nervous system. *Mol Pharmacol* **63**:463-468.

Watts VJ (2007) Adenylyl cyclase isoforms as novel therapeutic targets: an exciting example of excitotoxicity neuroprotection. *Mol Interv* **7**:70-73.

Whisnant RE, Gilman AG and Dessauer CW (1996) Interaction of the two cytosolic domains of mammalian adenylyl cyclase. *Proc Natl Acad Sci USA* **93**:6621-6625.

Wolska BM and Solaro RJ (1996) Method for isolation of adult mouse cardiac myocytes for studies of contraction and microfluorimetry. *Am J Physiol* **271**:H1250-1255.

Wu ZL, Thomas SA, Villacres EC, Xia Z, Simmons ML, Chavkin C, Palmiter RD and Storm DR (1995) Altered behavior and long-term potentiation in type I adenylyl cyclase mutant mice. *Proc Natl Acad Sci USA* **92**:220-224.

Yamaoka K and Kameyama M (2003) Regulation of L-type Ca^{2+} channels in the heart: overview of recent advances. *Mol Cell Biochem* **253**:3-13.

Yan L, Vatner DE, O'Connor JP, Ivessa A, Ge H, Chen W, Hirotani S, Ishikawa Y, Sadoshima J and Vatner SF (2007) Type 5 adenylyl cyclase disruption increases longevity and protects against stress. *Cell* **130**:247-258.

Yan SZ, Huang ZH, Andrews RK and Tang WJ (1998) Conversion of forskolin-insensitive to forskolin-sensitive (mouse-type IX) adenylyl cyclase. *Mol Pharmacol* **53**:182-187.

Yazawa K, Kameyama A, Yasui K, Li JM and Kameyama M (1997) ATP regulates cardiac Ca^{2+} channel activity via a mechanism independent of protein phosphorylation. *Pflüger's Arch* **433**:557-562.

Zhang G, Liu Y, Ruoho AE and Hurley JH (1997) Structure of the adenylyl cyclase catalytic core. *Nature* **386**:247-253.

8. Supplementary Data

8.1. Western blot

- **Sample preparation and SDS-PAGE (2.2.1.9)**
- **Transfer of proteins to nitrocellulose membrane (0.45 µm)**

1.	Fresh preparation of blotting buffer (1.0 L / buffer tank) Per gel holder cassette: two foam pads, four sheets of filter paper and one nitrocellulose membrane – soaking in buffer Place on the black side of the gel holder cassette (not the clear side!!!): one foam pad, two sheets of filter paper
2.	Remove one side of the gel cassette, cut off the loading gel from the separating gel
3.	Soak the gel with water until it does not stick to the gel cassette anymore and can be moved to the filter paper → place the nitrocellulose membrane on top of the gel
4.	Place two filter papers on top of the membrane, removal of air bubbles with a pen Place one foam pad on top of the filter papers Close the gel holder cassette and put it with the black side to the black side of the electrophoresis blotting module
5.	Blotting at 4°C (in refrigerator) for 120 min, Power Pac basic power supply: 0.15 A

- **Blocking unspecific binding**

1.	Fresh preparation of 1x TBS-T buffer (Tween 0.1% m/v) Dilute 5 g skimmed milk in 100 ml TBS-T buffer (5% m/v)
2.	Open the gel holder cassette, remove the membrane; Check blotting result by staining membrane with Ponceau S 0.1% (m/v) for 1 min. Cleaning with H_2O_{dest}.
3.	Incubate membrane 1 – 2 h in 5% (m/v) skimmed milk (TBS-T) on a shaker
4.	Remove milk and wash membrane 2x 5 - 10 min in TBS-T buffer (without milk!)

- **Detection of proteins *via* Chemiluminescence**

1.	Primary antibody in TBS-T, containing sodium azide 0.05% (m/v) and BSA 1% (m/v) (10 - 20 ml solution of 1st antibody in a 50 ml Falcon tube, storage in refrigerator)
2.	Take nitrocellulose membrane and place it in 50 ml Falcon tube
3.	Incubate overnight at 4°C (cold room) using a vertical rotation mixer
4.	Remove membrane from 50 ml Falcon tube and wash 3x 15 min in TBS-T buffer
5.	Dilute secondary antibody in 5% skimmed milk (1:1000) Place membrane on parafilm in a Petri dish (no airbubbles) and soak it with 2nd antibody solution (~ 4 ml), incubate 1 h at room temperature
6.	Remove milk and wash 3x 15 min in TBS-T buffer

- **Chemiluminescence**

1.	Drain membrane on a filter paper and put it on a Petri dish (no airbubbles!) → membrane should not be wet anymore
2.	Take 2 ml of solution 1 and 2 from ECL-Kit (4 ml / membrane), mix it and put it on top of the membrane for 1 min
3.	Drain membrane on filter paper and put it between two plastic foils, remove ECL rest
4.	Put the plastic foil in a X-ray film cassette for ~ 1 min (depends on amount of protein)
5.	Develop film with X-ray film processor

8.1.1. VC1 purification

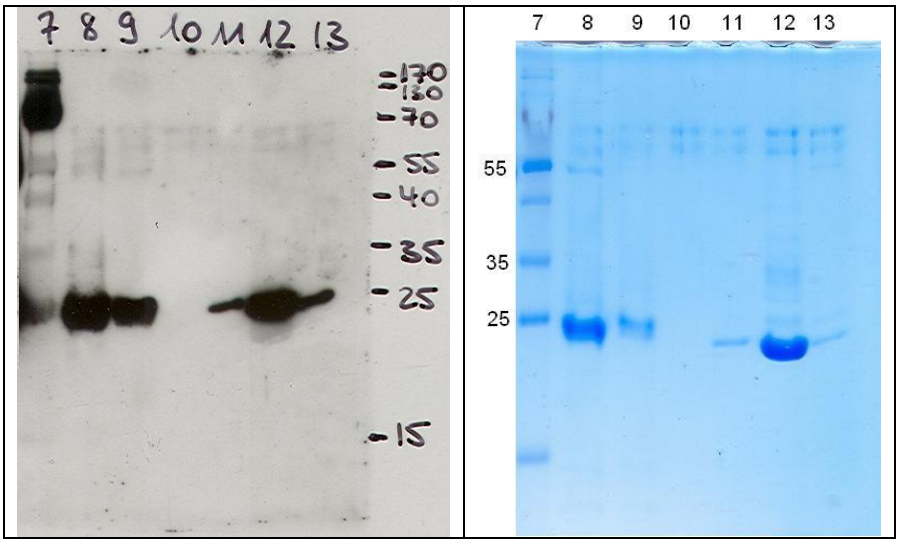

Supplementary Figure 1. Western Blot of VC1 protein detected with HIS-antibody.
The protein is expressed with a hexahistidine tag.
Lane 7 is the protein standard and lanes 8-13 show collected fractions after ion exchange.

8.1.2. $G_{s\alpha}$ purification

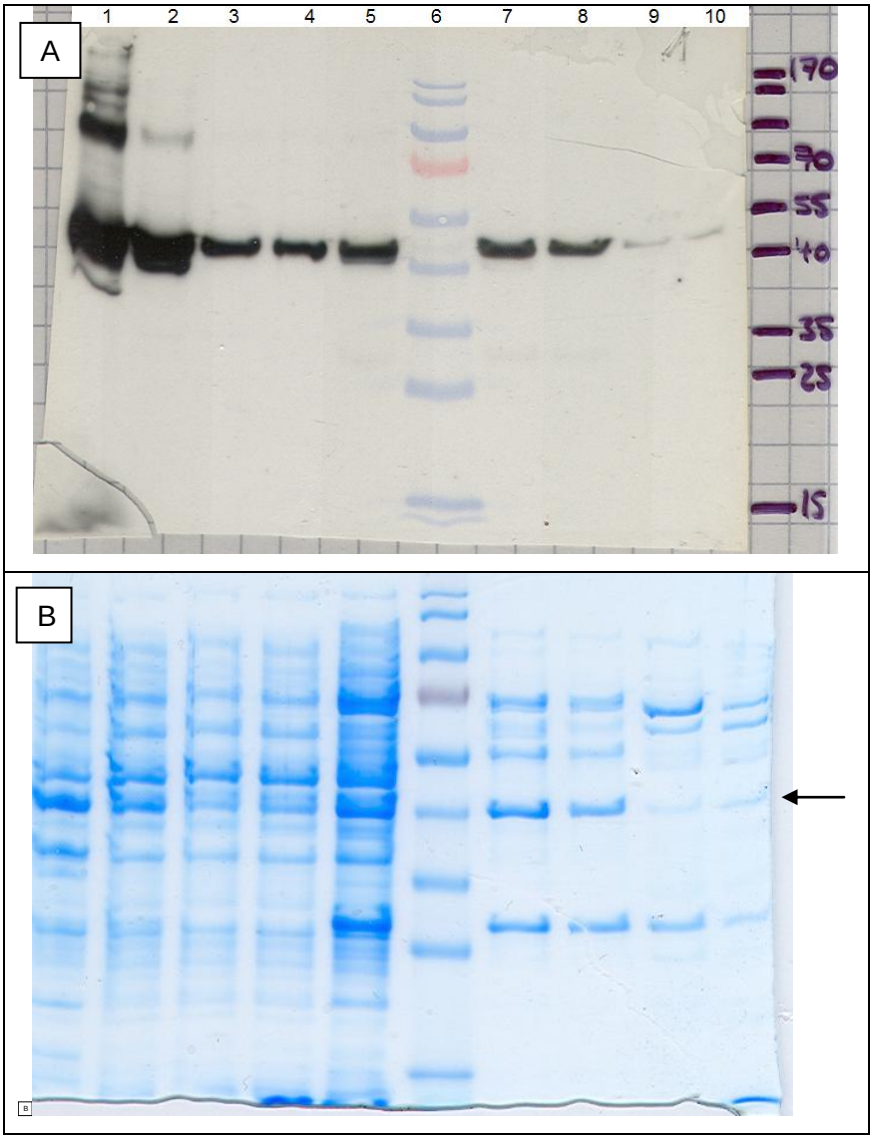

Supplementary Figure 2. Lysis and purification of $G_{s\alpha}$ with Ni-NTA column.
A. Western Blot of $G_{s\alpha}$ with HIS-Antibody, in comparison to the Coomassie stained SDS-PAGE, illustrated in **B.**
Lane

1 Pellet
2 Lysate
3 Load I
4 Load II
5 Wash
6 Standard
7 Fraction 1
8 Fraction 2
9 Fraction 6
10 Fraction 10

Gsα is eluted at ~ 46 kDa and indicated in the SDS-PAGE by a black arrow.

8.2. Protein purification of VC1

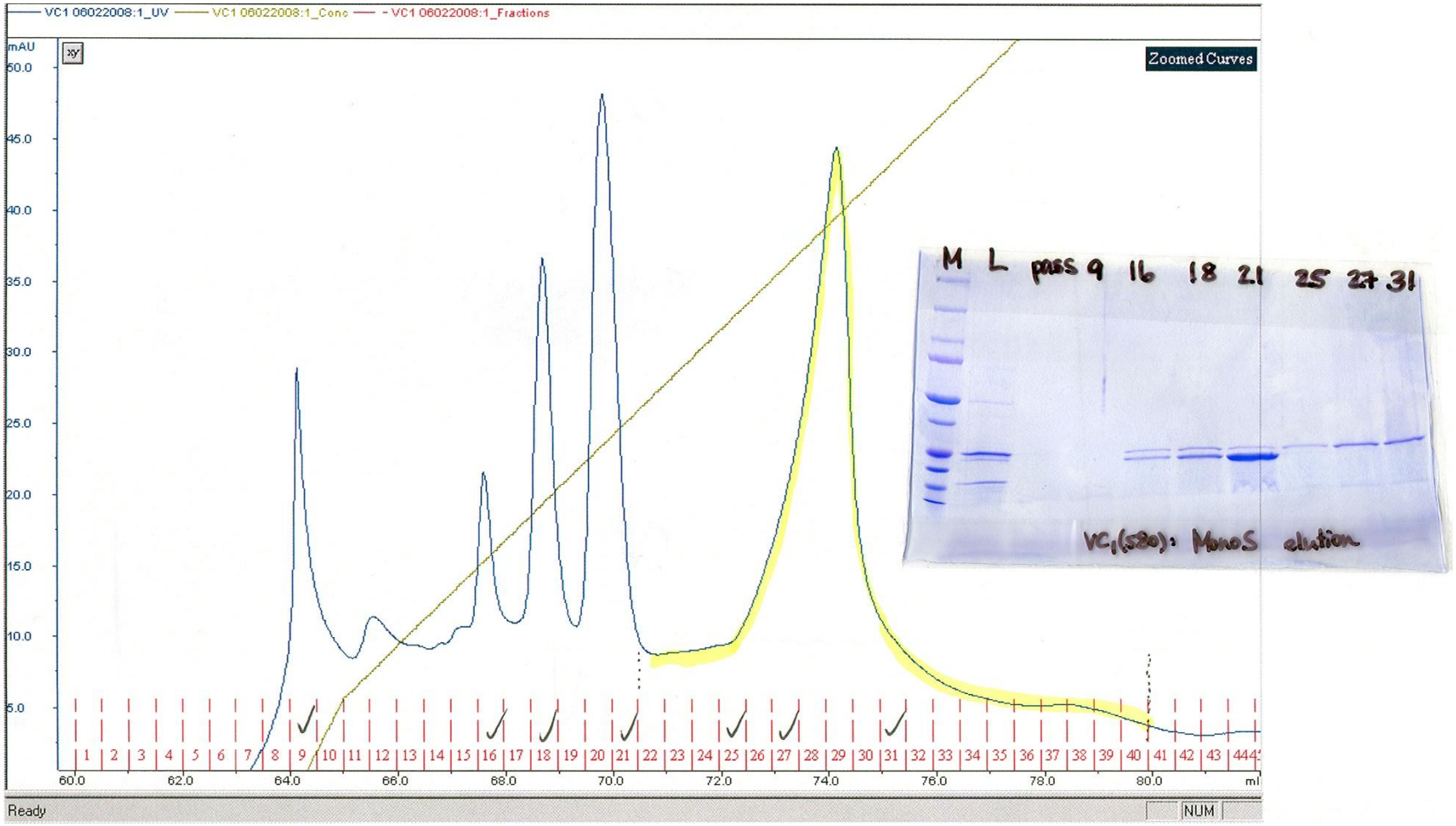

Supplementary Figure 3. Chromatogram of VC1 purification. The figure shows the elution of VC1 from Mono S column using a gradient to NaCl 1M (brown straight line). The yellow peak represents VC1, also indicated in the corresponding SDS-PAGE gel (fractions 25-31).

8.3. Gel filtration of AC-complex with 6-Acetyl-7-Deacetyl-FS

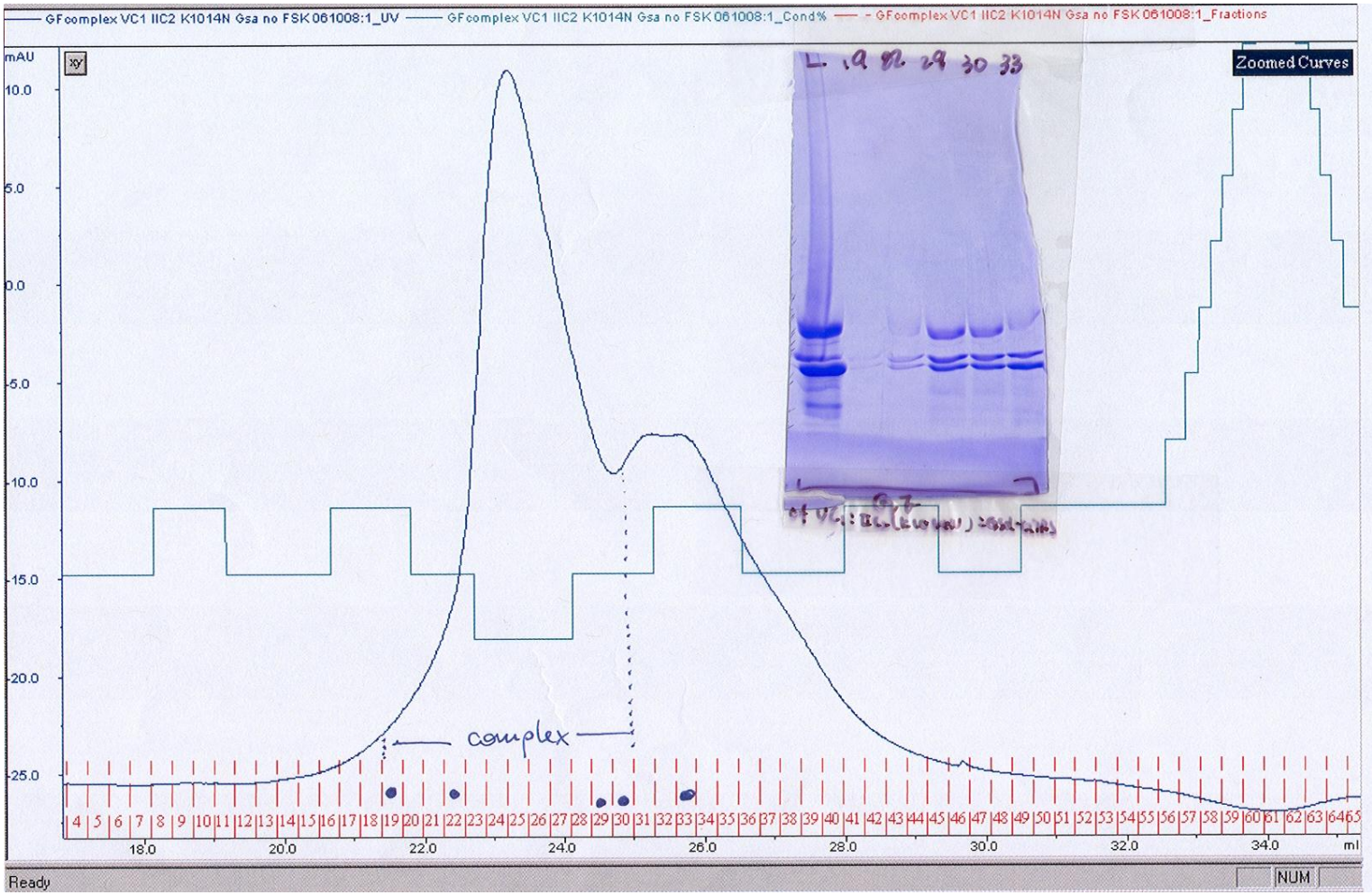

Supplementary Figure 4. Size exclusion chromatography of $G_{s\alpha}$-stimulated VC1/IIC2 (K1014N) complex with FS analog. Chromatogram and the gel show clearly that the complex was formed without FS, but with the help of 6-acetyl-7-deacetyl-FS. However, we never obtained crystals with FS analogs.

8.4. Crystal tray preparation

TRAY NAME: __VC1/IIC2/$G_{s\alpha}$/FS__# 5
DATE: _____03/21/2008___
ADDITIVE: _____non_____
PROTEIN(S): complex of 03/19/2008

TEMPERATURE: ____4 / 12 / **16** / 20°C
BUFFER: __HEPES buffer pH 8.0
SEEDING: Y / N FROM: _____
CONCENTRATION: 9 mg/ml

	1	2	3	4	5	6
A	**7.0% (v/v) PEG 8K** 50% (v/v) PEG 8K 140 µl 5 M NaCl 100 µl 1 M MES **pH 5.4** 100 µl dd water 660 µl	**7.2% (v/v) PEG 8K** 50% (v/v) PEG 8K 144 µl 5 M NaCl 100 µl 1 M MES pH 5.4 100 µl dd water 656 µl	**7.4% (v/v) PEG 8K** 50%(v/v) PEG 8K 148 µl 5 M NaCl 100 µl 1 M MES pH 5.4 100 µl dd water 652 µl	**7.6% (v/v) PEG 8K** 50% (v/v) PEG 8K 152 µl 5 M NaCl 100 µl 1 M MES pH 5.4 100 µl dd water 648 µl	**7.8% (v/v) PEG 8K** 50% (v/v) PEG 8K 156 µl 5 M NaCl 100 µl 1 M MES pH 5.4 100 µl dd water 644 µl	**8.0% (v/v) PEG 8K** 50%(v/v) PEG 8K 160 µl 5 M NaCl 100 µl 1 M MES pH 5.4 100 µl dd water 640 µl
B	7.0% (v/v) PEG 8K 50% (v/v) PEG 8K 140 µl 5 M NaCl 100 µl 1 M MES **pH 5.5** 100 µl dd water 660 µl	7.2% (v/v) PEG 8K 50%(v/v) PEG 8K 144 µl 5 M NaCl 100 µl 1 M MES pH 5.5 100 µl dd water 656 µl	7.4% (v/v) PEG 8K 50% (v/v) PEG 8K 148 µl 5 M NaCl 100 µl 1 M MES pH 5.5 100 µl dd water 652 µl	7.6% (v/v) PEG 8K 50% (v/v) PEG 8K 152 µl 5 M NaCl 100 µl 1 M MES pH 5.5 100 µl dd water 648 µl	7.8% (v/v) PEG 8K 50% (v/v) PEG 8K 156 µl 5 M NaCl 100 µl 1 M MES pH 5.5 100 µl dd water 644 µl	8.0% (v/v) PEG 8K 50% (v/v) PEG 8K 160 µl 5 M NaCl 100 µl 1 M MES pH 5.5 100 µl dd water 640 µl
C	7.0% (v/v) PEG 8K 50% (v/v) PEG 8K 140 µl 5 M NaCl 100 µl 1 M MES **pH 5.6** 100 µl dd water 660 µl	7.2% (v/v) PEG 8K 50% (v/v) PEG 8K 144 µl 5 M NaCl 100 µl 1 M MES pH 5.6 100 µl dd water 656 µl	7.4% (v/v) PEG 8K 50% (v/v) PEG 8K 148 µl 5 M NaCl 100 µl 1 M MES pH 5.6 100 µl dd water 652 µl	7.6% (v/v) PEG 8K 50% (v/v) PEG 8K 152 µl 5 M NaCl 100 µl 1 M MES pH 5.6 100 µl dd water 648 µl	7.8% (v/v) PEG 8K 50% (v/v) PEG 8K 156 µl 5 M NaCl 100 µl 1 M MES pH 5.6 100 µl dd water 644 µl	8.0% (v/v) PEG 8K 50% (v/v) PEG 8K 160 µl 5 M NaCl 100 µl 1 M MES pH 5.6 100 µl dd water 640 µl
D	7.0% (v/v) PEG 8K 50% (v/v) PEG 8K 140 µl 5 M NaCl 100 µl 1 M MES **pH 5.7** 100 µl dd water 660 µl	7.2% (v/v) PEG 8K 50% (v/v) PEG 8K 144 µl 5 M NaCl 100 µl 1 M MES pH 5.7 100 µl dd water 656 µl	7.4% (v/v) PEG 8K 50% (v/v) PEG 8K 148 µl 5 M NaCl 100 µl 1 M MES pH 5.7 100 µl dd water 652 µl	7.6% (v/v) PEG 8K 50% (v/v) PEG 8K 152 µl 5 M NaCl 100 µl 1 M MES pH 5.7 100 µl dd water 648 µl	7.8% (v/v) PEG 8K 50% (v/v) PEG 8K 156 µl 5 M NaCl 100 µl 1 M MES pH 5.7 100 µl dd water 644 µl	8.0% (v/v) PEG 8K 50% (v/v) PEG 8K 160 µl 5 M NaCl 100 µl 1 M MES pH 5.7 100 µl dd water 640 µl

Supplementary Figure 5. The table illustrates a 24 well plate used for crystallization. Each well contains 1 ml of reservoir solution, containing PEG, NaCl and MES buffer.

9. Publications and Poster Presentations

Publications:

2008

Pinto C, Papa D, Hübner M, Mou TC, Lushington GH and Seifert R (2008) Activation and inhibition of adenylyl cyclase isoforms by forskolin analogs. *J Pharmacol Exp Ther* **325**:27-36.

2009

Pinto C, Hübner M, Gille A, Richter M, Mou TC, Sprang SR and Seifert R (2009) Differential interactions of the catalytic subunits of adenylyl cyclase with forskolin analogs. *Biochem Pharmacol* **78**:62-69.

Suryanarayana S, Göttle M, Hübner M, Gille A, Mou TC, Sprang SR, Richter M and Seifert R (2009) Differential inhibition of various adenylyl cyclase isoforms and soluble guanylyl cyclase by 2',3'-O-(2,4,6-trinitrophenyl)-substituted nucleoside 5'-triphosphates. *J Pharmacol Exp Ther* **330**:687-695.

Egger M, Prantik M,Hübner M, Seifert R and König B (2009) Synthesis and pharmacological properties of new tetracyclic forskolin analogues. *Eur J of Org Chem* **21**:3613-3618.

2010

Hübner M, Mou TC, Lushington GH, Pinto C, Gille A, Geduhn J, König B, Sprang SR and Seifert R (2010) Structural Basis for the High-Affinity Inhibition of Mammalian Membranous Adenylyl Cyclase by 2',3'-*O*-(*N*-Methylanthraniloyl)-Inosine 5'-Triphosphate. *Mol Pharmacol* (in revision)

Hübner M, Dizayee S, Matthes J, Seifert R and Herzig S, Effect of MANT-nucleotides on basal L-type calcium currents in murine cardiomyocytes. *Naunyn Schmiedebergs Arch Pharmacol* (in submission)

Poster presentation:

Effect of MANT-nucleotides on basal L-type calcium currents in murine cardiomyocytes.
51st Annual meeting of the German Society of Pharmacology and Toxicology (DGPT), Mainz, *Naunyn Schmiedebergs Arch Pharmacol* (2010) **381 (Suppl 1)**:1-92

Effect of the competitive adenylyl cyclases inhibitor MANT-ITP on L-type calcium currents in murine cardiomyocytes.
Annual Meeting of the German Pharmaceutical Society (DPhG), Jena, October 2009

Effect of the selective adenylyl cyclase inhibitor MANT-ITP on L-type calcium currents in murine cardiomyocytes.
33rd Meeting of the European Working Group of Cardiac Cellular Electrophysiology (EWGCCE), Cologne, September 2009

Crystal structure of MANT-ITP – membranous adenylyl cyclase complex.
50th Annual meeting of the German Society of Pharmacology and Toxicology (DGPT), Mainz; *Naunyn Schmiedebergs Arch Pharmacol* (2009) **379 (Suppl 1)**:1-100

Interaction of MANT-ITP with adenylyl cyclase.
Symposium “Signal transduction”, Hannover Medical School, Hannover, November 2008

Interaction of MANT-ITP with adenylyl cyclase.
4th Summer School “Medicinal Chemistry” (GRK 760), Regensburg, October 2008

Oral Presentations:

Effect of MANT nucleotides on cardiomyocytes using patch clamp technique.
Workshop meeting of the graduate college “Medicinal Chemistry” (GRK 760), Regensburg, May 2010

Analysis of Adenylyl Cyclase Inhibition by MANT nucleotides.
Working group meeting of the Department of Pharmacology at the University of Cologne, Cologne, March 2010

Adenylyl cyclase – Inhibition with MANT nucleotides.
Working group meeting of the Department of Pharmacology at the Hannover Medical School, Hannover, November 2009

Using protein crystallography to investigate protein-drug interaction.
Christmas colloquium of the Department of Organic Chemistry, Regensburg, December 2008

Crystallography of MANT-ITP-adenylyl cyclase complex.
Workshop meeting of the graduate college “Medicinal Chemistry” (GRK 760), Regensburg, October 2008

Protein Purification and Crystallography.
Workshop meeting, Center for Biomolecular Structure and Dynamics, University of Montana, July 2008

Studying Forskolin and FS analogs as potential therapeutics.
Workshop meeting, Center for Biomolecular Structure and Dynamics, University of Montana, May 2008

10. Curriculum Vitae

Name:	Melanie Hübner
Date/Place of birth:	13.02.1981 in Dresden
Address:	Liskircher Strasse 13, 93049 Regensburg
Nationality:	German

Education

Since 03/2007	PhD at the University of Regensburg Department of Pharmacology and Toxicology Supervisor: Prof. Dr. Roland Seifert
03/2008 – 08/2008	Graduate Student, University of Montana, Missoula, USA Center for Biomolecular Structure and Dynamics, Prof. Dr. Steve Sprang
04/2004	2nd state examination (1.75), Free University, Berlin
10/1999 – 04/2004	Free University Berlin, Pharmacy studies
09/2002 – 05/2003	Undergraduate Student, University of Toronto, Canada, Faculty of Pharmacy
1992 – 1999	Gymnasium Dresden-Plauen, A-level (1.9)

Working experience and Practical Training

12/2006 – 03/2007	Pharmacist, Panorama-Apothecary, Dresden
01/2006 – 11/2006	Graduate teaching assistant, Ludwig-Maximilians University Munich, Department of Pharmaceutical Technology and Biopharmacy, supervisor: Prof. Dr. W. Frieß
06/2005 – 12/2005	Pharmacist, Panorama-Apothecary, Dresden
11/2004 – 05/2005	Practical training period, University of Florida, Gainesville, USA Department of Pharmaceutics, supervisor: Prof. H. Derendorf
05/2004 – 10/2004	Practical training period, Hoheluft-Apothecary, Hamburg
11/2002 – 04/2003	Undergraduate assistant, University of Toronto, Canada Department of Adverse Drug Reactions, Prof. Uetrecht
03/2002 – 08/2002	Alexandrinen-Apothecary, Berlin
02/2001 – 05/2001	Undergraduate training, Department of Pharmaceutical Technology, Université de Nancy, France, Prof. Maincent
08/2000	clinical traineeship, hospital pharmacy, Berlin-Wannsee

Qualifications:

Since 01/2008	Associate member of the Research Training Group (Graduiertenkolleg 760) *"Medicinal Chemistry: Molecular Recognition – Ligand Receptor Interactions"*
Since 11/2007	Scholarship for highly gifted graduates (Stipendium des Bayerischen Elitenetzwerks)
12/2001-03/2004	Undergraduate scholarship, Foundation of the German Economy (Stiftung der Deutschen Wirtschaft, sdw)

Professional Training:

Advanced training
Gentechnik-Fortbildungsveranstaltung nach §§ 15 und 17 der Gentechniksicherheits-verordnung
Prof. Dr. S. Modrow
Regensburg, April 2010

Advanced Courses in Pharmacology I
Methoden zur Analyse G-Protein-gekoppelter Rezeptoren
Mainz, March 2010

Advanced Courses in Pharmacology II
Moderne Massenspektrometrie in Pharmakologie und Toxikologie
Mainz, March 2010

Advanced Courses in Pharmacology I
Neue Tiermodelle in der pharmakologischen Forschung
Mainz, March 2009

Advanced Courses in Pharmacology II
Arzneimittelinteraktionen, -metabolismus und –transport
Mainz, March 2009

4th International Summer School Medicinal Chemistry
Regensburg, September 2008

Advanced training
Umgang mit offenen radioaktiven Stoffen
Dr. R. Schupfner
Regensburg, October 2007

Eidesstattliche Erklärung

Ich erkläre hiermit an Eides statt, dass ich die vorliegende Arbeit ohne unzulässige Hilfe Dritter und ohne Benutzung anderer als der angegebenen Hilfsmittel angefertigt habe. Die aus anderen Quellen direkt oder indirekt übernommenen Daten und Konzepte sind unter Angabe des Literaturzitats gekennzeichnet. Weitere Personen waren an der inhaltlich-materiellen Herstellung der vorliegenden Arbeit nicht beteiligt.
Insbesondere habe ich hierfür nicht die entgeltliche Hilfe eines Promotionsberaters oder anderer Personen in Anspruch genommen. Niemand hat von mir weder unmittelbar noch mittelbar geldwerte Leistungen für Arbeiten erhalten, die im Zusammenhang mit dem Inhalt der vorgelegten Dissertation stehen. Die Arbeit wurde bisher weder im In- noch im Ausland in gleicher oder ähnlicher Form einer anderen Prüfungsbehörde vorgelegt.

Regensburg, den 27.08.2010

Melanie Hübner